REPUBLIQUE DU CAMEROUN
Paix – Travail – Patrie
****
UNIVERSITE DE YAOUNDE I
FACULTE DES SCIENCES
DEPARTEMENT DE PHYSIQUE
****
CENTRE DE RECHERCHE ET DE FORMATION DOCTORALE EN SCIENCES TECHNOLOGIES ET GEOSCIENCES
Laboratoire de Physique de l'Environnement Terrestre

REPUBLIC OF CAMEROUN
Peace – Work – Fatherland
****
UNIVERSITY OF YAOUNDE I
FACULTY OF SCIENCE
DEPARTMENT OF PHYSICS
****
POSTGRADUATE SCHOOL OF SCIENCE TECHNOLOGY AND GÉOSCIENCE
Laboratory of Earth's Environment Physics

Hydrological modeling of climate change impacts on water resources and hydropower potential in the headwaters of the Benue River Basin, Northern Cameroon.

Thesis submitted in partial fulfillment of the requirements for the degree of Doctor/PhD in physics

Par : **NONKI Rodric Merimé**
Master's degree in Physics

Sous la direction de
LENOUO André
Professor
University of Douala
TCHAWOUA Clément
Professor
University of Yaoundé 1

Année Académique : 2021

UNIVERSITÉ DE YAOUNDÉ I
THE UNIVERSITY OF YAOUNDE I

FACULTÉ DES SCIENCES
FACULTY OF SCIENCE

DÉPARTEMENT DE PHYSIQUE
DEPARTMENT OF PHYSICS

ATTESTATION DE CORRECTION DE LA THÈSE DE DOCTORAT/Ph.D

Nous, Professeur **SIEWE SIEWE Martin** et Professeur **MKANKAM KAMGA François**, respectivement Examinateur et Président du jury de la Thèse de Doctorat/Ph.D de Monsieur **NONKI Rodric Mérimé**, Matricule **07W730**, préparée sous la direction du Professeur **LENOUO André** et du Professeur **TCHAWOUA Clément,** intitulée : « **Hydrological modeling of climate change impacts on water resources and hydropower potential in the headwaters of the Benue River Basin, Northern Cameroon**», soutenue le **Lundi, 19 Avril 2021**, en vue de l'obtention du grade de Docteur/Ph.D en Physique, Spécialité **Physique de l'Environnement Terrestre,** Option **Sciences de l'Atmosphère,** attestons que toutes les corrections demandées par le jury de soutenance ont été effectuées.

En foi de quoi, la présente attestation lui est délivrée pour servir et valoir ce que de droit.

Fait à Yaoundé le 25 MAI 2021

Examinateur	Le Chef de Département de Physique	Le Président du jury
Pr SIEWE SIEWE Martin	Pr NDJAKA Jean-Marie Bienvenu	Pr MKANKAM KAMGA François

Dedication

To my mother Jeanne Kenné...

In memory of my late father, Isaac Tanoh...

Acknowledgments

First and foremost, thanks to the almighty God for granting me his limitless care, love and blessings all along the way.

My greatest thanks go to my first supervisor Professor LENOUO André for having guided, supported and accompanied me through the journey towards becoming a scientist. Thanks also for having greatly contributed to this Ph.D study with your vast experience, technical advices and support.

I would like to acknowledge my second supervisor Professor TCHAWOUA Clément for his kind support, guidance, encouragement and constructive comments. I am grateful for the time you dedicated to review my work, and I have surely learnt a lot during the entire period of this research.

Beside my supervisors, of very important is the contribution of Professor TSHIMANGA MUAMBA Raphael of the University of Kinshasa whom I owe a lot of gratitude for the eventual completion of this work. He has remained my pillar of support even when it was almost impossible for me to move forward. I would also like to extend my sincere gratitude to Doctor LENNARD Christopher of the University of Cape Town for his invaluable advices, suggestions and help. So also are the supports of Professor AGHAKOUCHAK Amir of the University of California Irvine for providing me the matlab code of the HBV model.

I would like to thank Professor MKANKAM KAMGA François the founder of the Laboratory for Environmental Modeling and Atmospheric Physics (LEMAP) and all the members of LEMAP group for their constructive comments to this research with great enthusiasm, a lot of ideas and continuous encouragement.

I will not forget to thank Professor NDJAKA Jean-Marie Bienvenu the head of the Physics Department and all the teachers of the Physics Department who contributed significantly to this work with their training courses since I was registered at the University of Yaoundé 1.

My thanks also go to all offices, institutions, personalities and projects who provided the needed data for my research, some financial support to attend conferences, workshops and summer schools, specially UNESCO, IRD, CORDEX Framework, GMES-Africa project during this research work.

I am also thinking of all the other researchers at the University of Yaounde 1 with whom I have been able to discuss science or other things during these years, as well as my classmate.

Knowing that Adam could not achieve much alone, God created Eve! Thus, to my wife, WAMENE TINKENG Blandine and children, I say thank you indeed for their love, patience and support to

achieve this goal, and also for keeping the home during my period of absence. And to my mother KENNE Jeanne, I wish you long life so that you could reap the fruit of your good work.

I wish to express my unreserved and profound gratitude to my family and friends, specifically DJEUSSE Joseph and PIATA TAKALA Honoré, for their incomparable financial and moral support and constant prayers which kept me motivated.

I will not end these acknowledgments without sending particular gratitude to all the scientific personalities who made me the honor to judge this work:

- Professor MKANKAM KAMGA François of the University of Yaoundé 1 and founder of the LEMAP, for having admitted me in his Laboratory and accepted to chair the Jury of this defense.

- Professor LENOUO André of the University of Douala and Professor TCHAWOUA Clément of the University of Yaoundé 1; I renew my gratitude not only for having directed this thesis, but also for having supervised me since the Master degree.

- Professor NDJAKA Jean-Marie Bienvenu, head of the Physics Department of the University of Yaoundé 1 and Professor NOUAYOU Robert of the University of Yaoundé 1, Who not only accepted to be members of this jury, but who also participated respectively as president and rapporteur of the pre-defense jury of this thesis. I gratefully acknowledge their constructive comments and valuable suggestions which enormously improved the presentation of the final document.

- Professor SIEWE SIEWE Martin of the University of Yaoundé 1, who not only kindly accepted to participate in this examination committee, but also for the interest he showed in this work by giving a favourable opinion twice in a row so that this defense could take place, firstly as a rapporteur during the audition phase and secondly as an internal expert during the evaluation phase. I also gratefully acknowledge his valuable comments and suggestions which improved the quality of this thesis.

- Professor NGUIYA Sévérin of the University of Douala, who accepted to be a member of this jury and who showed particular interest in this study by giving a favorable opinion as an external expert during the evaluation phase.

Contents

List of figures

List of tables

List of abbreviations and acronyms

AET or ETa:	Actual EvapoTranspiration
AIM:	Asia-Pacific Integrated Model
AMIP:	Atmospheric Model Intercomparison Project
ANN:	Artificial Neural Network
AR4:	4^{th} Assessment Report
AR5:	5^{th} Assessment Report
ARMA:	Auto Regressive Moving Average
AOGCMs:	Atmosphere-Ocean General Circulation Models
BALTEX:	BALTIC Sea Experiment
CA:	Central Africa
CC:	Climate Change
CCA:	Canonical Correlation Analysis
CCS:	Climate Change Signal
CMIP:	Coupled Model Intercomparison Project
CORDEX:	COordinated Regional climate Downscaling EXperiment
CRA:	Climate Risk Assessment
CRU:	Climate Research Unit
DD:	Dynamical downscaling
DEM:	Digital Elevation Model
DJF:	December-January-February
DOE:	Department of Energy
DNM:	Direction of the National Meteorology of Cameroon
ECHAM:	European Centre-HAMburg
ECMWF:	European Centre for Medium Range Weather Forecasts
EC-ESM:	European-wide Consortium-Earth system model
ERAIN:	ERA-Interim
ET:	EvapoTranspiration
ETP:	EvapoTranspiration Potentielle
FAOSTAT:	Food and Agriculture Organization Corporate Statistical Database
FISRWG:	Federal Interagency Stream Restoration Working Group
GCAM:	Global Change Assessment Mode
GCMs:	Global Climate Models
GES:	Gaz à Effet de Serre

GHGs:	GreenHouse Gases
GMES:	Global Monitoring for Environment and Security
GPCP:	Global Precipitation Climatology Project
GWP:	Global Water Partnership
HadCM:	Hadley Center
HAMOCC	HAmburg Model of Ocean Carbon Cycling
HBRB:	Headwaters of the Benue River Basin
HBV:	Hydrologiska Byråns Vattenavdelning, in English: Hydrological Bureau Water Balance section
HEBB:	Hautes Eaux du Bassin de la Bénoué
ICTP:	International Centre for Theoretical Physics
IFS:	Integrated Forecast System
IMAGE:	Integrated Model to Assess the Global Environment
IPCC:	International Panel on Climate Change
IRD:	Institut de Récherche Pour le Developpement
IRAP:	International Rivers Africa Program
IS92:	Integrated Science scenarios published in 1992
ITCZ:	InterTropical Convergence Zone
JJA:	June-July-August
JSBACH:	Jena Scheme for Biosphere-Atmosphere Coupling in Hamburg
LAM:	Limited Area Model
LARS-WG:	Long Ashton Research Station Weather Generator
LBCs:	Lateral Boundary Conditions
LEMAP:	Laboratory for Environmental Modeling and Atmospheric Physics
LR:	Low Resolution
MAM:	March-April-May
MCGs:	Modèles Climatiques Globaux
MCS:	Monte Carlo Simulations
MINEE:	Ministère de l'Eau et de l'Energie
MINEP:	Ministry of Environment and Protection of Nature
MPI-ESM:	Max Planck Institute-Earth System Model
MPIM:	Max Plan Institut für Meteorology
MPIOM:	Max Planck Institute Ocean Model
NCAR:	National Centers for Atmospheric Research
NCEP:	National Centers for Environmental Prediction
NEMO:	Nucleus for European Modelling of the Ocean
NHHM:	Non-homogeneous Hidden Markov Model
NOAA:	National Oceanic and Atmospheric Administration
NRB:	Niger River Basin
NSE:	Nash-Sutcliffe Efficiency
ORSTOM:	Office de la Récherche Scientifique et Technique Outre-Mer
PARI:	Program of Accompanying Research for Agricultural Innovation
PBIAS:	Percent BIAS

PET:	Potential EvapoTranspiration
RCMs:	Regional Climate Models
RegCM:	Regional Climate Model of ICTP
REMO:	REgional MOdel
RCPs:	Representative Concentration Pathways
RF:	Radiation Forcing
RMSE:	Root Mean Square Error
RSR:	RMSE-Standard deviation Ratio
SA:	Sensitivity Analysis
SDSM:	Statistical DownScaling Model
SEE:	Standard Error of Estimation
SIEREM:	Système d'Informations Environnementales sur les Ressources en Eau et leur Modélisation
SMHI:	Swedish Meteorological and Hydrological Institute
SON:	September-October-November
SRES:	Special Report on Emission Scenarios
SD:	Statistical Downscaling
STARDEX:	Statistical and Regional dynamical Downscaling of Extremes
StD:	Standard Deviation
UA:	Uncertainty Analysis
UMR:	Unité Mixte de Récherche
UNDP:	United Nations Development Programme
UNESCO:	United Nations Educational, Scientific and Cultural Organization
UNFCCC:	United Nations Framework Convention on Climate Change
VBSA:	Variance-based Sensitivity Analysis
WAM:	West African Monsoon
WCA:	West and Central Africa
WCRP:	World Climate Research Program
WRM:	Water Resources Management

List of symbols

C_P:	Specific heat at constant pressure,1.013×10^{-3} $[MJ.K_g^{-1}.^oC^{-1}]$
e_a:	Actual vapor pressure, $[KP_a]$
e_s:	Saturation vapor pressure, $[KP_a]$
$e_s - e_a$:	Saturation vapor pressure deficit , $[KP_a]$
g:	acceleration due to gravity, $[m.s^{-2}$
N:	Maximum possible sunshine duration in a day or daylight hours, $[hour]$
n:	Mean daily sunshine duration, $[hour]$
$\frac{n}{N}$:	Relative sunshine duration, $[-]$
p:	Pressure, $[KP_a]$
R_a:	extraterrestrial radiation, $[MJ.m^{-2}.jour^{-1}]$
R_g:	Mean daily global radiation, $[MJ.m^{-2}.jour^{-1}]$
R_n:	Mean daily net radiation, $[MJ.m^{-2}.jour^{-1}]$
R_h:	Mean daily relative humidity, [٪]
T_a:	Mean daily air temperature at 2 m height, [℃]
T_{max}:	Mean daily maximum air temperature, [℃]
T_m:	Mean monthly air temperature, $[K]$
T_{min}:	Mean daily minimum air temperature, [℃]
U:	Mean daily wind speed at 2 m height, $[m.s^{-1}]$
z:	Elevation of the station, $[m]$
α:	Albedo, $[-]$
γ:	Psychometric constant, $[KP_a.^oC^{-1}]$.
Δ:	Slope of saturation vapor pressure versus air temperature curve, $[KP_a.^oC^{-1}]$
λ:	Latent heat of vaporization, 2.45 $[MJ.K_g^{-1}]$
ρ_a:	Density of the air mass, $[K_g.m^{-3}]$
ρ_ω:	water density, 1000 $[K_g.m^{-3}]$
η:	Overall plant efficiency

Abstract

The Headwaters of the Benue River Basin (HBRB) located in the northern Cameroon, is the second largest river in Cameroon and a major tributary of the Niger River Basin (NRB). It serves many water resources functions including irrigation, hydropower production and navigation. The population in the basin is mainly dependent on rain-fed agriculture and hydroelectricity represents more than 95% of electricity production, therefore highly vulnerable to the spatial and temporal variability of rainfall and Climate Change (CC). Recently, northern Cameroon has experienced water-related disasters such as floods and droughts. This research aims to assess the potential impacts of CC on water resources and hydropower potential in the HBRB. Hydrological simulations were performed with the use of calibrated HBV-Light hydrological model and historical and projected scenarios of dynamically downscaled temperature and precipitation from the REMO regional climate model (RCM) forced by the boundary conditions data of the Europe-wide Consortium Earth System Model (EC-ESM) and the Max Planck Institute-Earth System Model (MPI-ESM) general circulation models (GCMs).

Calibration and validation of the hydrological model is done again on measured discharge at three outlet gage stations (Buffle Noir, Riao and Garoua), whereby the most sensitive out the numerous "tuneable" calibration parameters in HBV-Light model have been selected by means of a sophisticated sensitivity analysis. The uncertainties arising from the problem of identifying representative model parameters in a hydrological model were investigated by using the Monte-Carlo procedure and the sensitivity of the model outputs due to different Potential evapotranspiration (PET) inputs was conducted through the dynamic and static sensitivity approaches. Consequently, a good calibration/validation model performance with a high Nash and Sutcliffe Efficiency (NSE) range between $0.66 - 0.89$ is obtained. The results also revealed that the best simulations as well as the measured streamflows lie inside the 95% uncertainty band of model predictions, indicating the insignificant implications of the model parameters uncertainties to the model predictions. The different PET inputs were found to have no or moderate impact on the model performance when we followed the dynamic or static sensitivity analysis approaches respectively..

The ability of REMO RCM to simulate present climate in the HBRB was assessed and the mean climate and hydrological variables for the historical ($1981 - 2005$) and the two future periods ($2041 - 2065$ and $2071 - 2095$) were compared to assess the potential impact of CC on water resources and hydropower potential in the middle and late twenty-first century under three greenhouse gases

(GHGs) concentration scenarios, the Representative Concentration Pathways (RCPs) 2.6, 4.5 and 8.5. Our results show that (a) the REMO model was found to reproduce the annual cycle of rainfall, 2-m temperature and PET well, although some relative low biases still exist; (b) annual precipitation will decrease between 1 and 10% while both annual temperature and PET will increase between $8-18$ and $6-30\%$, respectively, under scenarios, models and future periods; c) the combination of reduced precipitation and increase of PET results in a significant decrease in streamflow in the HBRB (up to 51%) and this will negatively impact the hydropower potential of the Lagdo dam with a decrease. The results also revealed that this region will be moved to extreme environmental drier conditions due to the increase of PET greater than increase of actual ET.

Key words: Climate change, Water resources, Hydropower potential, HBV-Light hydrological model, Regional climate model REMO

Résumé

Le Bassin de la Bénoué, situé au Nord - Cameroun, est le deuxième plus grand fleuve du Cameroun et un affluent majeur du bassin du fleuve Niger. Il possède un potentiel énorme en ressources en eau, notamment l'irrigation, la production de l'hydroélectricité et la navigation. La population du bassin est principalement dépendante de l'agriculture pluviale et l'hydroélectricité représente plus de 95 % de la production d'électricité, donc très vulnérable à la variabilité spatiale et temporelle des précipitations et aux changements climatiques (CC). Récemment, le Nord-Cameroun a connu d'importantes catastrophes liées à l'eau telles que des inondations et des sécheresses. Cette étude vise à évaluer les impacts des CC sur les ressources en eau et le potentiel hydroélectrique dans les hautes eaux du Bassin de la Bénoué (HEBB). Les débits ont été simulés à l'aide du modèle hydrologique HBV-Light forcé par les données de températures et de précipitations historiques et futures issues de la descente d'échelle dynamique de deux modèles climatiques globaux (MCGs: EC-ESM et MPI-ESM) par le modèle climatique régional REMO.

L'évaluation du modèle hydrologique s'est faite au moyen du test de calage/validation en utilisant des débits mesurés à trois stations de jaugeage (Buffle Noir, Riao et Garoua), et les paramètres du modèle les plus sensibles ont été sélectionnés au moyen d'une analyse de sensibilité. Les incertitudes dues à la détermination des paramètres du modèle ont été analysées grâce à la procédure Monte-Carlo. L'impact des différentes méthodes d'estimation de l'évapotranspiration potentielle (ETP) sur la performance du modèle a été réalisé par les approches dynamiques et statiques de l'analyse de sensibilité. Les résultats ont montré une bonne performance du modèle à simuler les débits aussi bien en période de calage que de validation avec le critère d'efficacité de Nash et Sutcliffe (NSE) élévé et compris entre $0,66$ et $0,89$. Les résultats ont également révélé que la meilleure simulation ainsi que les débits mesurés se situent dans la bande d'incertitude à 95% des prévisions du modèle, indiquant des implications insignifiantes des incertitudes dues aux paramètres du modèle sur les prévisions du modèle. Les différentes entrées de l'ETP se sont avérées avoir un impact significatif ou pas sur la performance du modèle en suivant les approches statique ou dynamique respectivement.

La capacité de REMO à simuler le climat actuel dans les HEBB a été évaluée et les variables climatiques et hydrologiques pour la période historique ($1981-2005$) et les deux périodes futures ($2041-2065$ et $2071-2095$) ont été comparées pour évaluer l'impact potentiel du CC sur les ressources en eau et le potentiel hydroélectrique au milieu et à la fin du XXIe siècle selon trois scénarii d'émission

des gaz à effet de serre (GES) RCP2.6, 4.5 et 8.5. Nos résultats montrent que a) REMO reproduit bien le cycle annuel des précipitations, de la température à 2 m d'altitude et de l'ETP, bien que certains biais relativement faibles existent; b) les précipitations annuelles diminueront de 1 à 10% alors que la température annuelle et l'ETP augmenteront respectivement de $8-18\%$ et $6-30\%$, selon les scénarii, les modèles et les périodes futures ; c) la réduction des précipitations combinée à l'augmentation de l'ETP entraîneront une diminution importante des débits dans les HEBB (jusqu'à 51%), ayant comme conséquence directe une réduction du potentiel hydroélectrique du barrage Lagdo. Cette région connaîtra des conditions environnementales extrêmement sèches en raison d'une augmentation de l'ETP supérieure à l'augmentation de l'ET réelle.

Mots clés: Changements climatiques, Ressources en eau, Potentiel hydroélectrique, Modèle hydrologique HBV-Light, modèle climatique régional REMO

General introduction

Freshwater, known as earth's fundamental natural resource, has various functions and is needed in all aspects of life. Freshwater serves as drinking water for humans and animals, is needed for sanitation issues and is vital to ecology, agriculture, economy, hydropower production and transport. In sub-Saharan Africa continent, water is recognized as the most important impediment for socio-economic development because more than 70% of the population practices rain-fed agriculture, which occupies about 95% of the land use (Tarhule et al., 2009). Good crop development depends on precipitation to maintain the needed level of soil water reserve. It is not the only activity dependent on water resources: hydro-electricity production represents more than 80 to 90% of electricity in this region (Magrin, 2007).

However, the last two decades have witnessed increasing pressure on the available African water resources due to increased trend in population growth as well as land use and climate change, which also triggered the prospect of water crisis in Africa. The water crisis of Cape-Town in 2018, the decrease of water level of the Ubangui River in the Congo basin with implication on economic navigation, and the shrinking of the Lake Tchad are just some of the few cases that we could mention, and that reveal the urgent need of sustainable water resources management in the African continent. In addition, West and Central Africa (WCA) are identified by the United Nations as one of the nine climate change "hot spots" due to decrease on rainfall (Nicholson et al., 2000; Mahé and Paturel, 2009) which has broadly brought a depletion of water resources (Abrate et al., 2013), whereas populations' water demands grow increasingly (FAOSTAT, 2012). It is also clear that developing regions, such as WCA, are the most vulnerable region under global warming because of their poor adaptive capabilities occasioned by lack of technical knowhow and poverty (Callaway, 2004; Solomon et al., 2007). The United Nations Framework Convention on Climate Change (UNFCCC, 2007) further observed that regions of the world that are least culpable for climate change are the most susceptible to the projected climate change impacts. For instance, whereas the African region contributes less to global warming because of the general low level of industrialization, warming is likely to be larger than the global annual average over the continent (Christensen et al., 2007). Moreover, there is a clear consensus amongst climate models on the increased warming over Central Africa (CA) towards 2100 (Mkankam, 2001; Haensler et al., 2013; Fotso-Nguemo et al., 2016; Mba et al., 2018). On the other

hand, while there is no agreement amongst models as regards the direction of the future evolution of precipitation, there is evidence that precipitation will change over CA towards 2100 (Fotso-Nguemo et al., 2016; Sonkoué et al., 2018; Tamoffo et al., 2018; Mba et al., 2018).

As key components of the hydrological cycle, any change in climate that affect rainfall and temperature will have proportionate impacts on the hydrological system in the area especially at the basin scale. According to Pal and Al-Tabbaa (2011), any change in the hydrological cycle due to global warming is likely to affect the distribution of water resources and consequently agriculture and hydropower production in the region as well as the availability and quality of freshwater. The Fifth Assessment Report (AR5) of the Intergovernmental Panel on Climate Change (IPCC, 2013) also argued that the risk of water disasters, such as flood, drought and water shortage, will be exacerbated due to climate change. Many authors also believe that the discharge and water quality are strongly controlled by the rainy event (Khan et al., 2016; Sakho et al., 2017).

Cameroon is one of the countries blessed with abundant water resources, both surface and groundwater. It contributes significantly to the economy of Central Africa (CA), its water resources being a major source of this importance. Cameroon is the second country in Africa (after the Democratic Republic of Congo) in terms of quantity of available water resources and hydropower potential (Mafany et al., 2006). It has a dense network of rivers most of which arise from the Adamawa Plateau of the country and flow north and southwards. There are five main river basins in Cameroon: Lake Chad, Niger, Sanaga, Congo and Coastal Rivers Basins, three of them (Lake Chad, Niger and Congo Basins) are shared with neighboring countries. Cameroon is ranked 49^{th} out of 182 countries in the world in terms of abundant water supply (Rosen, 2000). However, due to variations in the topography, rainfall pattern and climatic zones in Cameroon, these water resources are unequally distributed between the northern and southern parts. The southern part (up to 6°N) experiences a wet sub-tropical climate with annual precipitation ranging between 1500 and 4000 mm. In the northern part, the climate is semi-arid to arid Sahelian with annual rainfall less than 400 mm in the northernmost (13°N) part (Kamga 2001) and where many rivers dry up a few months after the rainy season. The Niger River Basin (NRB) is a only perennial river in Northern Cameroon and holds huge water resource potential.

The Niger River Basin (NRB), home to approximately 100 million people, a third longest river (4,200 Km) in Africa, is a vital, and complex asset for WCA. It is a trans-boundary river basin which traverses nine countries (Benin, Burkina Faso, Cameroon, Chad, Ivory Coast, Guinea, Mali, Niger, and Nigeria) of WCA. The NRB basin represents a great socio-economic importance in these areas because their main socio-economic activities depend on their available water resources (Ogilvie et al., 2010). For example, agricultural production including fishing which employs over 60% of the people of the area relies on irrigation water supply from the basin. In addition, the NRB is the main source of water supply for industrial and municipal use for the people through the construction of reservoirs

at several points. Furthermore, a greater percentage of electricity supply in some of the countries in the basin is through hydropower generation made possible by the dams constructed along the river valleys at different points. As at the last count, over 260 dams of different sizes were said to have been constructed in the basin to achieve the aforementioned purposes (Lienou, 2013). The river also provides opportunities for transportation across and within the countries especially during the period of high flows. However, despite his importance, recent reports have shown that the basin is drying out and experiencing low flow especially within the Cameroonian catchment due to climate change and poor management (Lienou, 2013; Dassou, 2019).

The headwaters of the Benue River Basin (HBRB), the main interest of this study, is the Cameroonian part of the NRB and occupies 4.4% (66,000 km^2) of the overall basin . It's the second-largest river in Cameroon and a major tributary for the NRB (Oguntunde and Abiodun, 2013). It is a perennial river in Northern Cameroon where many rivers dry up a few months after the rainy season. The HBRB holds huge water resources potential including hydropower, irrigation, and navigation due to the construction of the Lagdo dam and its hydro power plant in 1982. The population of this region practices rain-fed agriculture which is the main socio-economic activity of this region. Until the recent improvement of the surface transportation system in Nigeria, the River Benue served as a major navigation route from Lokoja to Garoua in the Cameroons during wet months; during recent decades, along the river from the Nigerian-Cameroon border, several settlements and socio-economic activities have emerged (Toro, 1997). Given also his great importance of water resources functions, current projects include industrial plantations of irrigated rice, sugar cane, cotton and vegetable, alongside the more traditional sorghum, maize and millet have been developed. The Lagdo dam is also known at present as the main hydroelectricity plant in this region and neighboring areas. The entire northern part of Cameroon is currently supplied with electricity from Lagdo, but, because of a low development level of the region, only one third of the installed production capacity of 300 GWh/year is exploited. It is planned to supply the Chad Republic in the near future and both northern Nigeria and part of the Central African Republic in 5–10 years (Mkankam, 2001). In this context, in 2007, the World Bank approved the second phase of the project known as "Niger Basin Water Resources Development and Sustainable Ecosystems Management Project" with aims to increase hydropower and irrigation capacity of the Lagdo dam (IRAP, 2015). In addition, Donfack et al. (2018) showed that in irrigated agriculture, maize yield increases significantly in the dry season, which can equal that of the rainy season in northern Cameroon.

However, northern Cameroon experiences water-related disasters such as floods (Sighomnou et al., 2013) and droughts (Molua and Lambi, 2006; Gao et al., 2011). Additionally, water shortages in northern Cameroon are also the result of population growth, which naturally increases the water demand, poor water resources management (WRM), and changing environmental conditions (Cheo

et al., 2013). Guenang and Mkankam (2014) found that the drought magnitude and duration increased with time for both short and long time scales in the North of Cameroon, as a response of a reduction in precipitation due to climate change. Arétouyap et al. (2014) showed an increase of temperature, decrease of annual precipitation and standardized precipitation index (SPI) in the Northern Cameroon during 1960-2010, with some visible consequences such as wetlands draining, wells dryness, rise of static and piezometric levels in boreholes drilled. Dassou et al. (2016) also found the negative trends of precipitation in the Northern Cameroon during the time period 1950-2013, while Oguntunde et al. (2018) shown an increase in drought intensity and frequency over the NRB as a result of statistically significant correlation between runoff and drought indices. Nonki et al. (2019) also found that the HBRB will move to an extreme environmental drier conditions due to a decrease in excess water and increase in evaporative demand under changing environmental conditions. Therefore, proper planning of water resources in space and time under CC becomes a great priority to propose the precise solutions in the water resources management (WRM) and development projects in a country. It is also important and urgent to build the tools that can help the decision-makers and water planners to better manage the water resources (planning, design, operation, and management of water resources systems). However, managing water resources in the large river basins of Africa involves problems of data paucity, lack of technical resources and the sheer scale of the problem. These river basins are located in regions that are characterized by poverty, low levels of economic development and little food security.

Nowadays, hydrological models are important and powerful tools for addressing the challenge of present and future water management in the watershed (basin-scale level). The hydrological models are increasingly used to investigate water resources management scenarios, predict the impact of extreme events such as floods and drought, describe nonlinear hydrological process and to analyze the impact of future potential changes in climate and land use on water resources (Mkankam, 2001; Tshimanga and Hughes, 2012, 2014; Hakala et al., 2019). However, the study of the hydrological impacts caused by climate change has been widely applied on the regional scale using GCM simulations (Mkankam, 2001). According to Chou et al. (2014), CC impact assessment at the regional scale needs higher resolution spatial data. As impacts and vulnerabilities of a given region are linked to regional and local forcings, GCMs with a coarse horizontal grid resolution do not capture these local and regional effects Deb et al. (2015). It is therefore important to downscale the input variables for a hydrological model to the spatial and temporal scales that resolve the local climate features and are needed by the hydrological model. In this context, the Coordinated Regional Climate Downscaling EXperiment project (CORDEX; Giorgi et al. (2009); http://www.cordex.org), sponsored by the World Climate Research Program (WCRP; http://www.wcrp-climate.org/) has produced many downscaled climate data for Africa derived from several regional climate models (RCMs) that have downscaled many GCMs. The data derive from a set of dynamically downscaled models, forced by

GCMs from phase 5 of the Coupled Model Intercomparison Project (CMIP5).

Although downscaled climate data has been used to drive hydrological models in Africa catchments (e.g. Blanco, 2011; Cherie, 2013; Tramblay et al., 2013; Li et al., 2015; Oloruntade, 2017), to date, no study has assessed the impact of CC on water resources over this important watershed by using downscaled precipitation and temperature data. Existing studies were based on GCM data (Mkankam, 2001; Sighomnou, 2004). In this context, the main focus of this research is to assess the impacts of climate change on water resources and hydropower potential in the HBRB, Northern Cameroon through the hydrological modeling and downscaled data. This research will help towards the development of early warning systems and risk assessment in the HBRB so as to develop capabilities to mitigate the effects of climate uncertainty. It will also help to develop the new vision of water management, long term strategy for electricity production and planning of water needs. This study will be accomplished by addressing the following objectives:

1. Building a tool that can help decision-makers and water planners to better manage the water resources (planning, design, operation and management of water resources systems), through the calibration, validation, sensitivity and parameter uncertainty analysis and parameter optimization of the hydrological model.

2. Proposing a comprehensive study for sensitivity analysis of hydrological simulations for model input especially the potential evapotranspiration (PET) input, through the comparison between the dynamic and static approaches for sensitivity analysis.

3. Analyzing the potential impacts of climate change on water resources and hydro power potential in the HBRB by driving calibrated hydrological model with downscaled scenarios climate data (precipitation, temperature and PET).

4. Analyzing the ecohydrological status of the watershed using the concept of water-energy budget.

This thesis comprises three chapters, the first chapter covers the literature review, which discusses the earth climate system, climate change, the Representative Concentration Pathway (RCP) and climate models. It also contains methods of downscaling and the concept of hydrological modeling. Chapter two includes geographical localization of the study area, his topography, climate and hydrology. It further describes the data used, the statistical tools employed, the theoretical concepts of the hydrological model, HBV-Light and the general modeling procedure and chapter three presents the obtained results and their discussions. This thesis ended with a general conclusion, which includes the main findings of this research and forthcoming work.

Chapter 1

Literature review

Introduction

Climate is traditionally defined as the description in terms of the mean and variability of relevant atmospheric variables such as temperature, precipitation, wind etc. Nowadays, there is a clear consensus that climate is changing then goes affect the climate system and hydrological cycle. Given the fact that it is too difficult to look back to the recent past to get an idea of what can happen later in the Earth's natural systems, scientific communities usually used the climate and hydrological models to better understand the future climate and their impacts in order to develop adaptive strategies, plan and better manage the natural resources such as water resources. This chapter provides in the first part the description of the climate system, their main components and the main drivers of his change. In the second part, a brief description of mathematical formulation of the climate models, as well as the different techniques generally used to downscale these models from global scale to regional or local scale are provided. In the third part, an overview of the hydrology and hydrological modeling science is mentioned, while the last part focuses on the review of different impact studies done in the NRB and especially in Cameroon.

1.1 Climate and climate change

1.1.1 Climate system

The climate system is a complex, interactive system consisting of the atmosphere (the gaseous envelope surrounding the Earth), the hydrosphere (liquid water, i.e. ocean, lakes, underground water, etc), the cryosphere (solid water, i.e. sea ice, lake ice and river-ice, snow cover, glaciers, ice caps and ice sheets, and frozen ground), the land surface and the biosphere (all the living organisms) (IPCC, 2007, Fig. 1).

However, the climate system evolves in time under the influence of its own internal dynamics and

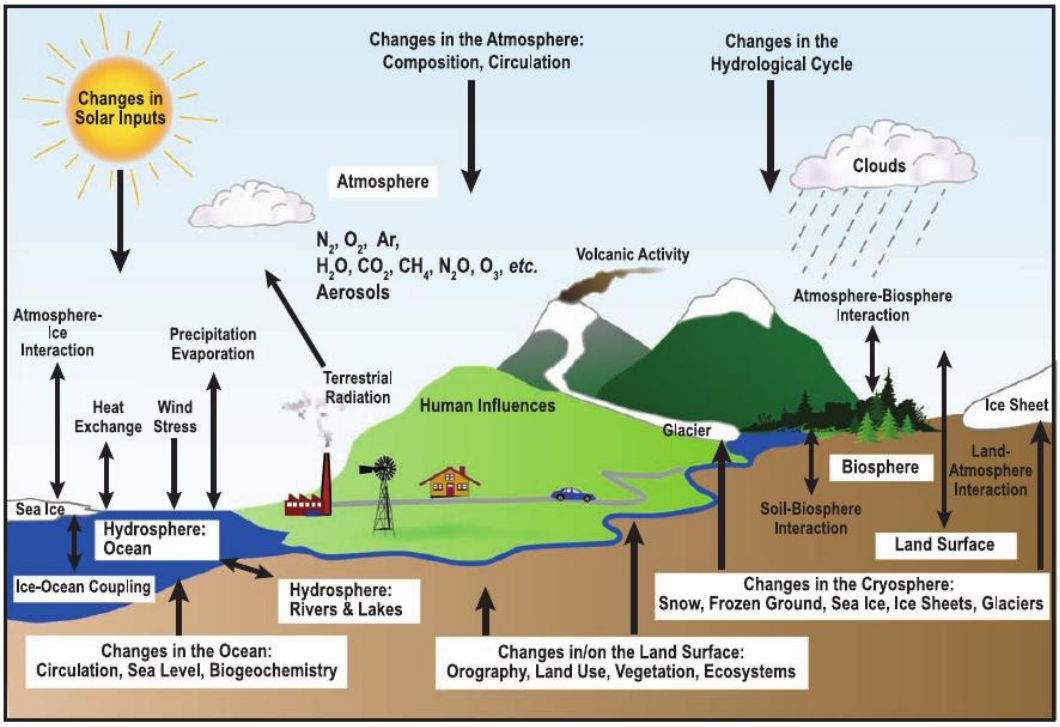

Figure 1: *Schematic view of the components of the climate system, their processes and interactions (IPCC, 2007).*

due to changes in external factors (called "forcing mechanisms"). External factors include natural phenomena such as volcanic eruptions and solar variations, as well as human induced factors, like the burning of fossil fuels and the depletion of the natural vegetation, both of which lead to changes in the atmospheric composition. Over the longest timescales, the amount of incoming solar radiation on the Earth's atmosphere and surface is in balance with the amount of outgoing radiation, whereby the latter is composed of short- and long-wave components. About half of the incoming solar radiation is absorbed by the Earth's surface. This energy is transferred in form of long-wave radiation back to the atmosphere whereby it is warming the air in contact with the surface (sensitivity heat), by evaporated water (latent heat) or is absorbed by clouds and greenhouse gases (GHGs). The atmosphere in turn radiates long wave energy back to Earth as well as out to space (Kiehl and Trenberth, 1997).

1.1.2 Climate change

According to IPCC, climate change is defined as a change in the state of the climate that can be identified by changes in the mean and /or the variability of its properties that persists for an extended period typically decades or longer (IPCC, 2007). Nowadays, there is evidence that the global climate is already changing and that further change is certain. For instance, during the last century (between 1906 and 2005), the average global temperature rose by about $0.74°C$ in two phases from 1910s and 1940s and more strongly from 1970s to the present (IPCC, 2007). In addition, as pointed out in the IPCC-report, there is now enough observational evidence of an increase of global average sea levels, while Northern hemisphere snow cover and ice amounts have also reduced (Fig. 2). As for the future

development of the earth's temperature, the IPCC (2007) states that the global average warming will be $1.1 - 6.4°C$ by 2090-2100.

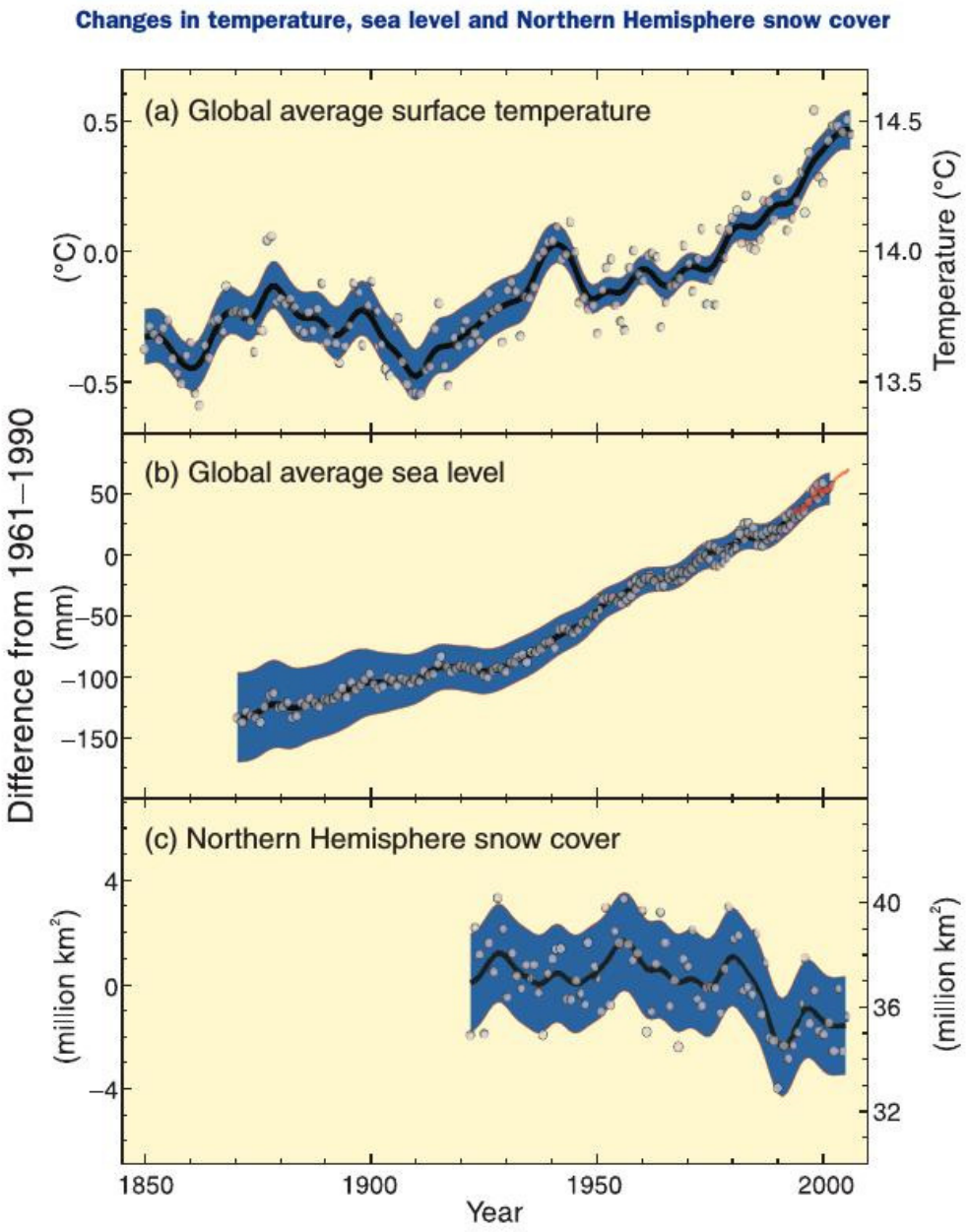

Figure 2: *Observed changes in (a) global average surface temperature; (b) global average sea level from tide gauge (blue) and satellite (red) data and (c) Northern Hemisphere snow cover for March-April. (IPCC, 2007)*

The most plausible cause of the global temperature change in the last 50 years and that to be expected for the near future is believed to be the presence of GHGs (Solomon et al., 2007), which act as a partial blanket for the long wave radiation emanated back from the Earth's surface. The most important GHG are carbon dioxide (CO_2), methane (CH_4), nitrous oxide (N_2O), Ozone (O_3), hydroflurocarbons ($HFCS$), Perfluorocarbons ($PFCs$) and sulphur hexafluoride (SF_6) and are the gases whose emissions are covered by the UNFCCC. They influence the absorption, scattering and

emission of radiation within the atmosphere and at the Earth's surface.

1.1.3 Drivers of climate change

Drivers of climate change are natural and man-made substances and processes that alter the Earth's energy budget (IPCC, 2013). They are also defined as the elements that contribute to GHG emissions, directly or indirectly (Blanco et al., 2014). Although interactions amongst the various constituents of the earth's climate system can lead to climate change, studies have shown that changes in climate that have been witnessed since 1950s are attributable to human activities (IPCC, 2001) and it is a lack of consensus according to literature about climate change drivers. Some researchers have distinguished between near and underlying or ultimate drivers (e.g. Angel et al., 1998; Geist and Lambin, 2002), in which near drivers are described as activities that are directly or closely related to the generation of GHGs and underlying or ultimate drivers are the ones that motivate the proximate drivers.

Given the difficulty to objectively define what the drivers can always be, there is not yet a unique method to identify the drivers of climate change, mainly because anthropogenic activities manifest themselves through a complicated network of interactions, and separating a clear cause-and-effect for a certain phenomenon purely through the lens of scientific observation is often difficult. Hence, the term 'driver' may not denote an actual causality but is used to signify a relationship to provide insights on what constitutes general changes in global GHG emissions (Blanco et al., 2014). Thus, within the literature, the major drivers of GHG emissions are consumption (Hertwich and Peters, 2009), international trade (Jakob et al., 2013), population growth (O'Neill et al., 2010), economic growth (Carson, 2009; Lim et al., 2009), structural change to a service economy (Nansai et al., 2009) and energy consumption (Malla, 2009). They have been so recognized because of their potential to contribute to increased GHG emissions within the global environment.

Nevertheless, IPCC (2007) often evaluates the influence of a driver of climate change, in terms of its radiative forcing (RF) and expressed in units of 'Watts per square meter'. RF is a measure of how the energy balance of the Earth-atmosphere system is influenced when drivers that affect climate are altered. RF is the change in energy rate per unit area of the globe caused by a driver, and is calculated at the top of the atmosphere. RF can be positive or negative, which means the energy of the Earth-Atmosphere system increases or decreases respectively and leads to a warming or to a cooling of the climate system (Fig. 3).

1.1.4 Emission scenarios

The impacts of climate change on the environment and society will depend not only on the response of the Earth system but also on how humankind responds through changes in technology, economy,

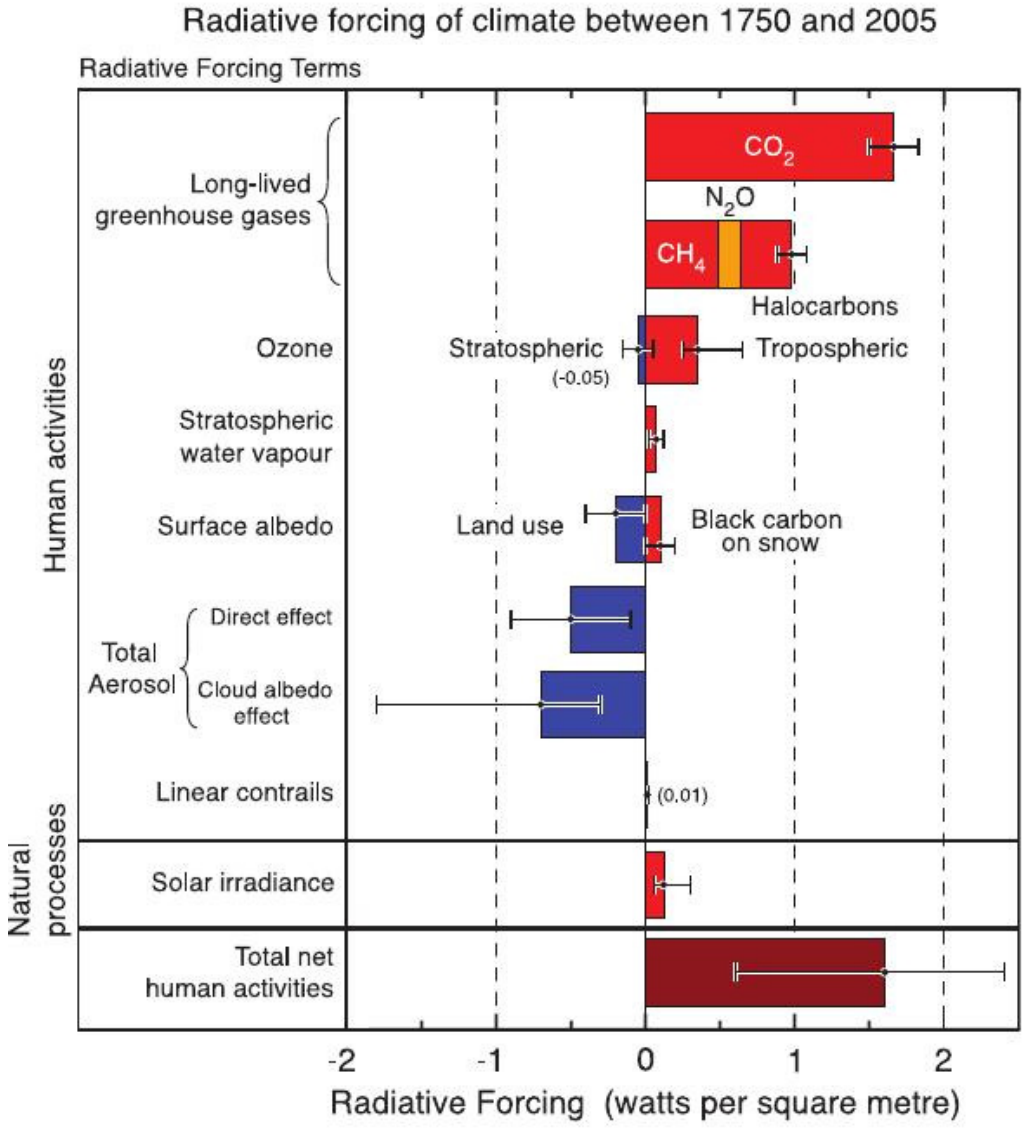

Figure 3: *Summary of the principal components of the radiative forcing of climate change. All these radiative forcings result from one or more factors that affect climate and are associated with human activities or natural processes as discussed in the text. The values represent the forcings in 2005 relative to the start of the industrial era (about 1750) (IPCC, 2007)*

lifestyle and policy. These responses are uncertain, so future scenarios are used to explore the consequences of different options. In climate change research, emissions scenarios describe plausible trajectories of different aspects of the future that are constructed to investigate the potential consequences of anthropogenic climate change. Scenarios represent many of the major driving forces - including processes, impacts (physical, ecological and socioeconomic), and potential responses that are important for informing climate change policy. They are used to hand off information from different research areas (e.g., from research on energy systems and greenhouse gas emissions to climate modeling). They are also used to explore the implications of climate change for decision making (e.g., exploring whether plans to develop water management infrastructure are robust to a range of uncertain future climate conditions). The goal of working with scenarios is not to predict the future but

to better understand uncertainties and alternative futures, in order to consider how robust different decisions or options may be under a wide range of possible futures". IPCC (2007) stated that one of the major reasons for developing emissions scenarios is to enhance coordinated studies of climate change, climate impacts, and mitigation options and strategies. They were also developed for better comparisons between various studies as well as easier communication of model results.

In order to address these issues, the IPCC published in 1992 the first set of climate change scenarios, called Integrated Science (IS92). Based on the number of inconsistencies and assumptions included in IS92 scenarios that are considered limited in the face of current uncertainty as to how the world will develop over the next century, a new set of emission scenarios called "Special Report on Emission Scenarios" (SRES) were approved for use by the IPCC in 2000 (Nakicenovic et al., 2000) and used in the Third and Fourth assessment reports of the IPCC. In This SRES, 40 SRES scenarios have been developed by six modeling teams and grouped into four qualitative storylines (include in Fig. 4) called "families" : A1, A2, B1, and B2.

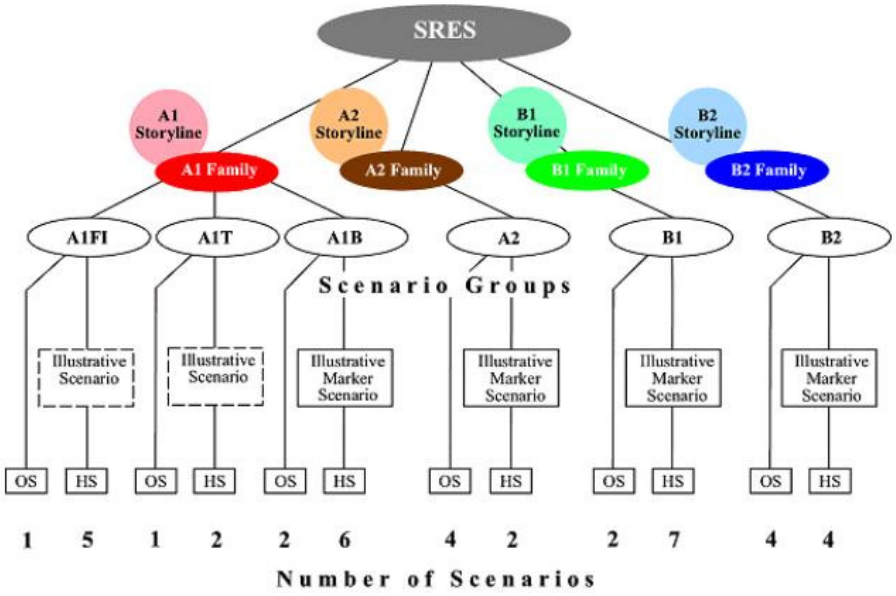

Figure 4: *Schematic illustration of SRES family storylines (Nakicenovic et al., 2000)*

Each storyline represents different demographic, social, economic, technological and environmental developments, which is described in Table 1.

One problem with the SRES scenarios indeed, a fair criticism of them is that they do not explicitly incorporate carbon emissions controls. While some of the scenarios involve storylines that embrace generic notions of sustainability and environmental protection, the scenarios do not envision explicit attempts to stabilize concentrations at any particular level. In the Fifth Assessment Report (AR5) of the IPCC, a new set of scenarios, called Representative Concentration Pathways (RCPs), has been introduced (IPCC, 2013).

Table 1: *Overview description of SRES storylines (Source: Nakicenovic et al., 2000).*

	A1 Storyline	**A2 Storyline**	**B1 Storyline**	**B2 Storyline**
World	Market-oriented	Heterogeneous	Convergent	Local solutions
Economy	faster per capita growth	Regionally oriented and lowest per capita growth	Service and information based; lower growth than A1	Intermediate economy development
Population	peaks in 2050, then decline	continuously increasing	same as A1	Moderate growth
Governance	strong regional interaction; income convergence	Self-reliance and preservation of local identities	Global solution to economic, social and environmental sustainability	Local and regional solutions to environmental and social equity
Technology	rapid introduction of new and more efficient technologies	Slowest and more fragmented development	Clean and resource efficient technology	less rapid and more diversified than in A1/B1

1.1.5 The Representative Concentration Pathway (RCP)

RCPs introduced in the IPCC AR5 and used in this research, are prescribed pathways for greenhouse gas and aerosol concentrations, together with land use change, that are consistent with a set of broad climate outcomes used by the climate modelling community. These pathways are characterized by the radiative forcing produced by the end of the 21st century. RCP scenarios are described to be "representative" because each of them represents a larger set of scenarios in the literature and are referred to as "pathways" in order to emphasize that their primary purpose is to provide internally consistent sets and time-dependent projections of atmospheric GHG concentrations (van Vuuren et al., 2011; IPCC, 2013). The RCPs are the product of an innovative collaboration between integrated assessment modelers, climate modelers, ecosystem modelers as well as social scientists working on emissions, economics, policy, vulnerability and impacts. The four RCPs are named according to radiative forcing target level in year 2100 relative to the pre-industrial year (1750) – RCP2.6 for 2.6 $W.m^{-2}$, RCP4.5 for 4.5 $W.m^{-2}$, RCP6.0 for 6.0 $W.m^{-2}$ and RCP8.5 for 8.5 $W.m^{-2}$. They include one mitigation scenario leading to a very low forcing level (RCP2.6), two medium stabilization scenarios (RCP4.5 and RCP6) and one very high baseline emission scenario (RCP8.5). Table 2 gives the overview description of each RCP, reference and model used to develop it.

The comparison between RCPs and SRES (Fig.5) scenarios reveals that the RCP8.5 is closest to A1FI, RCP6 is closest to A1B, RCP4.5 is similar to B1, and RCP2.6 is lower than any of the standard SRES scenarios.

Table 2: *Overview description of RCP scenarios (adopted from Moss et al., 2010)*

Name	**Radiative forcing**	**Atmospherics CO_2 equivalent (parts per million)**	**Pathway**	Model providing RCP*	Reference
RCP 8.5	>8,5 W.m^{-2} in 2100	>1370 equiv.- CO_2 in 2100	Rising	MESSAGE	Riahi et al., 2011
RCP 6.0	~6 W.m^{-2} at the stabilization level after 2100	~850 equiv.- CO_2 at the stabilization level after 2100	Stabilization without overshoot	IAM	Hijioka et al., 2008
RCP 4.5	~4,5 W.m^{-2} at the stabilization level after 2100	~660 equiv.- CO_2 at the stabilization level after 2100	Stabilization without overshoot	GCAM	Thomson et al., 2011
RCP 2.6	Peak at ~3 W.m^{-2} before 2100, declining to ~2.6 W.m^{-2} by 2100	Peak at ~490 equiv.- CO_2 before 2100 then decline	Peak and decline	IMAGE	van Vuuren et al., 2011

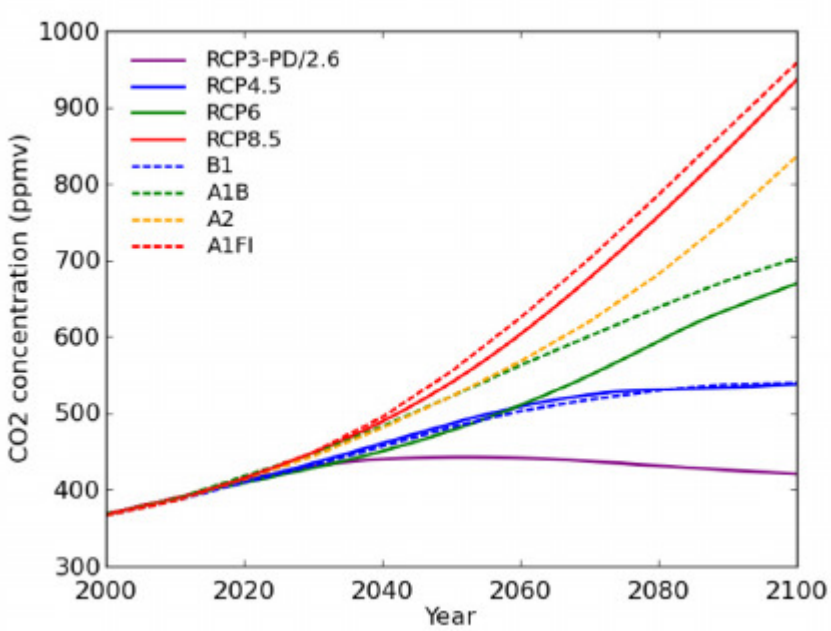

Figure 5: *Comparison of carbon dioxide concentrations for the 21st century from the RCPs and SRES scenarios (Source: Jubb et al., 2013).*

1.2 Climate models

Understanding past, present and future climate helps us to understand how Earth's systems naturally function. Since it is then impossible to look back to the recent past to get an idea of what can happen later, the only tools available to the scientific community to try to find out what can happen in the future are climate models, particularly global climate models (GCMs). Effects of the increases in atmospheric greenhouse gas concentrations on climate are also studied with climate model simulations. Climate models are a simplified and numerical representation of the climate system, its components and their interactions described through mathematical formulations of physical, biological and chemical principles (Fig. 6). Some on these fundamental conservation laws are namely: the first law of

thermodynamics (describing the movement of energy, Eq. 1.1), Newton's second law of motion (it's about momentum of a particle, Eq. 1.2), three continuity equations (the conservation of mass, Eq. 1.3) and the ideal gas law (for the water vapor, Eq. 1.4) (Fotso-Nguemo, 2018).

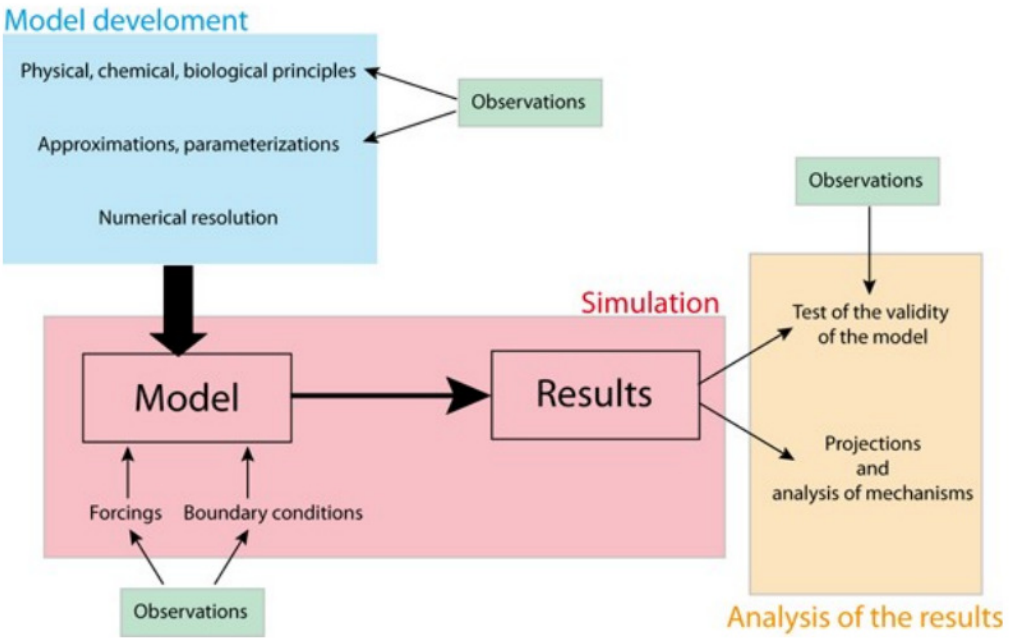

Figure 6: *Schematic representation of the development and use of a climate model (Source: Goosse et al., 2010)*

$$C_p\left(\frac{\partial T}{\partial t}+\overrightarrow{V}.\overrightarrow{\nabla}T\right)=\frac{1}{\rho_a}\frac{dp}{dt}+Q \tag{1.1}$$

$$\frac{\partial\overrightarrow{V}}{\partial t}+\overrightarrow{V}.\overrightarrow{\nabla}\overrightarrow{V}=-\frac{\overrightarrow{\nabla}p}{\rho_a}-2\overrightarrow{\Omega}\times\overrightarrow{V}+\overrightarrow{g}+\overrightarrow{F} \tag{1.2}$$

$$\frac{\partial\rho_a}{\partial t}+\overrightarrow{V}.\overrightarrow{\nabla}\rho_a=-\rho_a\overrightarrow{\nabla}.\overrightarrow{V} \tag{1.3}$$

$$p=\rho_a RT \tag{1.4}$$

In these equations,

C_p is a specific heat at constant pressure;

T is the air temperature;

$\overrightarrow{V}=u\overrightarrow{i}+v\overrightarrow{j}+w\overrightarrow{k}$ is the wind speed, with (u,v) his horizontal component (zonal and meridional respectively) and w his vertical component;

Q represents the sources and wells of internal heat from the sub-mesh processes;

p is the pressure;

ρ_a is the density of the air mass;

$\overrightarrow{\Omega}$ is the Earth's rotational speed;

$\overrightarrow{g}$ is the gravity containing the term of the centrifugal force then slightly deviating the direction of the gravity vector from the vertical;
$\overrightarrow{F} = F_x \overrightarrow{i} + F_y \overrightarrow{j} + F_z \overrightarrow{k}$ describes the sources and wells of the moment at scales smaller than the grid (friction force);
R is the specific gas constant.

The terms $-\frac{\overrightarrow{\nabla} p}{\rho_a}$, $-2\overrightarrow{\Omega} \times \overrightarrow{V}$, $C_p \left(\frac{\partial T}{\partial t} + \overrightarrow{V}.\overrightarrow{\nabla} T\right)$, $\frac{1}{\rho_a}\frac{dp}{dt}$ and $-\rho_a \overrightarrow{\nabla}.\overrightarrow{V}$ correspond respectively to the force of the pressure gradient that is directed towards the low pressures, the Coriolis force that acts on a moving particle, the internal energy of the system under consideration, the work and the term of compressibility. And the terms $\overrightarrow{V}.\overrightarrow{\nabla}\overrightarrow{V}$, $\overrightarrow{V}.\overrightarrow{\nabla} T$ and $\overrightarrow{V}.\overrightarrow{\nabla}\rho_a$ are the advection terms, introducing the non-linearity of the system. Indeed, non-linearity causes the sensitivity of the results to initial conditions and limits the predictability of the climate.

Given the complexity of these equations, they are usually solved numerically. Consequently, climate models provide a solution which is discrete in space and time, meaning that the results obtained represent averages over regions, whose size depends on model resolution and for specific times. Climate models used in climate research range from simple energy balance models to complex Earth System Models (ESMs) requiring state of the art high-performance computing. Nowadays, ESMs are the current state-of-the-art models, and they expand on Atmosphere Ocean General Circulation Models (AOGCMs) to include representation of various biogeochemical cycles such as those involved in the carbon cycle, the sulphur cycle, or ozone (Flato, 2011). These models provide the most comprehensive tools available for simulating past and future response of the climate system to external forcing, in which biogeochemical feedbacks play an important role.

1.2.1 Uncertainties in Global Circulation Models (GCMs)

GCMs integrate known atmospheric physical processes, such as the heating effect of the sun, the heat and moisture fluxes from oceans, the effect of land surface and vegetation, and the effect of GHGs on the atmospheric temperature profile, in an attempt to simulate the global climate system through time (Hewitson and Crane, 2006). Such processes are complex to integrate due to the scales at which they occur, and can only be resolved through parameterization of climate models, which leads to uncertainties in the outputs. Major sources of uncertainty in GCMs arise from the way they are parameterized to represent variables of the global climate system, the internal structures of the GCMs and the methods used to downscale the GCMs to allow projections at basin scales. This means that different GCMs will yield different output variables, especially in the prediction of precipitation changes (Haylock et al., 2006), depending on their skill to simulate the climate of a given region. Hence, it may be difficult to draw conclusions from a single model output. Given this situation, some recommended approaches to minimize uncertainties and to gain more confidence in the projection

of climate change are the inclusion of many different types of global models, downscaling techniques and emission scenarios as possible (Gachon and Dibike, 2007; Busuioc et al., 2006).

1.2.2 GCM Downscaling

Despite their advances and improvements in the modeling and their performance to reproduce the features of the global climate system (Flato et al., 2014), GCMs provide weather data at global scale and low resolution (currently about 200 km x 200 km) which are unable to resolve some important processes related to sub-grid scale clouds and topographic effects that are of significance in many impact studies (Fowler et al., 2007; Cherie, 2013). Therefore, it is important to downscale the GCMs data to the spatial and temporal scales that resolve the local climate features and are needed by the hydrological model. Thus, downscaling is the process of deriving finer resolution data (e.g. for a particular site) from coarser resolution GCM data. Figure 7 presents a visual representation of the concept of downscaling. Generally, there are two main approaches for downscaling: dynamical downscaling and statistical downscaling.

1.2.2.1 Dynamical Downscaling

Dynamical downscaling (DD) involves the use of an Limited Area Models (LAMs) or high resolution Regional Climate Models (RCMs) driven by the time-varying atmospheric lateral and data of GCMs as boundary conditions to simulate regional or local climate (Wilby et al., 2002). This approach is advantageous when supplied with appropriate sea surface and atmospheric boundary conditions. When used for downscaling, RCMs require, as inputs, specifications of the following parameters (Cherie, 2013):

- the initial state of the atmosphere and surface,
- time variations of any external forcing agents,
- the time-varying lateral fluxes of heat, mass, moisture, momentum and forcing agents (such as aerosols) derived from a global AOGCM or reanalysis,
- time variations of all surface variables that are not produced prognostically by RCM.

Downscaling using high-resolution global AOGCMs requires all of the above inputs, except for lateral fluxes.

1.2.2.2 Statistical Downscaling

The principle of statistical downscaling (SD) is based on the establishment of relationships between variables observed at the local scale (often at the climate station scale) called [predictands] and

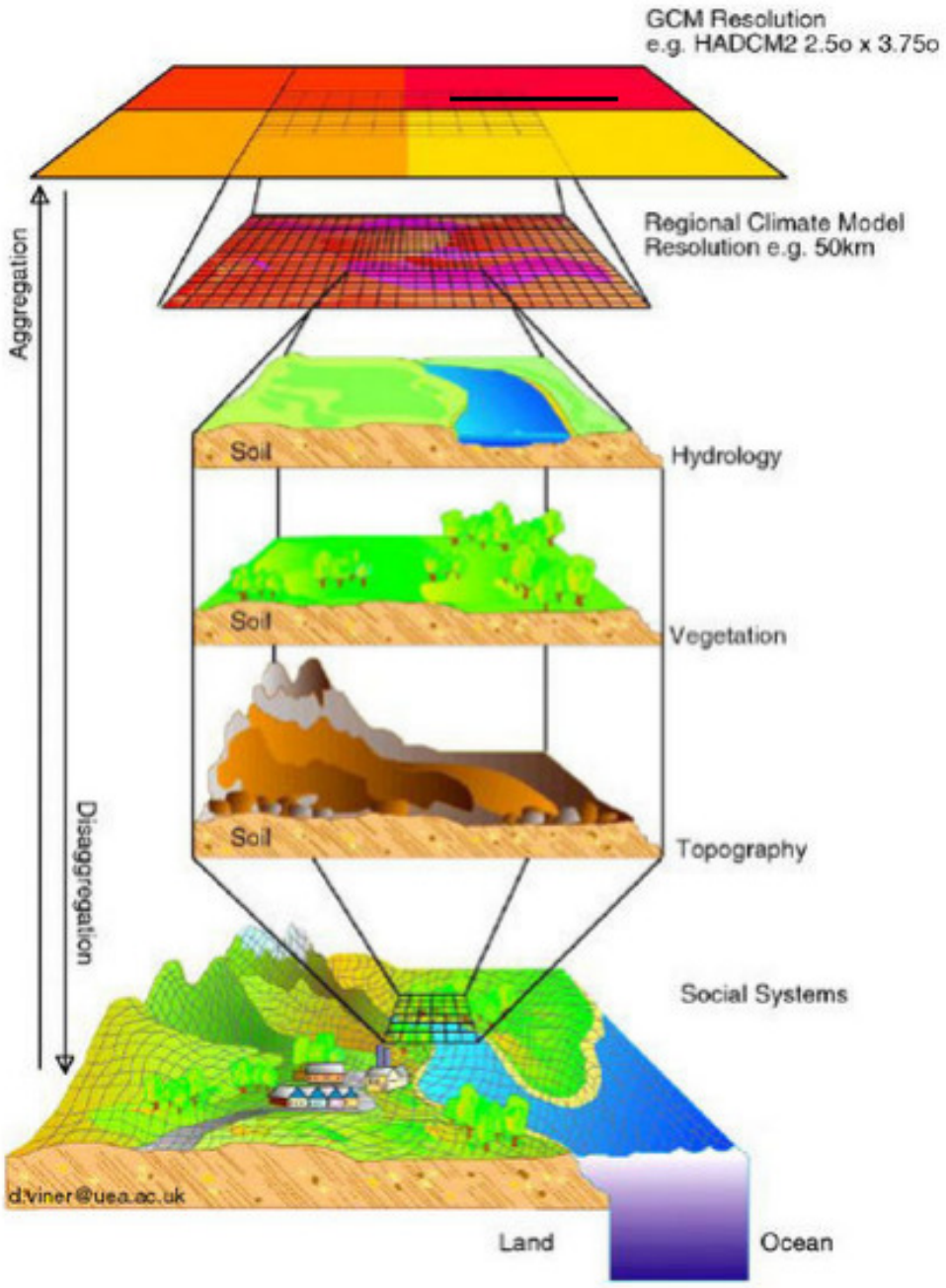

Figure 7: *Conceptual representation of downscaling (Source: Viner, 2000)*

variables characteristic of large-scale GCMs called [predictors]. SD allows the generation of long time series of variables from observational data and GCMs. SD uses several methods to develop the empirical predictand-predictor relationships, among which we can mention:

- **Linear methods** such as Delta method, simple and multiple linear regression method (Matulla et al., 2002), Canonical Correlation Analysis (CCA, von Storch et al., 1993) and Singular Value Decomposition (SVD) methods (Olsson et al., 2001). They have the merits to be relatively straightforward to apply, employ full range of available predictor variables. The greatest constraint is the requirement of a normal distribution of the predictor and the predictand values, which means that it cannot be used to predict the distribution of daily rainfall because it is

typically non-normal (frequent small amounts of rainfall and a few heavy events generally make the distribution not symmetrical).

- **Weather classifications** such as analog method, cluster analysis, Artificial Neural Network (ANN), Self-Organizing Map (SOM). These methods are particularly well suited for downscaling non-normal distributions, such as daily rainfall. However, a large amount of observational daily data (e.g., 30 years of daily data for the region of interest) is required in order to evaluate all possible weather conditions. In addition, these methods are more computationally demanding in comparison to linear ones, due to the large amount of daily data analyzed and generated.

- **Weather generators** such as Long Ashton Research Station Weather Generator (LARS-WG), Non-homogeneous Hidden Markov Model (NHMM). These methods are able to simulate length of wet and dry spells, to produce large number of series, which is valuable for uncertainty analysis. Weather generators are data-intensive, require long sequences of daily data, and are sensitive to missing or erroneous data in the calibration set (Wilby et al., 2009).

1.2.2.3 Summary and comparison of Statistical and Dynamical Downscaling

Despite the fact that both statistical and dynamical downscaling techniques own reasonable capacity to translate the coarse resolution of CGMs to a fine spatial resolution, there are also some drawbacks in their use. Some of the merits and demerits in the application of both techniques according to studies (e.g. Fowler et al., 2007; Wilby et al., 2009) are enumerated in Table 3.

Table 3: *Advantages, disadvantages, outputs, requirements and applications of dynamical and statistical downscaling (adopted from Trzaska and Schnarr, 2014)*

	Dynamical downscaling	**Statistical downscaling**
Provides	. 20–50 km grid cell information . Information at sites with no observational data . Daily and monthly time-series . Scenarios for extremes events	. Any scale, down to station-level information . Daily (only some methods) and monthly time-series . Scenarios for extremes events (only for some methods) and scenarios for any consistently observed variable
Requires	. High computational resources and expertise . High volume of data inputs . Reliable GCM simulations	. Medium/low computational resources . Medium/low volume of data inputs . Sufficient amount of good quality observational data . Reliable GCM simulations
Avantages	. Based on consistent, physical mechanism . Resolves atmospheric and surface processes occurring at sub-GCM grid scale . Not constrained by historical record so that novel scenarios can be simulated . Experiments involving an ensemble ofRCMs are becoming available for uncertainty analysis	. Computationally inexpensive and efficient, which allows for many different emissions scenarios and GCM pairings . Methods range from simple to elaborate and are flexible enough to tailor for specific purposes .The same method can be applied across regions or the entire globe, which facilitates comparisons across different case studies . Relies on the observed climate as a basis for driving future projections . Can provide point-scale climatic variables for GCM-scale output . Tools are freely available and easy to implement and interpret; some methods can capture extreme events
Disadvantages	. Computationally intensive . Due to computational demands, RCMs are typically driven by only one or two GMC/emission scenario simulations . Limited number of RCMs available and no model results for many parts of the globe . May require further downscaling and bias correction of RCM outputs . Results depend on RCM assumptions; different RCMs will give different results . Affected by bias of driving GCM	. High quality observed data may be unavailable for many areas or variables . Assumes that relationships between large and local-scale processes will remain the same in the future (stationarity assumptions) . The simplest methods may only provide projections at a monthly resolution

1.3 Hydrological modeling

1.3.1 Hydrological cycle and hydrology

The hydrological cycle describes the continuous movement and changes of the state of water between the atmosphere and the earth. This cycle includes the processes illustrated in Figure 8: evapotranspiration (water going into the atmosphere), condensation (forming of clouds); precipitation (in various forms, such as rain, snow, sleet and hail), runoff (flow of rainwater on the earth's surface and in surface water bodies) and percolation (water infiltrating into the earth to form and/or recharge groundwater bodies). The water movement from the earth's surface to the atmosphere is supported by the solar radiation, while the water movement at and below the surface of the earth is mainly driven by gravity. The main effect of the hydrological cycle is that of maintaining the heat balance of the earth, trough moving and redistributing water masses.

Hydrology is the science that studies the water cycle, with particular focus on the processes occurring at the land phase. The subject is very vast and complex, due to the huge variety of

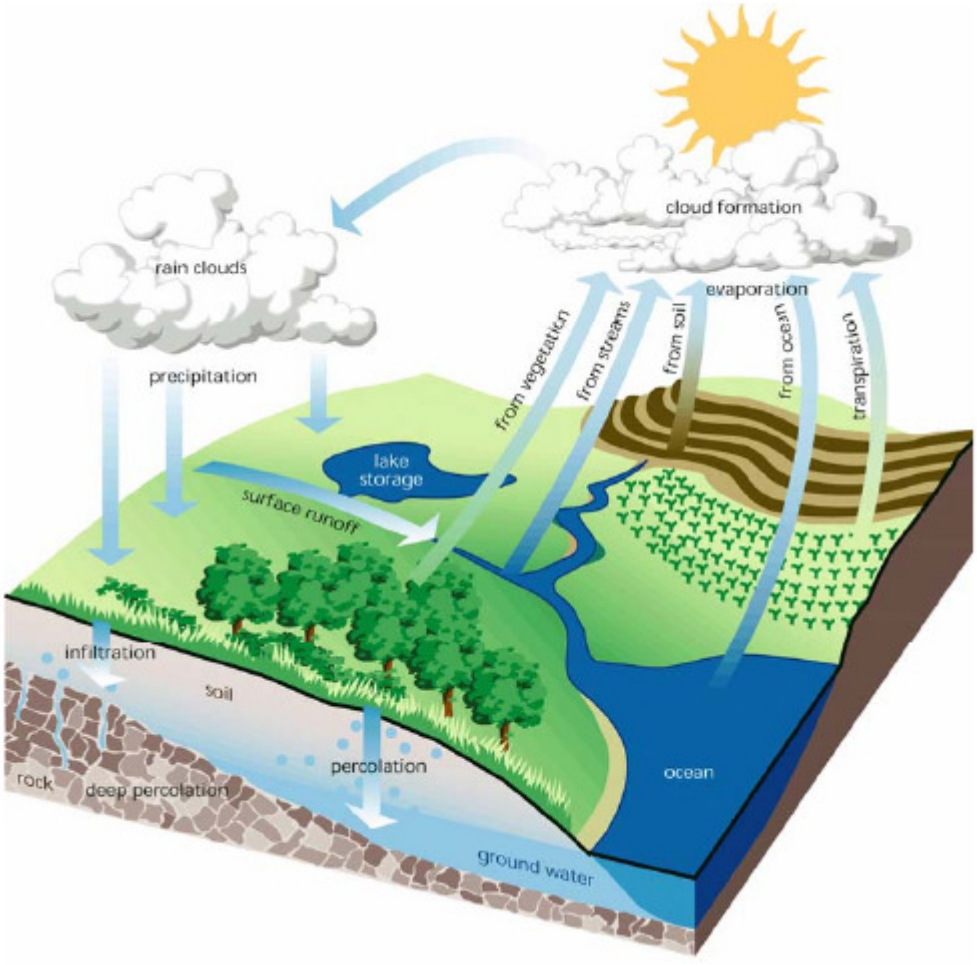

Figure 8: *The hydrological cycle (from FISRWG, 1998).*

processes involved in the cycle, their different temporal and spatial scales of occurrence and their interaction with other environmental components.

The humans life is deeply dependent on the water resources (particularly on freshwater), which are necessary for personal and domestic purposes, for recreation, as well as to support agriculture, fishery, hydropower generation, industries and various kinds of other uses. On the other hand, water can also constitute a threat, as, for example, in the case of floods. The strong connection between humans and water makes it necessary in several practical applications to have the best knowledge as possible on specific hydrological processes at the spatial and temporal scale of interest. This is essential to effectively plan, develop and manage the water resources, as well as to prevent its dangers. Hydrological models, which are introduced in the following part, are the primarily tools developed for hydrological predictions and for gaining more insight into the physical processes.

1.3.2 Hydrological modeling and hydrological models

Hydrological modelling is the discipline that tries to quantitatively describe the land phase processes of the hydrological cycle (Singh and Woolhiser, 2002). This is done by developing and setting up

mathematical models, i.e. sets of linked mathematical equations, which describe in a simplified form the behavior of the various components of the hydrological phenomena taking place in real hydrological systems. A hydrological system is defined as a structure or volume in space, surrounded by a boundary, that accepts water and other inputs, operates on them internally, and produces them as outputs (Chow et al., 1988).

In a general conceptualized form, a hydrological model can be represented as illustrated in Figure 9: it is an entity (a system of equations) that receives certain inputs (meteorological variables and model parameters) and transforms them into the desired output, the so-called model response. The model inputs comprise meteorological time series, also defined as forcing data, such as rainfall, snow, temperature and sunshine hours, as well as a set of model parameters, which describe the physical features of the hydrological system considered. The model parameters are divided into physical parameters, representing physically measurable properties of the system (for example the catchment area, the surface slopes and similar), and process parameters, describing characteristics that are not directly measurable (such as the average depth of the root zone, the time constants of various model storage blocks and similar). The outputs are defined depending on the system and the scope of the modeling. They can be, for example, river runoff, in the case of rainfall-runoff (RR) models, or groundwater flow and groundwater table elevation for groundwater (GW) models, while integrated models can simultaneously simulate surface and sub-surface processes and other parts of the hydrological cycle.

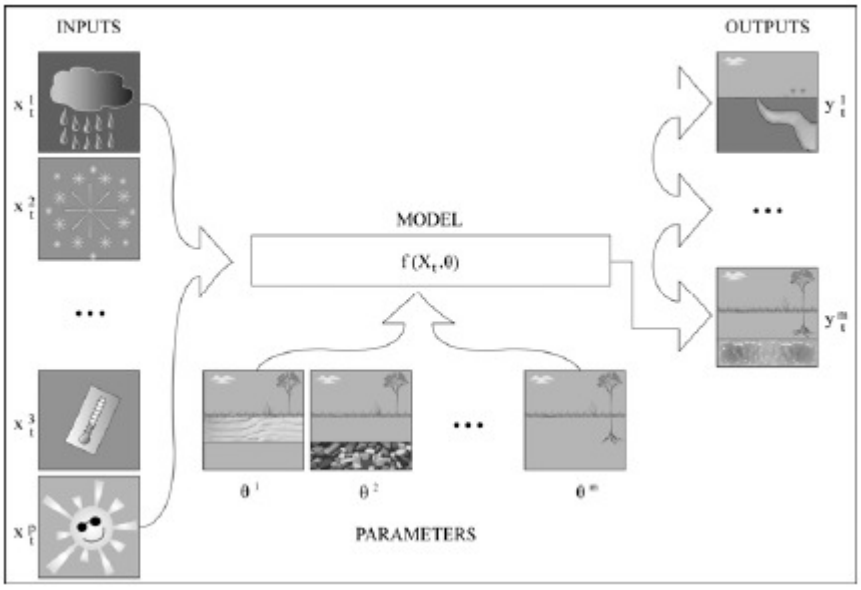

Figure 9: *Schematic representation of a hydrological model (from Blasone, 2007).*

The simplified mathematical form of a hydrological model is described in following equation:

$$Y_t = f(X_t, \Theta) \tag{1.5}$$

It is a system of equations, represented by the operator $f(.)$, which produces at every time step

t, a number m of outputs (hydrological responses), given by the vector Y_t:

$$Y_t = (y_t^1, ..., y_t^m) \tag{1.6}$$

The inputs of $f(.)$ are a vector of p meteorological inputs, X_t:

$$X_t = (x_t^1, ..., x_t^p) \tag{1.7}$$

and a vector of n model parameters Θ:

$$\Theta = (\Theta^1, ..., \Theta^n) \tag{1.8}$$

1.3.3 Classification of hydrological models

Nowadays, a large number of hydrological models are currently available and there are several criteria that can be used to classify them. Some important criteria are the degree of complexity of the different processes taking place in the model, the spatial resolution and the temporal variation of the processes in the model.

Based on the degree of complexity of the processes in the model, the hydrological models can be classified in three main groups:

- Physical-based models that try to accurately represent in a deterministic way all the processes occurring in the physical system and use partial differential equations in space and time.

- Black-box models that disregard any physical insight, often include stochastic components and just relate outputs to inputs through a set of empirical functions, such as simple mathematical expressions, time series equations, auto regressive moving average (ARMA) models and artificial neural networks (ANN).

- Conceptual models that are somewhere in between, since they represent all the relevant parts of hydrological processes but through a quite simplified description, often representing parts of the system as series of tanks that exchange water with one another.

  Based on the spatial resolution at which the processes are described, the models can be classified as:

  - Distributed in which the physical processes are represented, with varying degree of resolution, at various points in space and the model variables are also defined as functions of the space dimensions.

- Lumped opposite of distributed that consider the hydrological system as a unit block in which the properties are spatially averaged.
- Semi-distributed which are in between the first two, since the hydrological system is usually divided into smaller subsystems, each represented by a lumped model.

Based on the temporal variation of the processes (Chow et al., 1988), the flow conditions can be defined as steady and unsteady, the hydrological events can be accounted for in a continuous-time or event-based way and stochastic models can be classified as time-independent and time-correlated. However, steady conditions are normally assumed only in groundwater modeling applications, whereas continuous temporal variation is used to model faster response phenomena

1.3.4 Hydrological model selection

Despite the fact that several hydrological models are now currently available, the relationship between rainfall and runoff is a complex one as a result of landscape complexity brought about by tremendous heterogeneities and variability associated with the occurrence of connectivity, similarity and uniqueness of places at all scales (Wagener et al., 2007). For this reason, the selection of a hydrological model in river basins is usually carried out based some specific considerations (Wagener et al., 2004) such as:

- the model structure that is appropriate for the envisaged modeling purpose. The modeling purpose defines aspects such as which hydrological processes need to be considered and what modeling time step is required.
- the catchment characteristics. They are important criteria in determining what type of process description is suitable.
- the available data which enable a certain degree of causality of process description and allow a particular minimum spatial and temporal resolution.

Furthermore, the experience with a particular modeling code and the cost involved are equally important (Beven, 2001).

In this research, the HBV (Hydrologiska Byråns Vattenbalansavdelning) model was selected because it:

- is a conceptual model for runoff simulation,

- has a simple structure and is lumped or semi-distributed,
- is easy to understand, learn and apply,
- has been applied to many catchments in Sweden and abroad and provided good results in most applications,
- needs a moderate amount of input data, can be run on a PC (286 or better) and exists in different versions.

1.3.5 Uncertainties in hydrological modeling

Despite the recent advancements in developing hydrological models due to the actual level of knowledge of the physical processes of the hydrological system and the computational advances of the last years, hydrological modeling outputs are subject to uncertainty resulting from different sources of errors, which are generally grouped into three categories and discussed by Liu and Gupta (2007):

- input data error: they are generally come from both meteorological measurements and the hydrological observations used to evaluate the fit of the simulated outputs. This error affects both the magnitude and the timing of the model outputs.
- model parameters error that arises because of the uncertainty in determining the values of the model parameters. For calibrated models, this error also accounts for the fact that the parameter set adjustment can compensate for the other types of errors (Melching, 1995)
- model structural errors that can have several origins, such as incorrect representation of the processes (both in terms of physical description and of spatial and temporal discretization), disregarding of processes which are not represented and implementation errors in numerical algorithms and computer codes (Beven, 2005).

A realistic assessment of the uncertainty in model predictions is important for science-based decision making (Refsgaard et al., 2006) as well as to direct the research towards model structural improvements and uncertainty reduction. It is an accepted fact that hydrological model simulations should explicitly include an estimate of their associated uncertainty.

Uncertainty analysis (UA) is the discipline that tries to quantify the degree of confidence in the model outputs, based on the uncertainties in the model inputs (data or parameters). To date, many approaches to address the issues of UA in hydrological modeling prediction have been developed and grouped into two main categories according to Rosbjerg and Madsen (2006):

- First-order analysis also known as Local UA that can generally represent in a deterministic way only the uncertainty of the model output. This category includes Taylor-series expansion methods (Melching, 1995; Tsai and Franceschini, 2005), nonlinear regression methods (Vecchia and Cooley, 1987).

- Monte Carlo (MC) methods also known as Global UA, are stochastic techniques for probabilistic representation of uncertainty, which are based on running a certain number of model simulations (realizations) using a large random sample of the input variables. These methods can be used for analysis of error propagation in model simulations, if the sampled prior distributions of the inputs reflect the degree of knowledge on these variables. In this way, the input uncertainty is mapped into the output space and the structure of the distributions of model outputs can be defined. MC-based UA has become an active area of research in hydrological modeling and nowadays, different methods have been introduced. They are grouped based on the way in which they address the UA as: Bayesian methods (Thiemann et al., 2001; Vrugt et al., 2003; Freer et al., 1996), multiple criteria methods (Yapo et al., 1998; Boyle et al., 2000; Madsen, 2003), recursive and sequential data assimilation (Thiemann et al., 2001; Vrugt et al., 2005; Moradkhani et al., 2005), and set-theoretic methods (Klepper et al., 1991; van Straten and Keesman, 1991).

1.4 Climate change impact studies in Cameroon and neighboring areas

Cameroon is a sub-sahara Africa country and there is a clear consensus that the African climate has experienced some changes over the past few decades (Christensen et al., 2007) and the changing climate has impacted on many river basins in the region, including the Cameroonian rivers. For this reason, several studies have been conducted to ascertain the level of impact and as well as his possible future projections in many river basins in Africa. There is a general consensus that around 1970 an abrupt change in precipitation and runoff regimes across Cameroon and across West Africa in general, occurred (Tarhule et al., 2015; Liénou et al., 2008; Dzana et al., 2011; Amougou, 2018). However, only a few studies have been published regarding the potential future changes in river regime for Cameroon, particularly in such quantitative terms as required for this thesis and relevant for the planning of future hydropower development in Cameroon.

Mkankam (2001) studied the impact of climate change on the runoff in the Upper BRB. For this task, he used the calibrated Yates hydrological model forced by precipitation and temperature derived from two GCMs (HadCM2 and ECHAM4/OPYC3) under three emissions scenario IS92a, IS92c and IS92e. Compared to the baseline period (1961-1990), rainfall is expected to increase in the

range of 4–13% and temperature from 1 to 3°C. These lead to changes of 4–11% in annual potential evapotranspiration. Under the same conditions, changes in annual river flow range from -3 to +18%.

Penlap et al. (2004) used the Empirical orthogonal functions followed by Canonical Analysis to downscale statistically precipitation of ECHAM4/OPYC3 during the little rainy season (March-June) in Cameroon. His result showed an increase of precipitation from 4 to 44% for the 2010-2050 horizon in the North and North-West part of the country, and a decrease range between -14 to 4% in the Southern of the country relative to the baseline period 1961-2000.

Sighomnou et al. (2007) focused the impact of climate changes on the runoff regime in the Sanaga river during the 21st century. To this aim, runoff was simulated by driving GR2M hydrological model with precipitation and PET from HadCM3 GCM under the A2 emission scenario. compared to the baseline period (1971-2000), an increase of 3,4% in average annual precipitation is projected, along with a gradual increase in PET, in the order of 30% increase by 2100. As a result of such large increase in PET with only a modest increase in precipitation, runoff in the Sanaga basin could by 2100 decrease by as much as 20%.

Munang (2010) assessed climate change impacts on the hydro-energy potentials of the Sanaga basin by using trend analysis. the relationship between temperature, precipitation and river runoff from 1960–2007 was established based on regression analysis. Results showed an increase in temperature by 0.8°C, a decline in precipitation by 112 mm/yr or 6.5% and a decline in river runoff by 142 m^3/s or 7.5% for the Sanaga Basin. Projections of these trends to 2037 indicated a decrease in Sanaga river runoff by 355 m^3/s (or 19% compared to the 1960s), that will negatively affects the hydro-energy potential of the Sanaga River.

MINEP and UNDP (2012) studied the main risks of climate change on extreme climate risks such as droughts, erosion, high winds and flooding by using dynamically downscaled data of RegCM forced by the boundaries data conditions of one GCM (MPI-ECHAM5) under A1B emission scenario and agro-ecological zone. Their obtained results revealed a slight increase in precipitation until 2035, followed by a sharp and remarkable decrease by 2100 in nearly all agro-ecological zones except. The annual average temperatures would rise by the end of the 21st century from 0.7°C to 4.6°C in the northern part of Cameroon and from 0.5°C to 3.5°C in the forest zone in the South of the country.

The report of Grijsen (2014) presents a Climate Risk Assessment (CRA) for the five main river basins of Cameroon, focusing on the potential climate change impacts on water resources availability for hydro-energy generation, particularly in the Sanaga, Benue, Nyong and Ntem River Basins. For this job, 15 GCMs runs from phase 3 of the Coupled Model Intercomparison Project (CMIP3) under A1B emission scenario and the Turc-Pike rainfall runoff model were used. Results showed that the Lom Pangar and Nachtigal storage and hydropower projects in the Sanaga Basin are economically robust and climate resilient projects, but hydro-energy generated at Lagdo dam in the Benue basin may suffer a significant decrease due to climate change.

Conclusion

In this chapter, we have shown that the climate system is continually prone to the phenomenon of climate change as a result of both natural factors (such as volcanic eruptions and solar variations) and anthropogenic factors (such as the burning of fossils fuels and the depletion of the natural environment). Some of the impacts of climate change include increased warming of the earth surface that is usually aggravated by GHG emission to the atmosphere more especially since the second half of the 20^{th} century. In addition, high rainfall variability, sea level rise, increasing occurrence of floods and droughts have also been reported as the hydrological impacts of climate change. However, it has been revealed in the literature that the impacts of climate change will negatively impacted the water availability for both industrial and domestic purposes in the developing nations especially in Africa. The impacts on hydrology and water resources are already being felt and the situation could become worse in the future, especially in river basins such as the NRB. Nevertheless, most activities of the inhabitants of the NRB and particularly those living in the HBRB depend on the availability of water. This underscores the need for continuous understanding the impacts of the changing climate on water resources availability in the basin.

Although several studies in the literature review have focused on the impacts of climate change on the larger NRB and the entire Cameroonian catchment, most of them are limited by their inability to provide specific information needed for planning in the present study area, because those studies used GCMs data and scenarios without mitigation and adaptation strategies taking into account. Impacts and vulnerabilities of a given region are linked to regional and local forcings, GCMs with a coarse horizontal grid resolution do not capture these local and regional effects. Consequently, in order to fill the gaps, the present study embraces the application of a hydrological model and the use of downscaled GCMs data to ensure proper combination of the most probable physical and climatic conditions needed to mimic the climatic reality within the basin for the evaluation of the impacts of climate change to provide reliable information for future planning. Moreover, differently from the previous studies, this study includes scenarios that take into account the land use change, mitigation and adaptation strategies.

Chapter 2

Study area, data and methods

Introduction

Knowledge of the vegetation, climate and topography of the study area, as well as the techniques used, facilitates the interpretation and analysis of the obtained results. This chapter presents the study location, various data types and sources, and the analytical methods employed to achieve the objectives of the research work. First the sensitivity and uncertainty analysis of the hydrological model is examined, then the model optimization and performance assessment, followed by the RCMs data evaluation and lastly the evaluation of future climate change impacts in the basin. The flowchart of the research work is as shown in Figure 10.

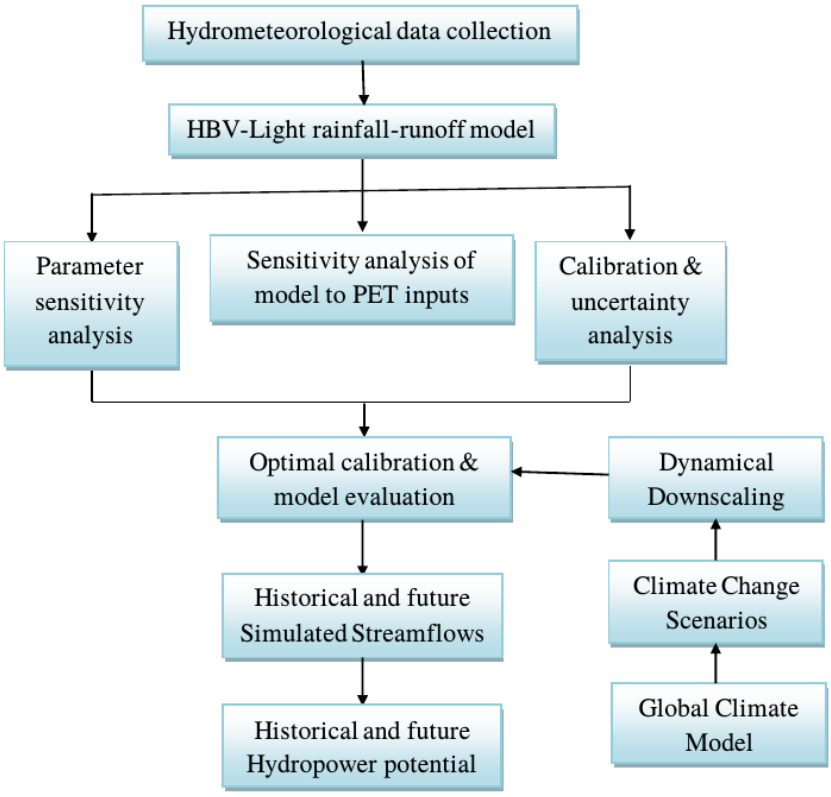

Figure 10: *Research Flowchart.*

2.1 Study area

2.1.1 Location

Generally, Cameroon is a Central African Nation located on the Gulf of Guinea between latitudes 2°N and 13°N of the equator and longitudes 8°E and 16°E of the Greenwich Meridian of the globe, with a total land mass of $475,650\ km^2$, shares its boundary with Nigeria to the west, Central African Republic and Chad to the east, Equatorial Guinea, Gabon and Congo to the south, and a small portion of Lake Chad to the north.

The Headwaters of the Benue River Basin (HBRB), a Cameroonian part of the Benue River Basin, and recognized as the important tributary of the Niger River Basin (NRB), is located in the Northern Cameroon between latitudes 7°N and 11°N and longitudes 12°E and 16°E (Fig. 11), with a drainage area of $66,000\ km^2$ and represents 4.4% of the total area of the NRB.

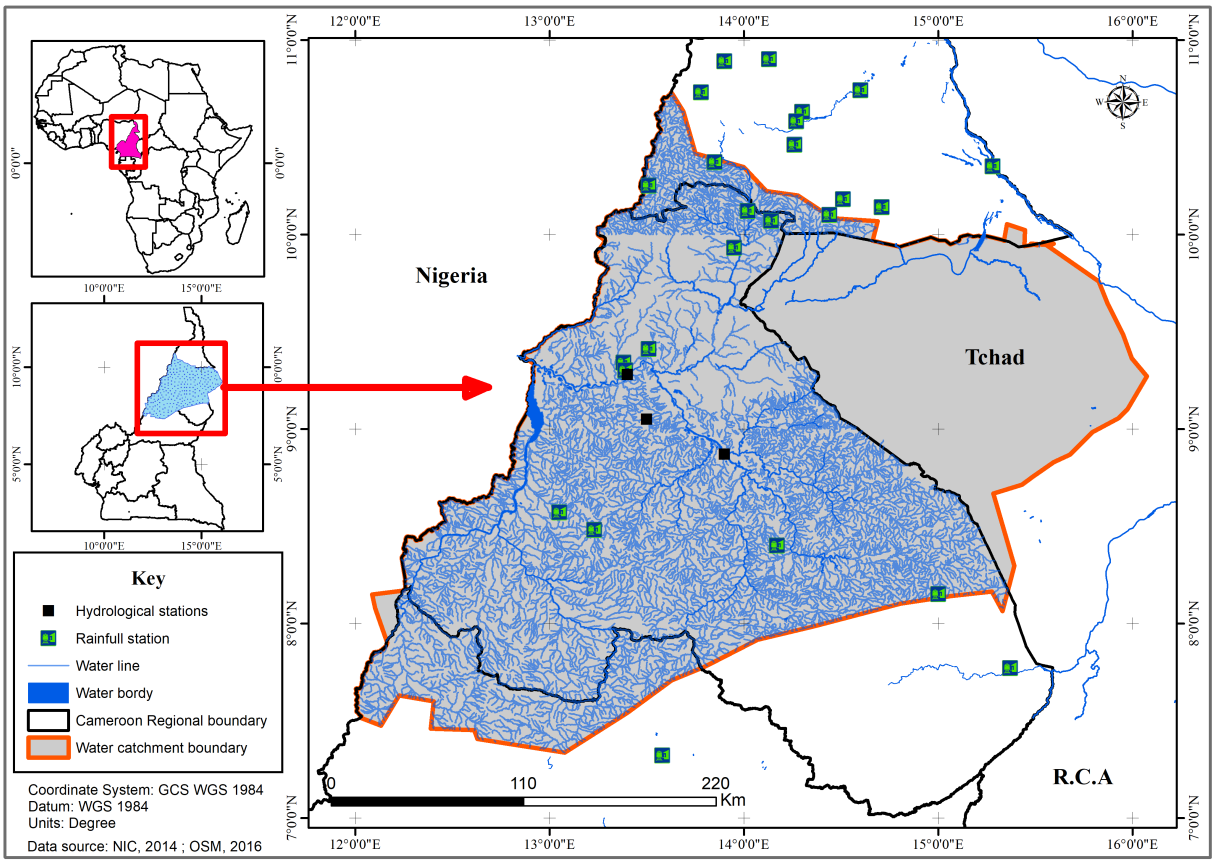

Figure 11: *Localization and drainage area of the HBRB.*

2.1.2 Topography

Based on the digital elevation matrix (DEM) at 90m, the elevations of the HBRB vary from 200 to 1800 m (Fig. 12) which can be divided into three main units (Dassou et al., 2016):

- The hilly regions which is characterized by the Mandara and Alantika Mountains. The elevation ranges between 900 - 1885 m;

- The Adamawa plateau (around 1100 m) in the southern part of the region which is surrounded by volcanic mountains reaching up to 2400 m;
- The Northward plain which is characterized by low altitudes around 300 m. It consists of degraded shrubby steppes on sandy clay soils.

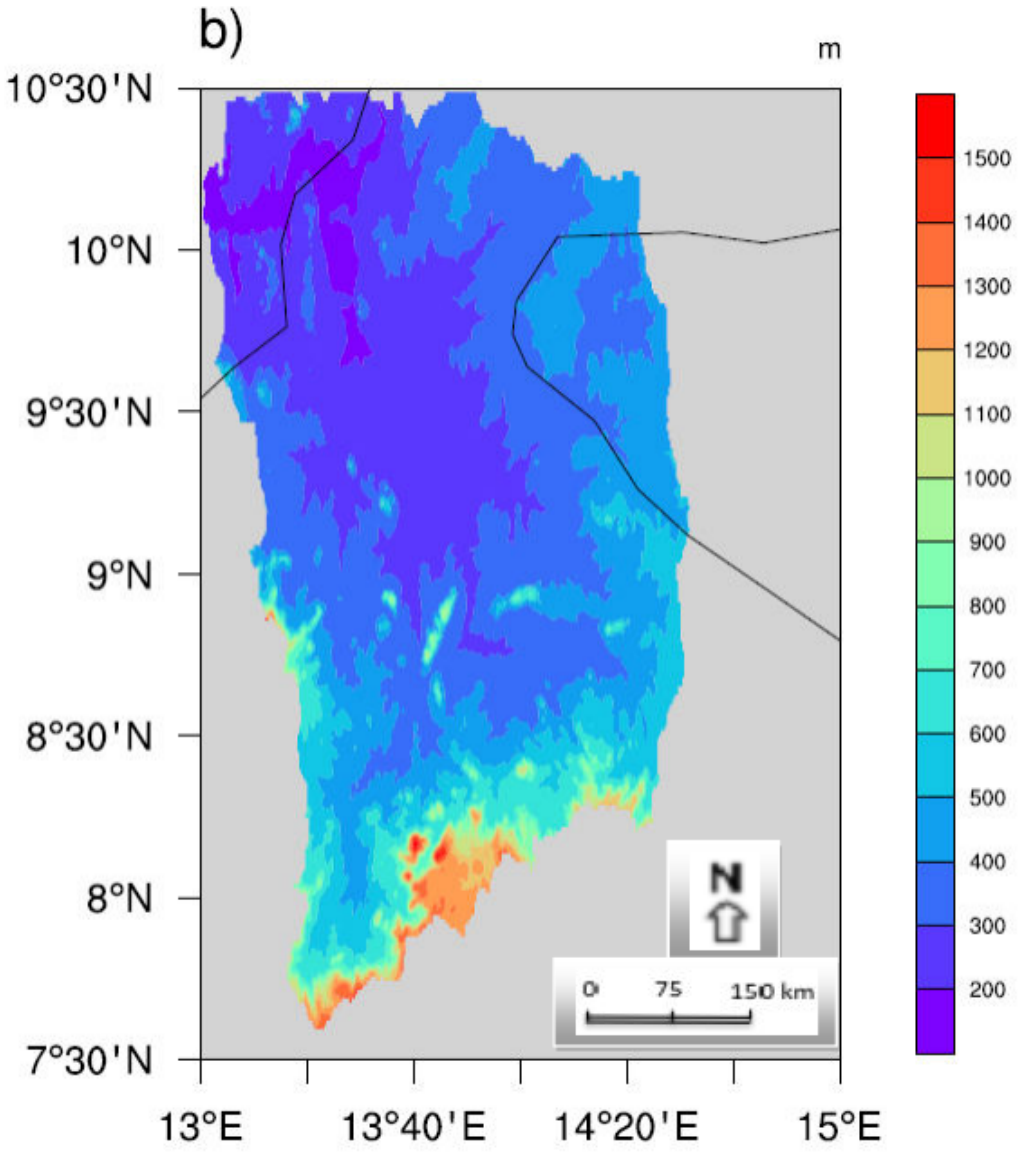

Figure 12: *Topography: Digital Elevation Model (DEM) at 90m of the HBRB.*

2.1.3 Climate

The HBRB is located in the transition zone between the tropical/equatorial climate in the Center and South of Cameroon and the Sahelian Climate in the Far North and enjoys a tropical humid climate (Sudan climate). This climate is characterized by a dry and hot season stretches from November to April and a wet and cooler season from May to October, during which rainfall occurs. It's unimodal rainfall region. The studied basin, like all the tropical regions of sub-Saharan Africa continent, is

under the influence of two air masses which control the shift in the position of the intertropical convergence zone (ITCZ, ground trace of the contact of the two air masses):

- Harmattan or continental tropical air, coming from the desert of Sahara, is a very dry air, at high temperatures in summer, with a general direction from the North-East;
- the Monsoon or equatorial maritime air, humid and unstable, with relatively cool temperature, come from the Saint Helena high, so from the southwest.

From November to April, under the influence of the Sahara high, the harmattan blows almost continuously from the northeast, slowly pushing the ITCZ towards the southwest which brings dryness. From May to October, a Saharan depression gradually replaces the previous high, while the Saint Helena high strengthens and moves a few degrees northward; the monsoon then invades upper Niger and then the lake area. The return of the ITCZ to the North is first accompanied by an increase in the hygrometric degree on the ground and dry tornadoes, then tornadoes short but violent.

2.1.3.1 Rainfall

Northern Cameroon's rainfall decreases gradually from the south (the highland of the Adamawa plateau) to the Far North (Chad plain). The length of the rainy season decreases from about six months in the Adamawa to four around Lake Chad and concentrated over four months: June, July, August and September. The annual rainfall in the Northern Cameroon ranges from 400 to 1800 mm (Dassou et al., 2016). The maximum monthly rainfall are in August and September with values of the same order for these two months. In October, the rainfall is decreasing very quickly (MINEE and GWP,).

2.1.3.2 Temperature

In contradiction to rainfall, northern Cameroon's temperature increases gradually from the south to the Far North. Due to the low altitude of the region, there is a significant increase in mean temperature of between 24 and 28.7°C in Tibati and Kaélé stations respectively. The maximum monthly mean temperatures are observed in March for the Tibati station (26.2°C) and in April for the Garoua (32.9°C), Kaélé (33.5°C) and Poli (29.6°C) stations. This marks the end of the dry season. The minimum monthly mean temperatures are observed in August for all stations, which corresponds to abundant rainfall (MINEE and GWP,).

2.1.4 Vegetation and agriculture

Cameroon has a diversified agricultural sector, resulting from various agro-ecological zones. It is characterized into five major agro-ecological zones with the major crops and livestock, production

activities for each zone (see Fig. 13). According to Okolle et al. (2016), the vegetation of the HBRB is mainly dominated by sudan and sahel savannah in the north and far north regions and high Guinea savannah in the Adamawa. The major crops and livestock production activities for the region are cotton, millet-sorghum, cowpea, onion, cattle, sesame, maize, yam and patatoes.

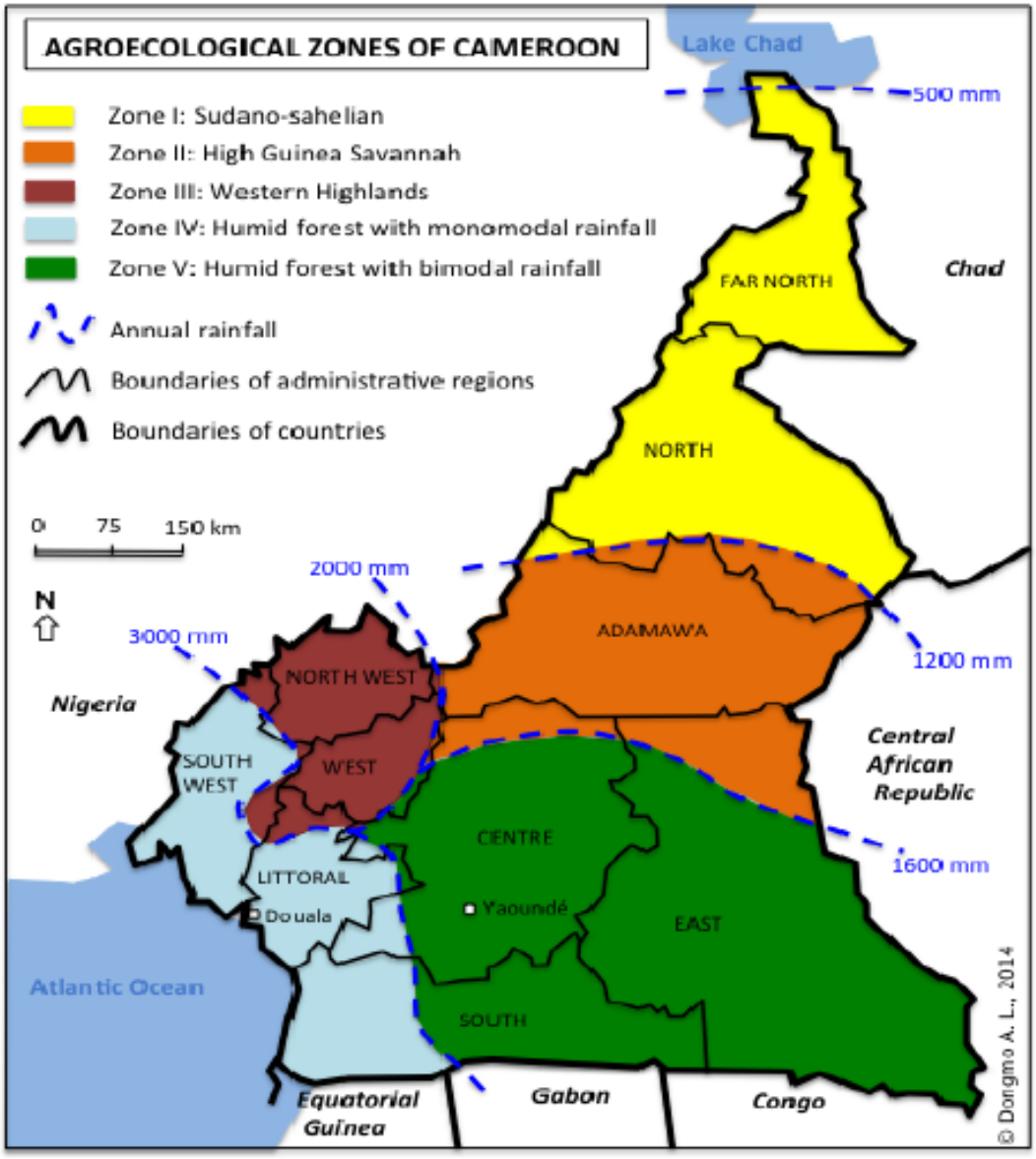

Figure 13: *Map of Cameroon showing the different regions and agro-ecological zones (Adapted from Okolle et al., 2016).*

2.1.5 Hydrology and water resources

The Benue River Basin (BRB) with an entire length of 1400 km has only 350 km within the Cameroon territory (Neba, 1987) and fed by tributaries from three catchment areas: the western highlands, the Adamawa highlands and the Mandara mountains and joins the Niger at Lokoja in Nigeria. It rises from the central northern slopes of the Adamawa plateau. Mayo Rey and Mayo Godi are the tributaries originate from the eastern sector. From the central region is the Mayo Farda from the Poli

mountains. The Faro, Mayo Njal and Mayo Deo, which form the western arm of the tributaries of the Benue, all converge to join the Benue at the exit point into Nigeria. In the western highlands, the tributaries of the Benue rise from the Bamenda highlands, the northern part of this catchment area. The main tributary from the Mandara mountains is the Mayo Louti. To the south of the Diamare plain is the Mayo Kebi and its tributaries flow through the Republic of Chad before meeting with Mayo Kebbi.

The HBRB holds huge potentials for water resources, including hydropower, irrigation, navigation, industry, domestic used and breeding. Table 4 summarized the water needs by sector in the HBRB (MINEE and GWP,).

Table 4: *Summary of water needs by sector in the HBRB (source: MINEE and GWP,).*

Sector	**Water volume** $10^{-3}.km^3.year^{-1}$	**Relative to the total needs (%)**
Domestic needs	65.9	0.82
Needs for breeding	13.29	0.17
Needs for irrigation	377.08	4.68
Needs for hydropower	7600	94.33
Needs for industry	0.33	0.004
Total	8056.6	100

Since the year 1982, the Lagdo dam which is the one largest Reservoir for Cameroon country was build by a combination of engineers and Chinese workers, along with Cameroonian laborers.

2.2 Data used

Data acquisition is the essential phase of any applied research. Data quality is a prerequisite for the quality of a study. In modelling, data are used not only to develop a model but also to evaluate it. Without data in sufficient quantity and quality, the model becomes unlikely efficient and operational. For our study, we needed the traditional data used in rainfall-runoff modelling (rainfall and stream-flows data) and specific data on climate variables (minimum, maximum and mean air temperatures, relative air humidity, wind speed, sunshine duration).

2.2.1 Hydrometeorological data

2.2.1.1 Meteorological data

Daily measured weather data (daily rainfall, mean, maximum and minimum air temperature at 2-m, solar radiation, relative humidity and potential evapotranspiration (PET) derived from Penman's formula) from the Direction of the National Meteorology of Cameroon (DNM), recorded at the different weather stations located in the Basin and neighboring areas, were used in this study. Figure 14 shows the geographical positions of the stations and Table 5 indicates the names, geographical positions (latitude and longitude), altitudes and record period of the stations.

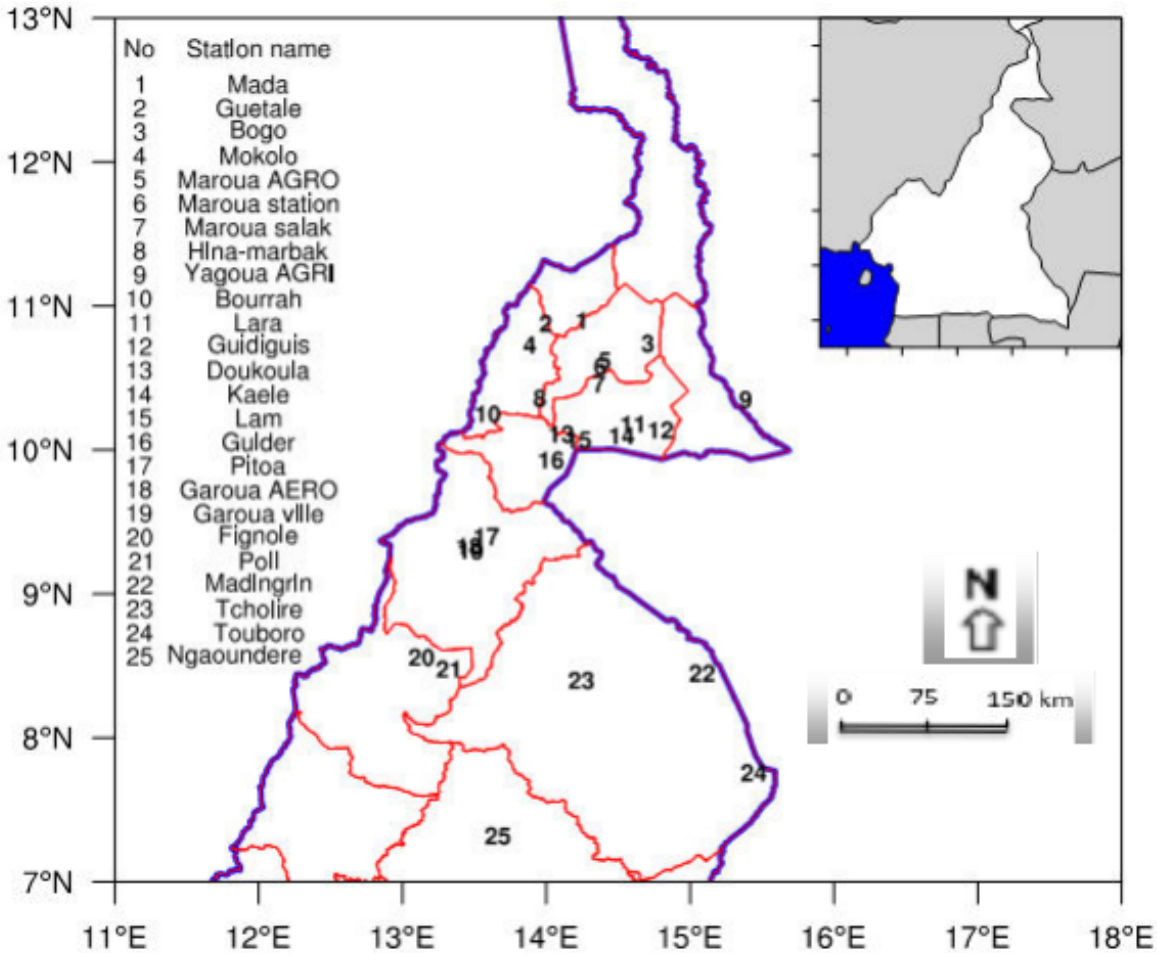

Figure 14: Study area with the geographical locations of rainfall stations (indicated by numbers).

Table 5: *Temporal and spatial characteristics of the 25 rainfall stations used.*

Station number	Station name	Latitude ($^\circ N$)	Longitude ($^\circ E$)	Altitude (m)	Record period	Missing (%)
1	Mada	10.9	14.13	750	1950-2004	0.15
2	Guetale	10.89	13.90	490	1948-2003	0.39
3	Bogo	10.74	14.6	340	1953-2003	0.20
4	Mokolo	10.73	13.78	795	1950-2003	0.04
5	Maroua AGRO	10.63	14.30	402	1946-1990	3.50
6	Maroua Station	10.58	14.27	428	1927-2003	0.00
7	Maroua Salak	10.46	14.26	423	1950-2004	0.33
8	Hina-marbak	10.37	13.85	544	1950-2003	0.10
9	Yagoua AGRI	10.35	15.28	325	1948-2003	0.01
10	Bourrah	10.25	13.51	775	1954-2003	0.64
11	Lara	10.18	14.51	416	1950-2003	0.01
12	Guidiguis	10.14	14.71	362	1961-2003	0.10
13	Doukoula	10.12	14.02	340	1955-2001	0.40
14	Kaele	10.10	14.44	388	1944-2003	0.02
15	Lam	10.07	14.14	430	1953-2003	0.85
16	Guider	9.93	13.95	356	1948-2003	0.00
17	Pitoa	9.41	13.51	274	1961-2003	0.01
18	Garoua AERO	9.34	13.38	242	1950-2004	0.59
19	Garoua Ville	9.30	13.39	213	1950-2003	0.41
20	Fignole	8.57	13.05	523	1961-2003	0.00
21	Poli	8.48	13.23	436	1950-1995	0.03
22	Madingrin	8.45	15.00	430	1961-2003	0.00
23	Tcholire	8.4	14.17	392	1950-2003	0.02
24	Touboro	7.77	15.37	500	1950-2003	0.00
25	Ngaoundere	7.32	13.58	1138	1950-2001	0.15

Only one station (Maroua AGRO) has the percentage of missing values equal to 3.5 %. The remaining stations have the missing values less than 1 %, while 05 of them have no missing values. The PET was provided by only few full meteorological stations (Ngaoundéré, Garoua, Kaele and Maroua). Rainfall data of some stations have been used to calibrate the Yates hydrological model in HBRB (Mkankam, 2001), to divide Cameroon into different climatic zones (Penlap et al., 2004), and to investigate the onset, retreat and length of the rainy season, and drought occurrence over Cameroon (Guenang and Mkankam, 2012, 2014).

2.2.1.2 Hydrological data

Daily streamflow time series for three (03) monitoring stations (Buffle Noir, Garoua and Riao) located in the basin, with different record periods, were obtained from the Hydrosciences Montpellier - Système d'Informations Environnementales database (Boyer et al., 2006, SIEREM, http://hydrosciences.fr/sierem). Table 6 gives the physiographic and hydrological characteristics of the available streamflow gauging sites in the UBRB considered here as sub-catchments, as well as the data quality analysis. The streamflow data of Riao gauging station were successfully used by Mkankam (2001) to investigate the performance of Yates hydrological model in the HBRB.

Table 6: *Physiographic and hydrological characteristics of the available streamflow gauging sites in the HBRB.*

characteristics	Garoua	Riao	Buffle Noir
Latitude (°N)	9.3	9.05	8.12
Longitude (°E)	13.38	13.68	13.83
Mean elevation (m $a.s.l.$)	174	185	350
Catchment size (km^2)	64,000	30,650	3,220
Mean annual precipitation ($mm/year$)	1,130	1,285	1,500
Mean annual discharge (m^3/s)	451.85	260.89	37.33
Extreme discharge (m^3/s)	5820	3320	738
	Land use		
Savannah	59%	16%	0%
Wooded savannah	38%	78%	0%
Highland meadow	3%	6%	100%
	Sub-catchment hypsometry		
% below 500 m $a.s.l.$	74.5%	63%	0%
% between 500 and 1,000 m $a.s.l.$	25.0%	35%	2%
% above 1,000 m $a.s.l.$	0.5%	2%	98%
	Daily streamflow data available		
Record period	1930-1995	1950-1999	1955-1995
Number of Months	776	591	480
Missing Months (%)	26.80	08.97	14.79

2.2.2 Climate scenarios data

In this research, CORDEX precipitation and temperature data derived from REMO model, which has been used in other studies over the region (Fotso-Nguemo et al., 2016, 2017; Vondou and Haensler, 2017; Tamoffo et al., 2018), were used to drive the hydrological model. The lateral boundary conditions (LBC) data of two GCMs, Europe-wide Consortium Earth System Model (EC-ESM) and Low Resolution of the Max Planck Institute-Earth System Model (MPI-ESM-LR) were downscaled by the REMO model over the CORDEX African domain (Giorgi et al., 2009) and are termed respectively REMO-EC and REMO-MPI. The REMO model is known to give a good representation of the present climate of the region (Fotso-Nguemo et al., 2016, 2017; Vondou and Haensler, 2017; Tamoffo et al., 2018).

2.2.2.1 REMO model description and experiment design

For the regional downscaling experiments, the hydrostatic version of the regional model REMO2009 is used (further denoted as REMO). REMO is a three-dimensional atmospheric model based on the "Europa-Model" system (Jacob, 2001b; Jacob et al., 2012; Teichmann et al., 2013). It has been developed in the context of the Baltic Sea Experiment (BALTEX) at the Max-Planck-Institute for

Meteorology in Hamburg by using the physical package of the global circulation model ECHAM4 (Roeckner et al., 1996). The finite difference equations are solved on an Arakawa-C grid. The model setup included a land surface scheme (Hagemann, 2002), radiation scheme (Morcrette, 1991) and a semi-lagrangian advection scheme as well as the parameterization of sub-grid scale processes such as convection (Tiedtke, 1989), cloud micro-physics (Lohmann and Roeckner, 1996) and turbulent vertical diffusion (Louis, 1979). The horizontal grid resolution was 0.44° x 0.44° as specified by CORDEX. More information about the model physics and dynamics is available in (Fotso-Nguemo, 2018) and at the REMO website (http://www.remo-rcm.de/).

The historical experiments are downscaled for 1950–2005 in which observed (GHGs) concentrations were used. The GCM projections are downscaled from 2006-2100 and three RCP scenarios are considered, namely, RCP2.6 (van Vuuren et al., 2011), RCP4.5 (Thomson et al., 2011) and RCP8.5 (Riahi et al., 2011).

2.2.2.2 Lateral boundary conditions data and experiments setup

The first GCM is EC-ESM version 2.3, which used the Integrated Forecasting System (IFS) from the European Centre for Medium-range Weather Forecast (ECMWF) to represent the atmosphere coupled to the Nucleus for European Modelling of the Ocean (NEMO) model. His spectral horizontal resolution is T159 (triangular truncation at wave-number 159, roughly 1.125° x 01.125°) with 62 vertical levels. The distance between levels increases gradually with height with typically about 20 levels to resolve the boundary layer. More information can be found at the website: http://ecearth.knmi.nl. Clouds are described by prognostic equations for cloud water content and cloud fraction and are distinguished in convective and stratiform clouds (Tiedtke, 1993). The parametrization of the former is based on the bulk mass flux approach (Tiedtke, 1989), whereas the formation of the latter is based on non-convective processes, such as large scale lifting and/or diabatic cooling (Jacob, 2001a).

The second GCM is MPI-ESM, which consists of the GCM for the atmosphere ECHAM6 (Stevens et al., 2013) coupled to the MPI Ocean Model (MPI-OM) (Jungclaus et al., 2013). The model system is further coupled to dynamic process models for marine biogeochemistry of the Hamburg Model of Ocean Carbon Cycling (HAMOCC5, Ilyina et al., 2013) and for the land biosphere of the Jena Scheme for Biosphere-Atmosphere Coupling in Hamburg (JSBACH, Brovkin et al., 2013). Here, we used the experiments conducted within the protocol of CMIP5 (Taylor et al., 2012) in the Low Resolution (LR) configuration with spectral truncation of T63 (approximately 1.875° x 1.875°) and 47 vertical levels. MPI–OM is used with a bi-polar grid at 1.5° horizontal resolution and 40 vertical levels.

The historical experiment of those two GCMs started in 1850 from a pre-industrial control simulation with a total length of 1,000 years with prescribed constant natural climate forcing. Starting from three different years of the pre-industrial control run, three realizations were integrated from 1850–2005 under observed natural and anthropogenic forcings, as well as anthropogenic land-cover

change (Giorgetta et al., 2013). In this research, the first realization from 1950–2005 for the downscaling experiments was used and the global climate change experiments are conducted for the period 2006–2100 following the Representative Concentration Pathway (RCP) scenarios developed by Moss et al. (2008) and anthropogenic land-use scenarios based on Hurtt et al. (2011).

2.2.3 Observation and reanalysis datasets

Assessing the model's ability to simulate the current climate is prior for impact studies. In order to take into account, the uncertainties associated with rainfall and 2-m temperature, we used different observational (in situ and satellite) and reanalysis datasets that include:

- Climate Research Unit data (CRU) version TS3.22 beginning in 1901 from the University of East Anglia that includes monthly precipitation and temperature at $0.5° \times 0.5°$ latitude-longitude resolution over land areas (Harris et al., 2014).
- National Center for Environmental Prediction/National Center for Atmospheric Research (NCEP/NCAR) Reanalysis data (NCEP1) spans from 1948 to present and includes 6 hourly daily precipitation rates and 2-m temperature at $2.5° \times 2.5°$ spatial resolution (Kalnay et al., 1996).
- The National Center for Environmental Prediction (NCEP) of the Department of Energy (DOE) Atmospheric Model Intercomparison Project (AMIP-II) reanalysis data (NCEP2) spans from 1979 to 2016 and includes 6 hourly daily precipitation rate and 2-m temperature at $2.5° \times 2.5°$ spatial resolution (Kanamitsu et al., 2002). NCEP2 is an improved version of NCEP1 that fixed errors and updated parameterization of physical processes.
- The ERA-Interim (ERAIN) Reanalysis data, which is the recently Reanalysis data for the European Centre for Medium-Range Weather Forecasts (ECMWF) that includes daily precipitation and 2-m temperature at $0.75° \times 0.75°$ spatial resolution (Dee et al., 2011).

2.3 Methodology

2.3.1 Hydrological model description: HBV-Light rainfall-runoff model concept

2.3.1.1 General description

The HBV-Light model (Seibert, 2005) selected for hydrological modeling in this research, was developed at Uppsala University in 1993 using Microsoft Visual Basic. It is a modified version on the HBV (Hydrologiska Byråns Vattenavdelning, in English: Hydrological Bureau Water Balance

section) model, originally developed by the water balance section of the Swedish Meteorological and Hydrological Institute (SMHI) to assist hydropower operations in the 1970s (Bergström and Forman, 1973; Bergström, 1976) in the context on a strong snow covert. The aim was to create a conceptual hydrological model with reasonable demands on computer facilities and calibration data. The name of the model HBV is adapted from institute name where it was developed. During the last few decades, the model was widely used in the Scandinavian and Sweden catchments (Bergström, 1992). HBV model was chosen due to the relatively low demand for input data and the unexcessive number of free model parameters compared with other models (Rusli et al., 2015). During the last few decades, the model has proved flexibility and robustness in solving water resources problems, and it is used for a broad range of applications in different version in many studies and projects in the World (Bergström, 2006). Additionally, in the West African context, the HBV model was also found to be suitable in simulating discharge and for global change impact studies (Cornelissen et al., 2013; Poméon et al., 2017; Kwakye and Bárdossy, 2020). The HBV-Light model (Seibert, 2005) used here has identical structure to the model of Bergström (1992), with two small changes. The firstly is inclusion of a spin-up period rather than requiring prescribed initial states, and secondly the MAXBAS routing parameter can assume non-integer values. It was used here because his Matlab version provided by Aghakouchak et al. (2013) includes Monte-Carlo procedure for calibration.

The model general water balance can be described as:

$$P - E - Q = \frac{d}{dt}[SP + SM + S_{UZ} + S_{LZ} + LAKES] \tag{2.1}$$

where P is precipitation, E is Evapotranspiration, Q is runoff, SP is snow pack, SM is Soil moisture, S_{UZ} is upper ground zone, S_{LZ} is lower ground zone and $LAKES$ is lakes water storage.

2.3.1.2 Model structure

The HBV model is classified as a conceptual hydrological model with either semi-distributed or lumped model domain. The model works at daily time step and simulates discharge using precipitation, temperature and long-term monthly potential evapotranspiration like input variables. It consists on four (04) main conceptual subroutines: the snow routine representing snow accumulation and snow melt by a degree-day method, the soil moisture and evaporative routine where groundwater recharge and actual evaporation are computed as functions of actual water storage, the response routine represented by three linear reservoir equations and channel routine modeled by a triangular weighting function (Aghakouchak and Habib, 2010).

Given that the study area is snow free, the snow subroutine has been removed and the main hydrological processes in the model are simplified by nine (09) model parameters, subdivided into two (02) categories, namely:

- the physical parameters that describe the physical properties of the watershed, include the

field capacity (FC) parameter that describes the maximum capacity of the soil moisture, the permanent soil wilt point (LP) which is the value of soil moisture for which the current (actual) evapotranspiration (AET) reaches the PET because soil moisture is a factor influencing the AET.

- Empirical parameters that have little or no physical significance but are used to describe conceptual processes include reservoir parameters (K_0, K_1, K_2, $PERC$ and UZL) representing respectively the storage coefficients of near-ground flow, hypodermic flow, base flow, constant percolation and threshold level in the upper reservoir, the shape coefficient (β) which determines the relative contribution to rainwater runoff and the $MAXBAS$ parameter which is a unit hydrograph of base time.

Model parameter, definitions, units and initial ranges are summarized in Table 7.

Table 7: *Main components of hydrological processes and the parameters designed to represent them in the HBV-Light model and their ranges used for the Monte Carlo simulations (source: Seibert and Vis, 2012.*

Main hydrological Processes	Parameter	Definition	Units	Minimum value	Maximum value
Soil and evaporation routine	**FC**	Maximum value of soil moisture storage	mm	50	500
	LP	Fraction of FC above which actual ET equals potential ET	–	0.3	1
	β	Shape parameter for the soil moisture distribution function	–	1	6
Groundwater and response routine	K_0	Near surface flow routing rate constant	day^{-1}	0.05	0.5
	K_1	Interflow routing rate constant	day^{-1}	0.01	0.3
	K_2	Baseflow routing rate constant	day^{-1}	0.001	0.1
	UZL	Threshold for Q_0 flow	mm	0	100
	$PERC$	Maximum rate of recharge between the upper and lower groundwater boxes	$mm.day^{-1}$	0	6
Routing routine	$MAXBAS$	Length of triangular weighting function in routing routine	day	1	5

For the soil moisture and evaporation routine, given that the watershed is snow-free, the rainfall (P [mm]) is divided into water infiltration and water recharge depending on the relation between the water content the soil box (SM [mm]) and its maximum value (FC [mm]). The second component, usually known as effective precipitation (P_{eff} [mm]) is computed as follows:

$$P_{eff} = P.(\frac{SM}{FC})^{\beta} \tag{2.2}$$

where a parameter β determines the relative contribution to runoff from a millimeter of rain at a given soil moisture deficit.

Then, the water content of the soil box is updated:

$$SM = SM + (P - P_{eff}) \tag{2.3}$$

The actual evapotranspiration (AET) is computed using the integrated converted method (Zhao et al., 2013). This method uses the soil moisture extraction function to convert PET into AET based on the following equation:

$$AET = PET.min(1, \frac{SM}{FC.LP}) \tag{2.4}$$

where LP is a parameter that controls the shape of the reduction curve for PET.

The water content of the soil box is updated again:

$$SM = max(0, SM - AET) \tag{2.5}$$

The runoff response routine is organized around two conceptual reservoirs, which have linear emptying laws, the first feeding the second by infiltration. The first reservoir receives the water recharge and empties into three components:

- a surface runoff, Q_0 takes place when the water level in the upper reservoir exceeds the threshold value, UZL

  $$Q_0 = max(0, K_0 \times (S_{UZ} - UZL)) \tag{2.6}$$

  where S_{UZ} is the water level filling the upper reservoir and K_0 is the near surface flow storage coefficient.

  Then, the water level filling the upper reservoir is updated:

  $$S_{UZ} = S_{UZ} - Q_0 \tag{2.7}$$

- a sub-surface runoff, Q_1

  $$Q_1 = K_1 \times S_{UZ} \tag{2.8}$$

  where K_1 is the interflow storage coefficient.

- a constant percolation, Q_{perc}

  $$Q_{perc} = PERC \times S_{UZ} \tag{2.9}$$

  where $PERC$ is the percolation storage coefficient.

Finally, the water level filling the upper reservoir is updated again:

$$S_{UZ} = S_{UZ} - (Q_1 + Q_{perc}) \tag{2.10}$$

The lower reservoir receives the constant percolation Q_{perc} and empties linearly into a base flow (groundwater contribution), Q_2

$$S_{LZ} = S_{LZ} + Q_{perc} \tag{2.11}$$

$$Q_2 = K_2 \times S_{LZ} \tag{2.12}$$

where S_{LZ} is the water level filling the lower reservoir and K_2 is the is baseflow storage coefficient.

Then, the water level filling the lower reservoir is updated:

$$S_{LZ} = S_{LZ} - Q_2 \tag{2.13}$$

The total runoff at the time step t, Q_{GW} is then transformed by the parameter MAXBAS $[day]$ to give the modeled streamflow, Q_{sim} $[mm.day^{-1}]$.

$$Q_{GW}\,(t) = Q_0 + Q_1 + Q_2 \tag{2.14}$$

$$Q_{sim}(t) = \sum_{i=1}^{MAXBAS} C(i)\, Q_{GW}(t-i+1) \tag{2.15}$$

where $C(i) = \int_{i-1}^{i}(\frac{2}{MAXBAS} - |u - \frac{MAXBAS}{2}| \times \frac{4}{MAXBAS^2})du$.

The schematic view of different processes that occurs in the HBV-Light rainfall-runoff model used in this study is presented in Figure 15.

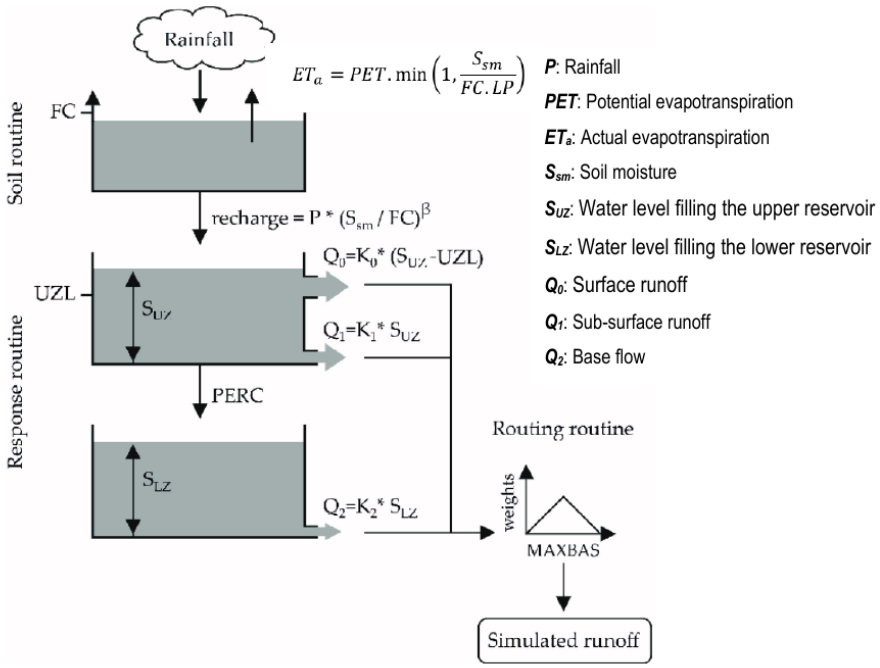

Figure 15: *Schematic view of the different hydrological processes in the HBV-Light model.(adopted from Seibert, 2005)*

The average value of input data over a catchment was computed using the Arithmetical Mean Method (Rakhecha and Singh, 2009) as shown in Eq. (2.16):

$$P_{avg} = \frac{1}{n}\sum_{i=1}^{n} P_i \tag{2.16}$$

where P_{avg} is the average of the climate variable P over the catchment area (for a given time period); n is the number of stations within the catchment; P_i is the value of the considering climate variable at station i.

2.3.2 Model calibration and validation

Since the main hydrological processes in hydrological models are simplified by the model parameters that cannot be determined directly from field measurements, their calibration is required. Calibration is a technique that allows one to choose the best parameter set of the model, by adjusting manually or automatically their numerical values to more reproduce the response at the outlet (Madsen et al., 2002; Wu et al., 2012). According to Blasone (2007), this process is also called "model optimization", considering that his scope is the reduction of the model error; and also defined as "inverse modelling",

since the observations of the model outputs are used to estimate the parameter values. This may be performed automatically, or manually. Manual calibration, which involve manual adjustment of the parameter values until a satisfactory level of model behavior is obtained, needs an experienced modeler who understands the behavior of the model and can be very time-consuming. A substitute to the manual procedure is automatic optimization. Automatic calibration involves the use of a search algorithm to determine best-fit parameters, and it offers a number of advantages over the manual approach.

The calibrated model parameters should necessarily be validated. A model validation, also called model testing is the process to check the reproducibility of the results by the calibrated parameters. This can be achieved by generating model simulations for independent events and/or at independent locations and verifying that the model fit to the observations is comparable to that achieved in the calibration. A new data set different from that in the phase of the calibration is used.

In this research, the automatic calibration procedure and the split-sample procedure recommended by Klemeš (1986) were used for calibration and validation. Our data time-series has been split into two sub-periods. The rainfall-runoff model is calibrated in the first sub-period using the Monte-Carlo simulations (Aghakouchak et al., 2013) and validated in the second sub-period, taking the first year of each sub-period as spin-up period. A MCS is in actuality a broad class of computational algorithms which employs random sampling algorithms used to obtain probability distributions of an unknown variable (Robert and Casella, 2013). It is the strategy of choice because it is more general and requires fewer assumptions than other methods (Mishra, 2009). In MCS, the uncertain parameters are sampled from distributions, and a large number of simulations are computed. Each simulation represents an independent and equally probable realization. MCS has several advantages: (1) it avoids errors associated with linearization of the model; (2) it produces a distribution for the uncertain output as well as the mean and standard deviation; (3) the method does not require the computation of derivatives; and (4) can handle correlated and independent parameters. However, MCS may not be the most efficient in terms of number of model runs when the parameter uncertainty is poorly defined or the outcomes of interest are limited in number (Mishra et al., 2003).

Given that it's often not possible to find one unique best parameters set, i.e. different parameter sets give similar good results during a calibration period, leading to uncertainties in the model output prediction (Uhlenbrook et al., 1999). Therefore, the assessment of uncertainty in hydrological modeling is important, especially when their results are used to support decisions about the management of water resources (Refsgaard et al., 2007). It is also an accepted fact that hydrological model simulations should explicitly include an estimate of their associated uncertainty (Blasone, 2007). Sensitivity analysis (SA) and parameter uncertainty analysis are the powerful tools used to reduce uncertainty in hydrological modeling prediction by identifying the influential parameters on model output, reducing the interaction between model parameters and time-consuming during the model calibration, and to

enhance the model optimization efficiency (Saltelli et al., 2006; Refsgaard et al., 2007).

2.3.3 Sensitivity analysis of model parameters

Sensitivity Analysis (SA) investigates how the variation in the output of a numerical model can be attributed to variations of its input factors. It is a powerful tool generally applied to hydrological models in order to identify the influential model parameters affecting most the hydrological response variations. The parameter will then say "influential" or "non-influential" if change in the parameter value affect the result of simulation of the hydrological response or not. The non-influential parameters could be used to reduce the number of parameters to be calibrated in the model. There are generally two approaches for SA: local and global SA methods. The choice of the method highly depends of the purposes of SA since differents methods are better suited to address differents questions (Pianosi et al., 2016). Given that the main objective of this research is to provide an optimal calibration model for the basin, it is therefore important to provide insights on how variations in the uncertain parameters map onto variations of the performance metric that measures the model fit. For this task, the local SA method especially One-factor-At-Time (OAT) method is highly recommended (Pianosi et al., 2016). The model was first calibrated using different Multi-objective functions and the best parameter set that reproduces the streamflow well was obtained. By using the random numbers from a uniform distribution within the given ranges for each parameter, we generated 100 values of each model parameter and the model was run by varying one parameter, while keeping the other parameters constant and observe the results for the Absolute Percent Bias (PBIAS, refer to Eq. 2.20) and the normalized Root Mean Square Error (RSR, refer to Eq. 2.21) in order to find the parameter controlling the total volume error and high-flow series respectively (Abebe et al., 2010) (refer to "Optimal calibration and model performance assessment" to found the equations of those criteria).

2.3.4 Parameter identifiability and uncertainty analysis

The uncertainty in model parameters is the problems in identifying and calibration parameters. Reliable hydrological models simulations require that model parameters are precisely identified. In constraining model parameters to small ranges, high parameter identifiability is achieved. To identify appropriate model parameter values, typically, a large number of model simulations with different parameter combinations is carried out and analysed according to their impact on performance criterion. For this, we used the Monte Carlo (MC) method. Fifty thousand (50,000) parameter sets were generated using the random numbers from a uniform distribution within the given ranges for each parameter. The model was run for each parameter set and the value of Nash-Sutcliffe efficiency (NSE, Nash and Sutcliffe, 1970, Eq. 2.17) greater or equal to 0.70 was taken as acceptable simulations.

NSE is a normalized dimensionless method that determines the relative magnitude of the residual

variance ("noise") compared to the measured data variance ("information"). It is range between $-\infty$ to $+1$, with optimal value equal to 1. $NSE = 0$ indicates that the model predictions matching the mean of the measured data, while a negative NSE shows that the measured mean is a better predictor than the model. It is common and widely used method by the hydro-geologists to assess the efficiency of the model (Moussa, 2008) and computed as follow:

$$NSE = 1 - \frac{\sum_{t=1}^{n}(Q_{obs,t} - Q_{sim,t})^2}{\sum_{t=1}^{n}(Q_{obs,t} - \overline{Q_{obs}})^2} \tag{2.17}$$

Where $Q_{obs,t}$ and $Q_{sim,t}$ are the observed and simulated stream flows in the time step t respectively. $\overline{Q_{obs}}$ is the average of observed stream flows and n the total number of time step in the period of simulation.

The parameter will then say "Good/well" or "badly/ill" defined if it gives acceptable simulations with a small or wide range of variations respectively (assessed using boxplot). The more the model parameter ranges are reduced, the more precisely a parameter is identified. This also reduces the impact of equifinality and thus reduces the uncertainty in selecting adequate parameter values (Shin et al., 2015). It can be qualitatively assessed by plotting NSE (vertical axis) against the model parameter values (horizontal axis), in which for a well-defined parameter, the upper boundary should have a distinct peak while in ill-defined parameters the upper boundary will have a broad plateau. Quantitatively, simple descriptive statistics such as the mean, range, standard deviation (StD, refer to Eq. 2.18), coefficient of variation (CV, refer to Eq. 2.19) and the determination of maximum (max) and minimum (min) values are also employed to gain preliminary understanding of the acceptable model parameters.

$$StD = \sqrt{\frac{\sum_{i=1}^{N}(\Theta_i - \overline{\Theta})^2}{N}} \tag{2.18}$$

$$CV = \frac{StD}{\overline{\Theta}} = \sqrt{\frac{\sum_{i=1}^{N}(\Theta_i - \overline{\Theta})^2}{N}}\frac{1}{\overline{\Theta}} \tag{2.19}$$

where Θ_i is the model parameter value for the acceptable simulation i, $\overline{\Theta} = \frac{\sum_{i=1}^{N}\Theta_i}{N}$ is the mean value of model parameter Θ for an ensemble of the acceptable simulations, and N the number of the acceptable simulations.

2.3.5 Optimal calibration and model performance assessment

During this stage, the model parameters identified as non-influential to total volume error and high-flow series are kept constant. The range of other parameters have been defined based on the lower and upper limits of the 95% confidence intervals for the acceptable simulations obtained during the calibration. Based on MC-Simulations, 50,000 parameter sets were derived and the model was run for each parameter set. Then, the optimized parameter set was obtained by optimizing the different objectives functions mentioned in the paragraph below. The best set of optimized parameters was then used in validation period and the performance of the model will be assessed.

To assess the model performance for the HBRB during the model calibration and validation phase, graphical and statistical techniques have been used (ASCE, 1993; Legates and McCabe, 1999). The graphical techniques include hydrographs used to identify the difference in timing and magnitude of peak flows, model bias and shape of the curves of recession (ASCE, 1993) and flow duration curves that can illustrate how well the model reproduces the frequency of measured daily flows throughout the calibration and validation periods (van Liew et al., 2007). In addition to the graphical technique, other statistical methods, in addition to the NSE criteria, will be used to evaluate the results of the calibration and validation. Those have been recommended by Moriasi et al. (2007) are described as follows:

Percent bias ($PBIAS$): $PBIAS$ is an index error that measures the average tendency of the modeled data to be larger or smaller than their observed counterparts (Gupta et al., 1999). His optimal value is 0.0, while the positive values indicate model underestimation bias, and negative values indicate model overestimation bias. $PBIAS$ is computed based on the following equation.

$$PBIAS = \frac{\sum_{t=1}^{n}(Q_{obs,t} - Q_{sim,t})}{\sum_{t=1}^{n}(Q_{obs,t})} \times 100 \tag{2.20}$$

RMSE-standard deviation ratio (RSR): it is also an error index statistic and includes a scaling/normalization factor. RSR is calculated as the ratio of the root mean square error ($RMSE$) and standard deviation of observed data (StD_{obs}), as shown in equation 2.20:

$$RSR = \frac{RMSE}{StD_{obs}} = \frac{\sqrt{\sum_{t=1}^{n}(Q_{obs,t} - Q_{sim,t})^2}}{\sqrt{\sum_{t=1}^{n}(Q_{obs,t} - \overline{Q_{obs}})^2}} \tag{2.21}$$

RSR varies from the optimal value of 0, which indicates zero $RMSE$ or residual variation and therefore, perfect model simulation, to a large positive value. The lower value of RSR implies the lower value of $RMSE$ and then the better model simulation performance.

The coefficient of correlation R^2 was also used in this study in order to describe the degree of collinearity between simulated and measured data. It ranges from 0 to 1, with 1 being the perfect fit between the simulated and the measured data and computed as follows:

$$R^2 = \frac{\sum_{t=1}^{n}(Q_{obs,t} - \overline{Q_{obs}})(Q_{sim,t} - \overline{Q_{sim}})}{\sqrt{\sum_{t=1}^{n}(Q_{obs,t} - \overline{Q_{obs}})^2}\sqrt{\sum_{t=1}^{n}(Q_{sim,t} - \overline{Q_{sim}})^2}} \tag{2.22}$$

where $\overline{Q_{sim}}$ is the average of modeled streamflows.

More details and descriptions of those statistical techniques can be found in ASCE (1993); Legates and McCabe (1999); Moriasi et al. (2007), while the table 8 gives their interpretation.

Table 8: *Interpretation of the statistical criteria obtained during the model calibration and validation (source: Moriasi et al., 2007).*

PBIAS	NSE	RSR	Interpretation model
$PBIAS < 10$	$0.75 < NSE \leq 1.0$	$0.00 \leq RSR < 0.50$	Very Good
$10 \leq PBIAS < 15$	$0.65 < NSE \leq 0.75$	$0.50 \leq RSR < 0.60$	Good
$15 \leq PBIAS < 25$	$0.50 < NSE \leq 0.65$	$0.60 \leq RSR < 0.70$	Satisfactory
$PBIAS \geq 25$	$NSE \leq 0.50$	$RSR \geq 0.70$	Unsatisfactory

2.3.6 Sensitivity analysis of HBV-Light model to PET input

Precipitation and evapotranspiration (ET) are the major components of water budget for a watershed, mainly because precipitation that includes ice (snow, hail, graupel, sleet) and water (rain, drizzle), is the main mechanism responsible for depositing the fresh water on the catchment, while ET, which is a sum of evaporation from the soil, sublimation and transpiration from the plant canopy, is the primary mechanism by which water is removed from a watershed. Also, quantification of AET is important to focus the land use change impacts on water yield, environmental assessment, and development of best management practices to protect the quality of both surface and ground water (Irmak et al., 2005). Moreover, precipitation and ET represent the key inputs for hydrological models. However, unlike precipitation, direct measurement of ET is hard, time consuming, and costly because ET is depended on a number of factors that may vary both spatially and/or temporally, including changes in leaf area, plant height, crop characteristics, rate of crop development, degree of canopy cover, canopy resistance, soil and climate conditions, and management practices (Doorenbos and Pruitt, 1977).

In the rainfall-runoff model, ET is estimated based on a theoretical climatic variable known as PET and depends on the soil moisture extraction function (Zhao et al., 2013). PET represents the upper limit of ET when soil water is in sufficient quantity. Due to the fact that this variable is difficult to measure, it is usually estimated based on other climatic variables like air temperature, relative humidity, sunshine duration and wind speed. However, these variables are often not available in data scarce regions like the Upper Benue River Basin in Northern Cameroon. Nowadays, several PET estimation methods exist that vary from temperature-based to physically-based process models (see Oudin et al., 2005; Djaman et al., 2019 for a comprehensive list).

Many studies have compared the performance of PET estimation methods under different climatic conditions zone (Nonki, 2014; Djaman et al., 2015, 2019) and they found significant difference between them. Although significant differences exist in estimating PET with different methods, there is not a clear consensus concerning the impact of PET estimation methods on stream flows simulations. Some authors found that the hydrological model is insensitive to PET input (Oudin et al., 2005, 2006; Wang et al., 2006; Jung et al., 2014; Spies et al., 2015; Bai et al., 2016), while another found that the simulated streamflow is strongly depended on the PET input (Vazquez and Feyen, 2003; Andreassian

et al., 2004; Samains and Pauwels, 2013). Consequently lack of consensus concerning the approach of sensitivity analysis (dynamic or static approach) as suggested by Andreassian et al. (2004) and Oudin et al. (2006), and also the use of the raw and rescaling PET inputs in the sensitivity studies. As far it is important to continuous search to improve our understanding about the influences of PET estimation methods on the hydrological modeling, here we evaluate the impact of PET estimation methods on the model parameters and efficiency of the hydrological model follow the dynamic and static sensitivity analysis approaches.

1. A dynamic sensitivity studies involve a re-calibration of the hydrological model using the raw and perfect PET estimation methods. The best set of optimized model parameter obtained using each PET methods is then used to compute the streamflow during the validation period and the model sensitivity is assessed by comparing modeled streamflows using each PET methods and observed streamflows.

2. A static sensitivity studies consist to calibrate the model with a perfect PET considered to be optimal. The best set of optimized parameters is leaving unchanged and the modeled streamflows is computed during the validation period using raw and perfect PET methods. Model sensitivity is then assessed by comparing modeled streamflows simulated using each PET methods and observed streamflows.

The comparison between modeled and measured streamflow is assessed here by using, in addition to NSE, RSR and R^2, the cumulative balance error (CB, Oudin et al., 2005) given by the following equation:

$$CB = 1 - |1 - \frac{\sum_{t=1}^{n} Q_{sim,t}}{\sum_{t=1}^{n} Q_{obs,t}}| \tag{2.23}$$

CB is used to compute the significant average values and to measure the ability of the model to successfully simulate streamflow volumes over the studied period. His range between $-\infty$ to $+1$, with optimal value equal to 1.

2.3.6.1 Different PET estimation methods used in this research

PET is calculated by using several methods that are applied to the mean daily data. These include two combinative methods (Penman, Priestley-Taylor), twelve radiation-based methods (Global Radiation, Net Radiation, Hargreaves-Samani, Trajkovic, Berti, Ravazzani, Makkink, McGuinness-Bordne, Jensen-Haise, Turc, Abtew, Caprio) and five temperature-based methods (Schendel, Thornthwaite, Hamon, Blaney-Criddle, Romanenko). However, the Penman PET data were used as the standard method to estimate daily PET because it is usually considered as the most appropriate by many hydrologists (Jensen et al., 1990; Shuttleworth, 1993). The selected PET methods were based on different climatic data need and available in the study area and on their performance tests and eval-

uations under Sahelian climate condition (Djaman et al., 2015). Methods used, formulation, and references can be found in Table 9.

Table 9: Different PET estimated methods used in this work (brief description in the text)

Methods name	**Formulation**	**References**
Penman (PEN)	$PET = \frac{\Delta\, R_n + \gamma\,(e_s - e_a) E_a}{\lambda\rho(\Delta+\gamma)}$ where $E_a = 2.63(1 + 0.536U)$	Penman, 1948
Priestley-Taylor (PT)	$PET = \frac{\alpha_{pt}\Delta\, R_n}{(\Delta+\gamma)\lambda}$, where $\alpha_{pt} = 1.26$	Oudin et al., 2005
Schendel (SCH)	$PET = 16\frac{T_a}{R_h}$	Djaman et al., 2015
Thornthwaite (TH)	$PET = 1.067\frac{N}{24}(\frac{10T_a}{I})^k$, where $I = \sum_{m=1}^{12}(\frac{T_m}{5})^{1.514}$ $k = 0.49 + 1.8(\frac{I}{100}) - 0.77(\frac{I}{100})^2 + 0.67(\frac{I}{100})^3$	Federer et al., 1996
Hamon (HAM)	$PET = 715.5\frac{N}{24}\frac{e_s}{(T_a+273.2)}$	Federer et al., 1996
Blaney-Criddle (BC)	$PET = k\frac{n}{N}(0.46T_a + 8.13)$ where $k = 0.45$	Oudin et al., 2005
Romanenko (RO)	$PET = 4.5(1 + \frac{T_a}{25})^2(1 - \frac{e_a}{e_s})$	Oudin et al., 2005
Global Radiation (GR)	$PET = -0.611 + 0.149\,R_g + 0.079\,T_a$	Irmak et al., 2003
Net Radiation (NR)	$PET = 0.489 + 0.289\,R_n + 0.023\,T_a$	Irmak et al., 2003
Hargreaves (HAR)	$PET = 0.0023\,\frac{R_a\sqrt{(T_{\max}-T_{\min})}}{\lambda}(T_a + 17.8)$	Xu and Singh, 2002
Trajkovic (TRA)	$PET = 0.0023\,\frac{R_a(T_{\max}-T_{\min})^{0.424}}{\lambda}(T_a + 17.8)$	Djaman et al., 2015
Berti (BER)	$PET = 0.00193\,\frac{R_a(T_{\max}-T_{\min})^{0.517}}{\lambda}(T_a + 17.8)$	Djaman et al., 2015
Ravazzani (RAV)	$PET = (0.817 + 0.00022Z)0.0023\,\frac{R_a(T_{\max}-T_{\min})^{0.5}}{\lambda}(T_a + 17.8)$	Djaman et al., 2015
Makkink (MA)	$PET = \frac{1}{\lambda}\left(0.7\,\frac{R_g\Delta}{(\Delta+\gamma)}\right)$	Xu and Singh, 2002
McGuinness-Bordne (MB)	$PET = \frac{R_a}{\lambda}\left(\frac{T_a+5}{68}\right)$	Oudin et al., 2005
Jensen-Haise (JH)	$PET = \frac{R_g(0.025\,T_a+0.08)}{\lambda}$	Xu and Singh, 2002
Turc (TU)	$PET = 0.013\frac{T_a}{T_a+15}(23.8846R_g + 50)(1 + \frac{50-R_h}{70})$ if $R_h > 50$, $PET = 0.013\frac{T_a}{T_a+15}(23.8846R_g + 50)$	Kostinakis et al., 2011
Abtew (AB)	$PET = 0.53\,\frac{R_g(1-\alpha)}{\lambda}$	Oudin et al., 2005
Caprio (CA)	$PET = \frac{6.1}{10^{-9}}R_g(1.8T_a + 1.0)$	Kostinakis et al., 2011

In Table 9, Δ is the slope of saturation vapor pressure versus air temperature curve ($KP_a.^oC^{-1}$); R_n is the mean daily net radiation ($MJ.m^{-2}.day^{-1}$); R_g the mean daily global radiation ($MJ.m^{-2}.day^{-1}$); γ the psychometric constant (0.0671 $KP_a.^oC^{-1}$ for 29.3m elevation (Z)); T_a the mean daily air temperature at 2m height [($T_a = (T_{max}+T_{min})/2$), ^oC]; T_{max} the daily maximum air temperature (^oC); T_{min} the daily minimum air temperature (^oC); T_m the mean monthly air temperature (^oC); e_s is the saturation vapor pressure KP_a; e_a the actual vapor pressure (KP_a) and $e_s - e_a$ the saturation vapor pressure deficit (KP_a). α=0.22 is the albedo for Savannah vegetation surface. R_h is the mean daily relative humidity; n the mean daily sunshine duration ($hour$). $\frac{n}{N}$ is the relative sunshine duration [$-$] where N represents maximum possible sunshine duration in a day or daylight hours. The latent heat of vaporization (λ) was taken as 2.45 [$MJ.K_g^{-1}$] and R_a is the extraterrestrial radiation ($MJ.m^{-2}.day^{-1}$). Brief description and equation for all the constant are given in Allen et al. (1998) and Nonki (2014).

The difference between those PET estimation methods was assessed by comparing PET values computed using each PET method and Penman's PET values considered here as the perfect PET method by using different statistical criteria such as Mean Bias (MB), RMSE, PBIAS, Standard Error of Estimation (SEE; Irmak et al., 2003 and Mean Ratio (MR; Djaman et al., 2015). Their equations

are given as follow:

$$MB = \frac{1}{n}\sum_{t=1}^{n}(x_i - y_i) \tag{2.24}$$

$$RMSE = \sqrt{\frac{\sum_{t=1}^{n}(x_i - y_i)^2}{n}} \tag{2.25}$$

$$SEE = \sqrt{[\frac{1}{n(n-2)}][n\sum_{i=1}^{n} y_i^2 - (\sum_{i=1}^{n} y_i)^2 - \frac{[n\sum_{i=1}^{n} x_i y_i - (\sum_{i=1}^{n} x_i)(\sum_{i=1}^{n} y_i)]^2}{n\sum_{i=1}^{n} x_i^2 - (\sum_{i=1}^{n} x_i)^2}]} \tag{2.26}$$

$$MR = \frac{1}{n}\sum_{i=1}^{n}\frac{y_i}{x_i} \tag{2.27}$$

where x_i is the Penman estimated PET; y_i is PET estimated by other equations in the time step i and n is the number of time step.

2.3.6.2 Rescaling factor of PET estimates to avoid systematic biases

Some PET formulas listed in Table 9 give mean accumulated PET values different from those given by the original Penman formula. In order to achieve similar accumulated PET values over the tested periods due to these under- or over-estimations which may yield systematic errors on stream flow simulations, we chose to apply a rescaling factor given by Oudin et al. (2005) for each formula in order to fit the annual mean Penman PET value by the following relation:

$$PET_{rescaling,j} = \frac{\sum_{j=1}^{n} PET_{Penman,j}}{\sum_{j=1}^{n} PET_{formula,j}} \times PET_{formula,j} \tag{2.28}$$

where $\sum_{j=1}^{n} PET_{Penman,j}$ is the sum of daily Penman PET, $\sum_{j=1}^{n} PET_{formula,j}$, $PET_{rescaling,j}$, $PET_{formula,j}$ represent respectively the sum of daily PET, the daily rescaling PET and daily PET computed using different methods.

Introducing this scaling factor, only the relative importance of PET fluctuations over the studied period for each PET method is tested, and thus to identify which atmospheric parameters would lead to the best temporal fluctuations in the evolution of the watershed evaporative demand. It also allows us to focus on the seasonal cycle of each formula in order to avoid the effects of systematic biases.

2.3.7 REMO model evaluation and performance assessment

Evaluation of a model is a process which determines how well the model's predictions are consistent with reality (Jørgensen and Bendoricchio, 2001) and the degree to which the model gives the users a realistic description of the real world. In this research, the ability of the REMO model to simulate present climate (1983–2005) was assessed by comparing the annual cycle of outputs of the REMO model with observational and reanalysis datasets and computed some statistic performance criteria such as the Root Mean Square Error ($RMSE$), Mean Bias (MB) and correlation coefficient (R^2).

2.3.8 Evaluation of climate change signal on hydro-climatic variables

The climate change signal (CCS) can be defined as the difference between the mean climatological values of the future and reference (or present, or baseline or historical) period. In this study, we defined two future periods termed mid of the 21st century (2041-2065) and late 21st century (2071-2095), while baseline period was spans from 1981-2005 as adopted by Tamoffo et al. (2018).

For each climate variable and water balance components simulated by the HBV-Light hydrological model, the CCS is computed as follows:

$$CCS = X_{future} - X_{present} \tag{2.29}$$

$$CCS(\%) = \frac{(X_{future} - X_{present})}{\overline{X_{present}}} \times 100 \tag{2.30}$$

where X_{future} and $X_{present}$ respectively represent the climatic or hydrological variables in the future and baseline period, and $\overline{X_{present}}$ is the average of this variable over the baseline present.

A positive value of CCS indicates an increase of the considerate climatic or hydrological variable, while a negative value indicates a decrease.

2.3.9 Hydropower potential estimation of the Lagdo Dam and his future change

Hydropower is energy from water sources such as the ocean, rivers and waterfalls. It is an efficient, reliable, and renewable source of energy, specially in developing countries like Cameroon, where hydropower potential is the main source of electricity production. It also represents an useful tool to reduce the atmospherics greenhouse gas concentrations caused by human activities. The cost of hydroelectricity is relatively low, making it a competitive source of renewable electricity. However, it is the most sensitive industry to the global warming, mainly because climate change will directly affect the quality, quantity of water resources (streamflow and runoff), which are the important drivers of hydropower potential.

The hydropower potential is the total energy from all natural runoff at stream gradient over the entire domain. It is achieved by converting the potential and kinetic energy of the water into electrical energy by electro-mechanical means (Turbines and Generators). The two vital factors to consider are the flow and the head of the stream or river. The flow is the volume of water which can be captured and re-directed to turn the turbine generator, and the head is the distance the water will fall on its way to the generator (see Fig. 16)

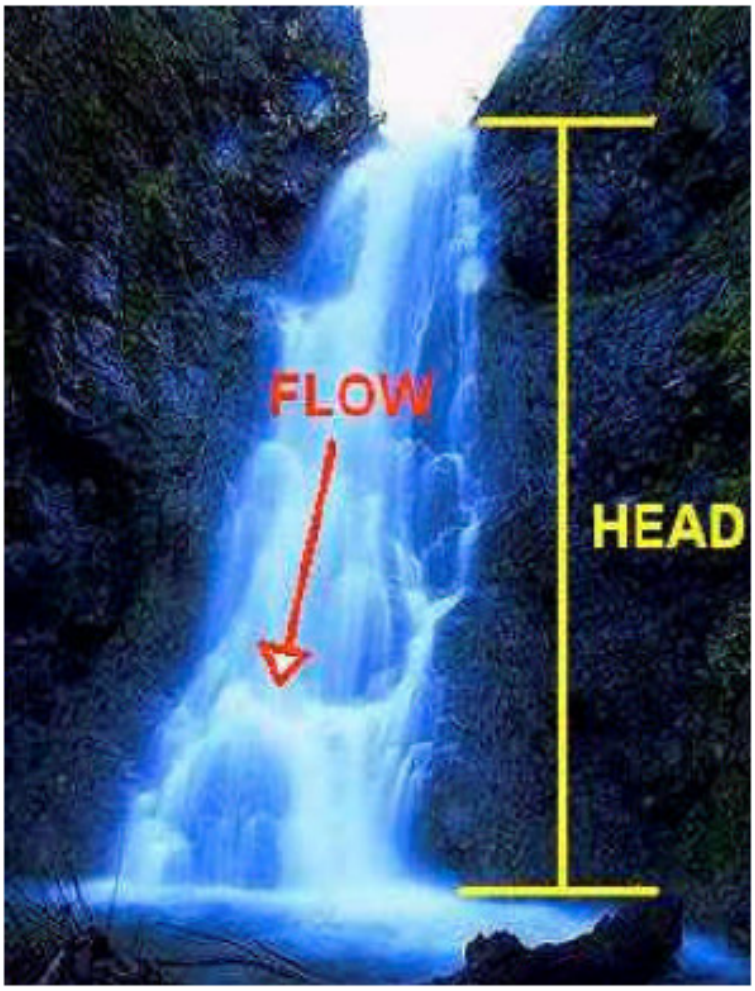

Figure 16: *Vital factors considered for hydropower generation.*

2.3.9.1 Mathematical formulation of the hydropower potential

The hydropower potential is computed follow different steps:

- Let us consider a volume of water dV that moves from position 1 to position 2, the work done by this volume of water is given by the following equation:

$$dW = \rho_w \times g \times dV \times H \tag{2.31}$$

  where dW is the Work done by mass of water in Joules, ρ_w is the water density in $k_g.m^{-3}$, g is the acceleration due to gravity, dV is a volume of water and H is the Vertical distance moved by the volume of water.

  This equation actually represents the energy that the volume of water has at position 1 with respect to position 2.

- Now, if this volume of water takes some time dt to move from 1 to 2, then the flow of water Q is determined as:

$$Q = \frac{dV}{dt} \tag{2.32}$$

- But the power extracted by the water is the rate of work done and can be mathematically written as:

$$P = \frac{dW}{dt} \tag{2.33}$$

After substituting equation 2.31 in equation 2.33, we obtain:

$$dp = \frac{\rho_w \times g \times dV \times h}{dt} \tag{2.34}$$

Equation 2.31 can also be written as $dV = Q \times dt$, therefore the previous equation can now be written as:

$$dp = \frac{\rho_w \times g \times Q \times dt \times H}{dt} \tag{2.35}$$

which after integration over time reduces to:

$$P = \rho_w \times g \times Q \times H \tag{2.36}$$

This equation actually gives the theoretical power expressed in Watts (W).

- Therefore, the actual output is reduced by the fact that the turbine and generator have losses in transforming the potential and kinetic energy into mechanical and electrical energy. Thus actual power output will be obtain using the following equation (de Oliveira et al., 2017):

$$N_p = \rho_w \times g \times Q \times H \times \eta \tag{2.37}$$

where N_p is the hydropower potential (W), ρ_w is the water density in (Kg/m^3), g is the acceleration due to gravity in (m/s^2), Q is the discharge through turbine in $((m^3/s))$, H is the Gross head in (m) known as elevation difference between headwater and tail water, and η is the overall plant efficiency.

2.3.9.2 Potential impacts of climate change on hydropower potential

Through Equation 2.37, reference and future simulated streamflows obtained by using the calibrated HBV-Light hydrological model were used to estimate the reference and future hydropower potential of the Lagdo dam. The potential impact of climate change on hydropower potential was computed by using the Equations 2.29 or 2.30.

2.3.10 Ecohydrological status of the watershed: the concept of water-energy budget

An ecohydrologic analysis of the watershed known as a concept of water-energy budget (Tomer and Schilling, 2009; Milne et al., 2002) is the approach used to evaluate the efficiency of water and energy used by an ecosystem, defined here as the vegetation within a watershed. It is also used to test the

validity in assessing the interaction between increase PET and precipitation change as projected by the RCM-GCM model. It is determined by plotting the unused water (P_{ex}, given by Equation 2.38) against unused energy (E_{ex}, given by Equation 2.39) in the watershed (Yira et al., 2017).

$$P_{ex} = \frac{(P - AET)}{P} \tag{2.38}$$

$$E_{ex} = \frac{(PET - AET)}{PET} \tag{2.39}$$

where P_{ex} is the unused water; E_{ex} is the unused energy; P is the precipitation; AET is the actual evapotranspiration; and PET is the potential evapotranspiration.

The shift in this status relative to the reference period detects the climate change signal, while the direction of the shift indicates whether the catchment experienced water stress or increased humidity (see Fig. 17).

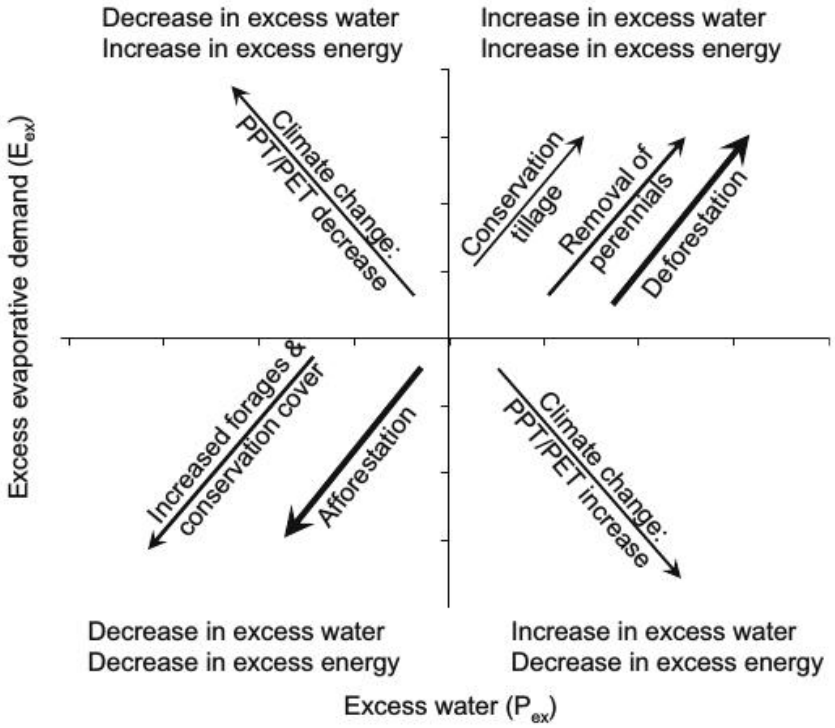

Figure 17: *Conceptual model of ecohydrological shifts associated with changes in climate and land use.(adopted from Tomer and Schilling, 2009).*

This concept is also used to assess the change of streamflow as response of climate or land use changes (Tomer and Schilling, 2009). Changes in land use will typically cause ecohydrologic shifts towards increased P_{ex} and E_{ex}, or decreased P_{ex} and E_{ex}. Changes in climate are required to cause increased P_{ex} and decreased E_{ex} (due to increase in P/PET ratio in time) or decreased P_{ex} and increased E_{ex} (due to decrease in P/PET ratio in time). The direction of change in the P/PET ratio indicates whether climate change results in increased or decreased humidity and precipitation at the regional scale.

Conclusion

In this chapter, we began with a detailed description of the study area. Next, we proposed an observation-Modeling framework to quantify the effect of climate change on water balance components and hydropower potential. The main parts of this framework are a hydrological model that can simulate the observed streamflow, a RCM model that can downscale the GCMs, and the mathematical formulation of the hydropower potential. The basic requirements of the framework are observed data: meteorological data of the entire period to run the hydrological model; hydrological data to assess the sensitivity and uncertainty analysis of the model parameter, and to calibrate and validate the hydrological model; and the observation and reanalysis data to evaluate the performance of the RCM model to simulate present climate in the study site.

Chapter 3

Results and discussions

Introduction

The purpose of this chapter is to present the results obtained with the observation-Modeling framework presented in the previous chapter. This includes the results of the hydrological modeling in the first part, the sensitivity analysis of PET inputs for the model simulations results in the second part, the results of climate change impacts assessment on the HBRB in the third part. The assessment includes an analysis of the performance of the REMO RCM for the main climate variables at the basin level, projections of water balance components and hydropower potential for the HBRB under climate change (monthly, seasonal and annual), and ecohydrologic status of the watershed.

3.1 Hydrological modeling results

This section presents the results of the hydrological modeling in the headwaters of the Benue River Basin. Sensitivity analysis, parameter identifiability, uncertainty analysis, parameter optimization, stream flows for calibration and validation periods, and statistical performance of the model are performed. Results show, in general, good model performance in representing the hydrological dynamic of the study basin.

3.1.1 Individual sensitivity analysis

Figures 18 and 19 represent the individual sensitivity analysis of each parameter to PBIAS and RSR respectively in the different gauging stations of the HBRB. The results indicate that the recession coefficients (K_0, K_1, K_2), the percolation coefficient (PERC) and the upper reservoir threshold (UZL) parameters are insensitive to the PBIAS (Fig. 18) in the different gaging stream stations. In addition, a routing routine parameter MAXBAS is insensitive to PBIAS in the Buffle Noir gaging station. Thus they are non-influential parameters to the total volume balance error of this catchment. On the other

hand, the soil and evaporation routine parameters (FC, β and LP), in addition with the recession coefficient (K_1) and the transformation routine parameter (MAXBAS) are the most or less influential parameters for RSR (Fig. 19), thus influence the high-flow series of the catchment. But the soil and evaporation routine parameters (FC, β and LP) are more sensitive to the volume balance error than to the high-flow series, while the recession coefficient (K_1) is the only routine response parameter most sensitive to high-flow series.

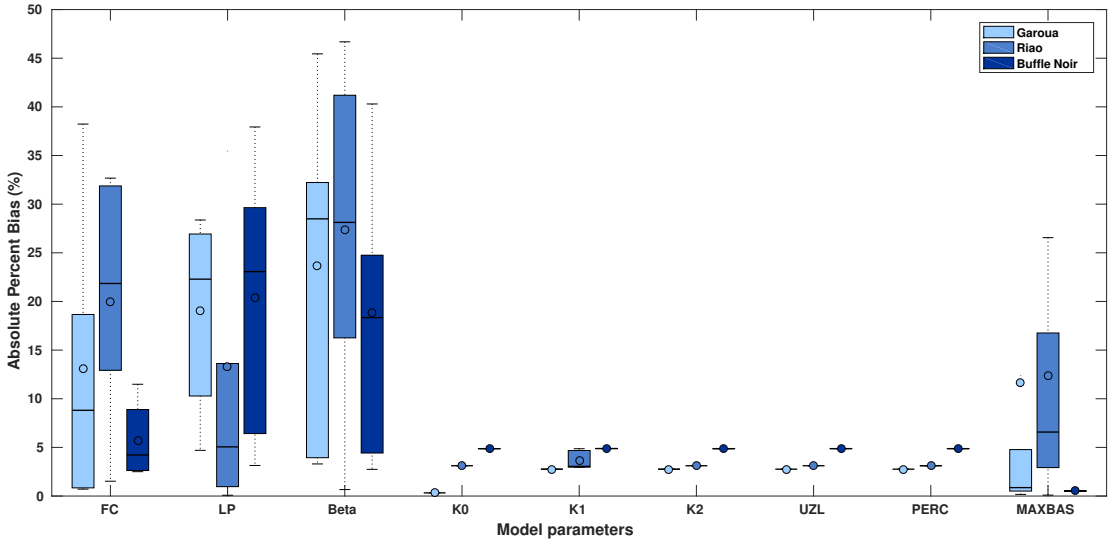

Figure 18: *Sensitivity boxplot of parameters with reference to PBIAS objective function.*

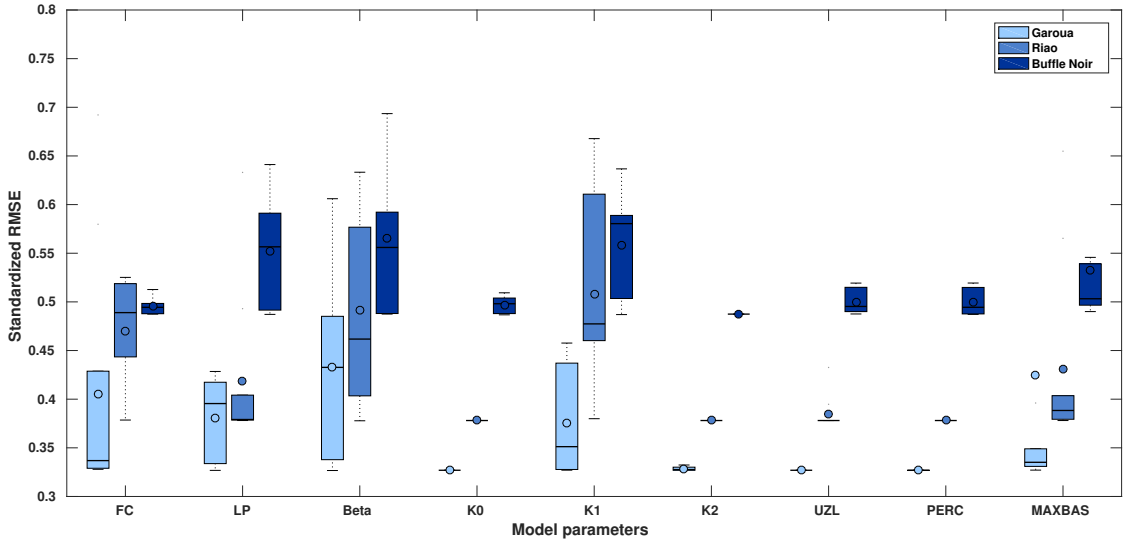

Figure 19: *Sensitivity boxplot of parameters with reference to RSR objective function.*

From the model structure and formulation, FC, β and LP are the parameters that control the water filling in the soil (infiltration), water lost (evapotranspiration) and water runoff. Thus, they

influence the volume balance more than the high-flow series (Table 10). Specifically, considered as key parameter in partitioning precipitation into soil moisture and runoff, a low value of FC implies that the soil water storage capacity is very low and means that there is a small quantity of water available for evapotranspiration and vice versa. This makes FC the main parameter to control volume error and thus the sensitivity of this parameter to the PBIAS measure. As a parameter β is an exponent of the ratio between soil moisture and his maximum value (FC), it represents the relative contribution of precipitation to runoff at a given soil moisture deficit. For specific amount of soil moisture, the higher value of β parameter implies the lower runoff, and vice versa. Then, it influences the amount of soil moisture available for evapotranspiration and therefore strongly affects the volume error and high-flow series. LP parameter, which controls the amount of water lost based on soil moisture deficiency, influences both volume error and high-flow series because, when LP is close to 1, the actual evapotranspiration will be higher, and vice versa.

Also based on model formulation, it is evident that parameters K_0, K_1, K_2, $PERC$ and UZL control the response routine, thus will influence the high-flow series than total volume error. But K_0, K_2, $PERC$ and UZL parameters are non-influential parameters for high-flow series and volume balance error. Specifically, K_0 controls the surface runoff when an effective precipitation is above threshold value UZL. Given the fact that the study catchment is a semi-arid zone (Guenang and Mkankam, 2012) where precipitation is absent during sixth to eight months on the year (Dassou et al., 2016), the received precipitation only contributes to the water feeling the soil box, water loosed and water feeling the upper runoff reservoir without exceed his threshold value UZL, thus only contributes to subsurface runoff. Therefore, the parameter KO that controls the surface runoff and the UZL parameter are non-influential parameters for both high-flow series and volume balance error, while the parameter K_1 that controls the subsurface runoff is sensitive to high-flow series. In addition, the percolation parameter $PERC$ which plays a simple role of partitioning the effective precipitation between the two runoff reservoirs based on the soil characteristics does not have an effect on both high-flow series and total volume error; while K_2 parameter, which controls the groundwater runoff or base flow, and which is relatively low compared to K_1 parameter is less sensitive to high-flow series and not sensitive to total volume error.

Table 10: *Statistical evaluation of the dispersion of PBIAS and RSR due to the variation of each model parameter (StD=Standard deviation; CV=Coefficient of variation).*

	Garoua outlet																	
Evaluation	**FC**		β		**LP**		**k0**		**k1**		**k2**		**UZL**		**PERC**		**MAXBAS**	
criteria	StD	CV(%)	StD	CV(%)	StD	CV(%)	StD	CV(%)	StD	CV(%)	StD	CV(%)	StD	CV(%)	StD	CV(%)	StD	CV(%)
PBIAS	13.33	102.2	8.66	45.45	15.24	64.42	0.0	0.0	0.0	0.0	0.0	0.0	0.0	0.0	0.0	0.0	29.12	249.25
RSR	0.13	31.58	0.04	11.02	0.09	22.02	0.0	0.0	0.05	14.15	0.002	0.59	0.0	0.0	0.0	0.0	0.26	62.13
	Riao outlet																	
PBIAS	12.0	60.19	19.52	148.79	16.53	60.38	0.0	0.0	0.86	23.62	0.001	0.03	0.004	0.12	0.0	0.0	17.16	133.71
RSR	0.05	11.52	0.08	19.95	0.1	20.79	0.0	0.0	0.1	20.34	0.0	0.0	0.02	4.53	0.0001	0.06	0.1	22.55
	Buffle Noir outlet																	
PBIAS	3.37	59.63	12.99	63.65	13.26	70.51	0.0	0.0	0.03	0.53	0.004	0.07	0.002	0.04	0.002	0.04	15.34	123.72
RSR	0.008	1.61	0.06	10.64	0.07	12.84	0.009	1.77	0.05	9.17	0.0	0.0	0.013	2.56	0.014	2.71	0.076	14.26

Overall, we found that for the nine parameters that represent the main components of hydrological processes in the HBV-Light model, four parameters (FC, β, LP and $MAXBAS$) are sensitive to a total volume error, while those four parameters in addition to K1 parameter are sensitive to high-flow series in the HBRB. This result is comfortable with those found by Abebe et al. (2010) and Zelelew and Alfredsen (2012). Abebe et al. (2010) used the Monte-Carlo procedure to identify the influential and non-influential model parameters to the model response variations on the HBV model in the semi-humid Leaf River catchment near Collins, Mississippi. They found that the parameters FC, β and LP influence the total volume error, while UZL, K_1, K_0, and $MAXBAS$ parameters that control the response and transformation routines are the parameters that control the high-flow series in this watershed. Zelelew and Alfredsen (2012) used the Sobol's variance-based sensitivity analysis method (VBSA, Sobol, 2001) in the twelve catchments located in Southern Norway to identify the sensitive and non sensitive HBV model parameters on the model simulations. Their results showed that for the fifteen free model parameters, they are four to six influential model parameters for high flow conditions, and up to a minimum of six influential model parameters for low flow conditions.

3.1.2 Parameter identifiability

When the model parameters were sampled simultaneously, for the 50,000 simulations, about 1669, 40 and 1157 model runs gave fits with NSE values above 0.85 in the Garoua and Riao stations and NSE above 0.70 in the Buffle Noir station respectively and identified as behavioral ones. The scatter plots between the behavioral parameters and the values of NSE, which met his threshold value are shown in Figure 20 to Figure 22 , while Figure 23 summarizes the uncertainty of the model parameters. Based on these figures, it is clear that good simulations were obtained within wide ranges of response routine parameters in the different gaging sites, except the recession parameter K_1. Thus, they are ill-defined or non-identifiable parameters in the HBV-Light model because there is not a distinct peak when plotting NSE (vertical axis) against those parameter values (horizontal axis). We also notice that the soil and evaporation routine parameters (FC, LP, β), in addition to recession parameter (K_1) and the routing routine parameter ($MAXBAS$) are found to be more or less well-defined or identifiable parameters in this catchment, with K_1 the most identifiable parameter. A closer look at the formulation of the model shows that these parameters are the most important in their respective model components. The results also reveal that FC shows more sensitivity in individual sensitivity analysis as compared to his identifiability.

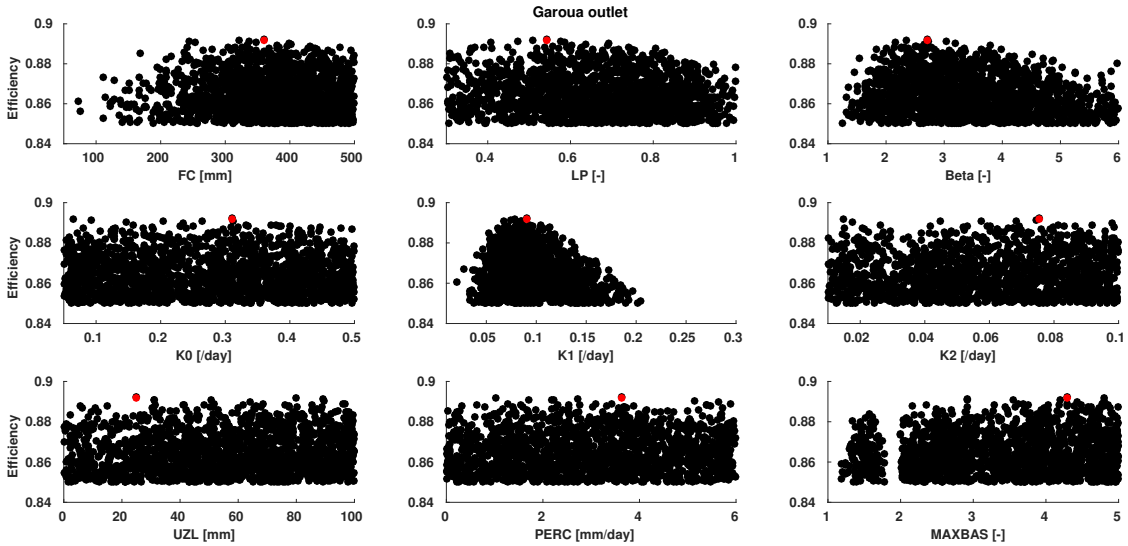

Figure 20: *Distribution of acceptable simulations of the nine model parameters after 50000 model runs at the Garoua gage station (each point represents one model run and the red points represent the optimal values of the objective function (NSE)).*

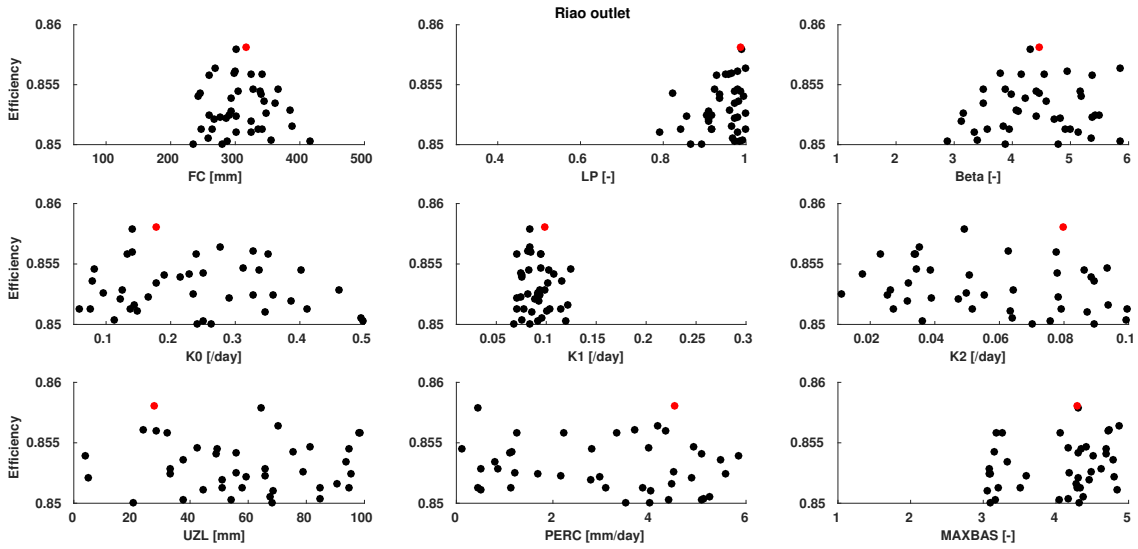

Figure 21: *Same as Figure 20 but at Riao gage station.*

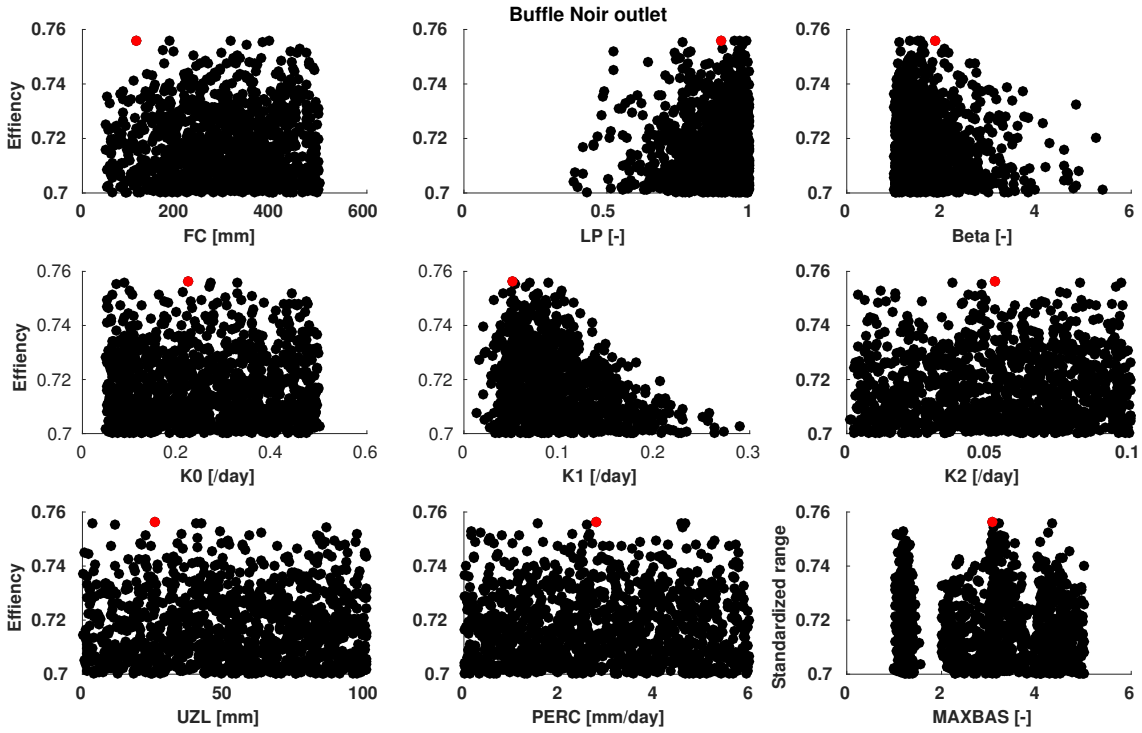

Figure 22: *Same as Figure 20 but at Buffle Noir gage station.*

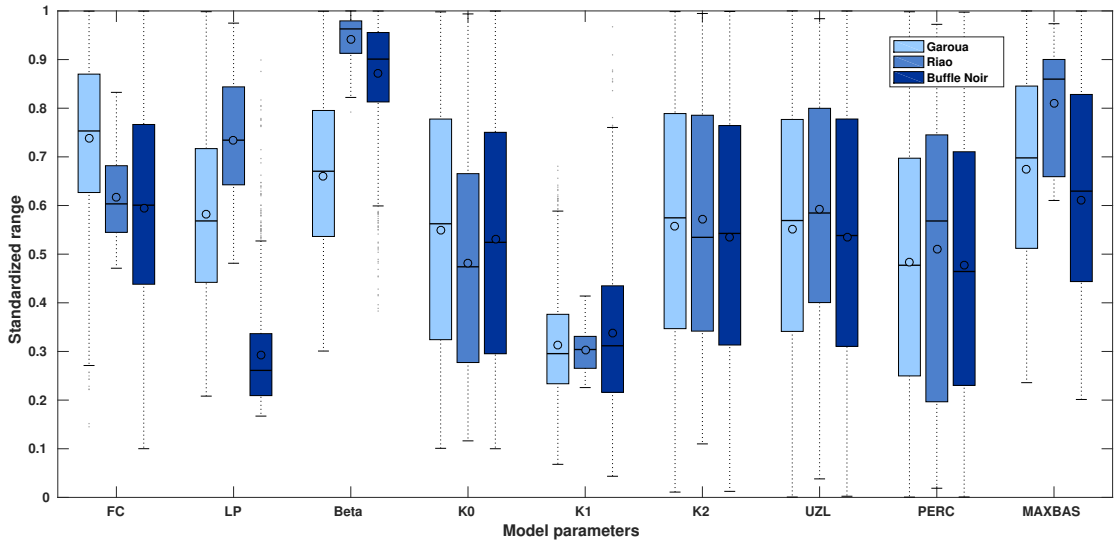

Figure 23: *Summary of the uncertainty of the model parameters, the standardized range refers to the ranges used for the Monte Carlo procedure (Table 3).*

In order to confirm this result, we expressed the uncertainty range of each parameter for acceptable simulations by the 95% confidence intervals and the coefficient of variation (CV) and consigned in Table 11.

Table 11: 95% confidence intervals and variation coefficients of model parameters.

Parameter	Garoua			Riao			Buffle Noir		
	95% confidence internal	**Mean value**	**CV (%)**	**95% confidence internal**	**Mean value**	**CV (%)**	**95% confidence internal**	**Mean value**	**CV (%)**
FC	186.6 - 491.3	368.8	22.6	239 - 401.9	308.1	14.2	78.3 - 485.8	269.7	37.1
LP	0.34 - 0.95	0.66	25.4	0.8 - 1	0.94	5.5	0.58 - 0.1	0.87	12.8
β	1.7 - 5.7	3.5	31.1	3 - 5.8	4.41	17.8	1.03 - 3.55	1.75	39.1
K_0	0.06 - 0.49	0.27	47.05	0.067 - 0.5	0.24	50.5	0.059 - 0.49	0.27	49.6
K_1	0.047 - 0.17	0.094	33.8	0.069 - 0.12	0.091	16.3	0.037 - 0.21	0.101	45.6
K_2	0.007 - 0.098	0.056	48.3	0.014 - 0.099	0.057	45.1	0.0055 - 0.097	0.053	51.4
UZL	3.27 - 98.3	55.2	49.2	4.3 - 98.2	59.1	43.3	3.5 - 98.6	53.4	52.2
$PERC$	0.14 - 5.8	2.9	57.3	0.28 - 5.7	3.1	57.9	0.13 - 5.8	2.86	59.2
$MAXBAS$	1.44 - 4.9	3.37	30.6	3.1 - 4.9	4.05	15.5	1.09 - 4.9	3.06	38.9

Table 11 shows that the confidence intervals for acceptable simulations of ill-defined parameters were not significantly smaller than their initial ranges (Table 3), while the more or less identifiable parameters have the confidence intervals relatively smaller than their initial ranges. For example, before uncertainty analysis was performed, the threshold of the upper reservoir (UZL) parameter had the value range [0, 100], but the confidence intervals for the acceptable simulations were [3.7, 98.3] (at Garoua station) and [4.3, 98.2] (at Riao station); while the initial range ([0.01, 0.3]) of the recession coefficient parameter (K_1) become [0.05, 0.17], [0.07, 0.12] and [0.04, 0.21] at Garoua, Riao and Buffle Noir stations respectively. It can also be seen from Table 11 that the CV of the ill-defined parameters were relatively large compared to those of most or less well-defined parameters.

3.1.3 Implications of the parameters uncertainties to the model predictions

Figures 24 and 25 show the results of the model predictions based on the 95% confidence intervals for the acceptable simulations during the calibration and validation periods respectively. These results reveal that the simulations show a less evenly distributed band of uncertainty around the observed streamflows. The results also show that there is a scope for using the Monte-Carlo procedure to calibrate and to increase confidence in parameter estimation procedures and model predictions in the HBRB. In all the gaging stations within the basin area, the best simulation as well as the observed streamflows lie within the uncertainty band of model predictions from low to high flows. Some discrepancies are noticed for the Buffle Noir outlet station where the high flows of the observed streamflows lie outside the uncertainty band. These findings give the merit to the Monte-Carlo procedure in calibrating, optimizing and predicting uncertainties in hydrological models because in this method, the interactions between model parameters are implicitly taken into account (Seibert, 1997; Steele-Dunne et al., 2008; Tshimanga, 2012).

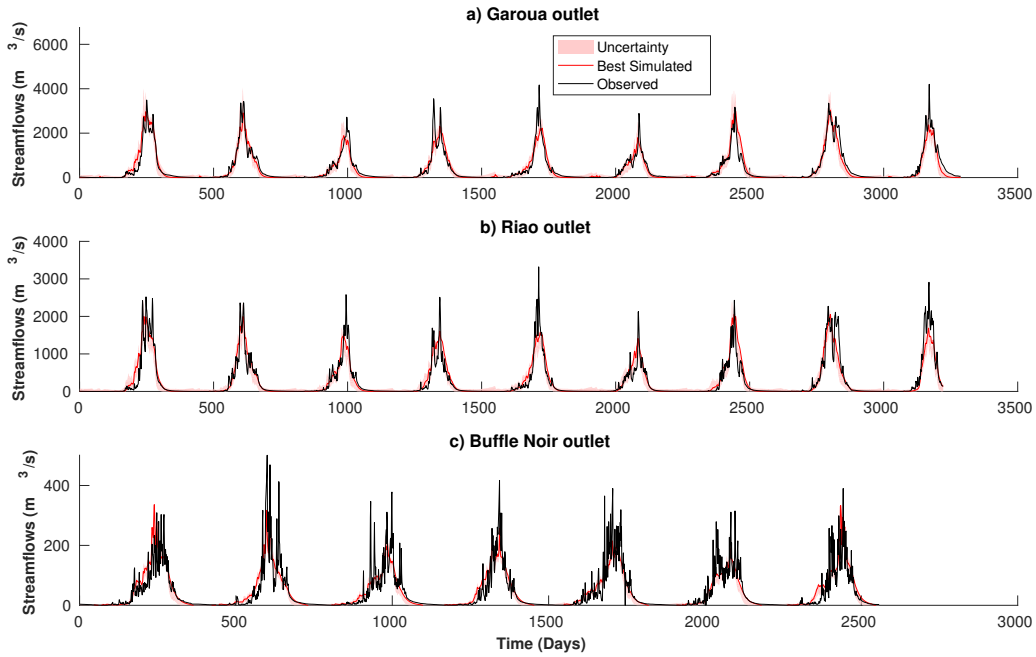

Figure 24: *Uncertainty band on the model simulations during the calibration period (envelope of the standard deviation generated from the mean of the acceptable simulations) as well as measured and best simulated discharge.*

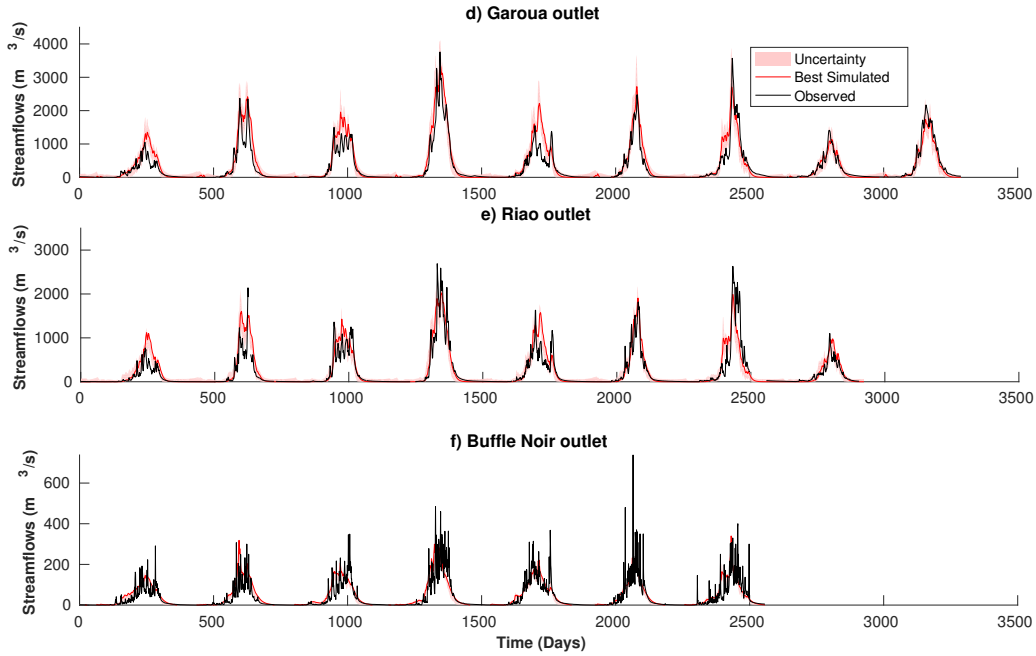

Figure 25: *Uncertainty band on the model predictions (envelope of the standard deviation generated from the mean of the model simulations using the behavioral parameters in the validation period) as well as measured and best simulated discharge .*

3.1.4 Optimal calibration and model performance evaluation

3.1.4.1 Optimized model parameters

Based on the lower and the upper limits of the 95% confidence intervals of the influential model parameters, the model was re-calibrated. After the 50,000 model runs, the best set of optimized model parameter which well performed the simulations in different outlets of the HBRB are given in Table 12. Large values of FC, β and $MAXBAS$ parameters are associated with more damped and even hydrographs, and with the increasing channel length (Steele-Dunne et al., 2008). Based on more damped and even hydrographs in a larger catchment, the recession coefficients (K_0, K_1 and K_2) are expected to decrease with increasing catchment size. The parameter K_0 varies in the opposite way. This can be explained by the fact that this parameter is the non-influential and worst defined parameter in the model structure.

Table 12: Optimized value of model parameter obtained during the recalibration.

Main hydrological Processes	**Parameter**	**Garoua**	**Riao**	Buffle Noir
	FC	313.7	321.05	282.07
Soil and evaporation	**LP**	0.64	0.99	0.98
routine	β	2.99	4.45	1.90
	K_0	0.46	0.42	0.103
Groundwater and	K_1	0.076	0.093	0.077
response routine	K_2	0.0776	0.0365	0.0801
	UZL	59.03	93.06	19.07
	$PERC$	4.45	2.88	2.78
Routing routine	$MAXBAS$	3.92	4.54	3.05

3.1.4.2 Calibration period

Figure 26 illustrates the model performance using daily observed and simulated hydro graphs as well as the flow duration curves during the calibration period at the three gage stations within the basin (Garoua, Riao and Buffle Noir). The model captures reasonably the timing and magnitude of high and low flows, although some bias still exist. The flow duration curves also show that the model reproduces the low flows more accurately than the high flows. Figure 27 shows the average monthly streamflows for the calibration period at different outlets. The model represents the seasonality of hydrological regime well with a maximum obtained in September, although a small difference exists in the Buffle Noir outlet. Relationships between daily simulated and observed streamflows show a strong correlation (Fig. 28), indicating good model performance (correlation greater than 0.90 at different gaging sites). The goodness-of-fit of the model is also supported by other performance criteria which are described with further detail in the statistical analysis section below.

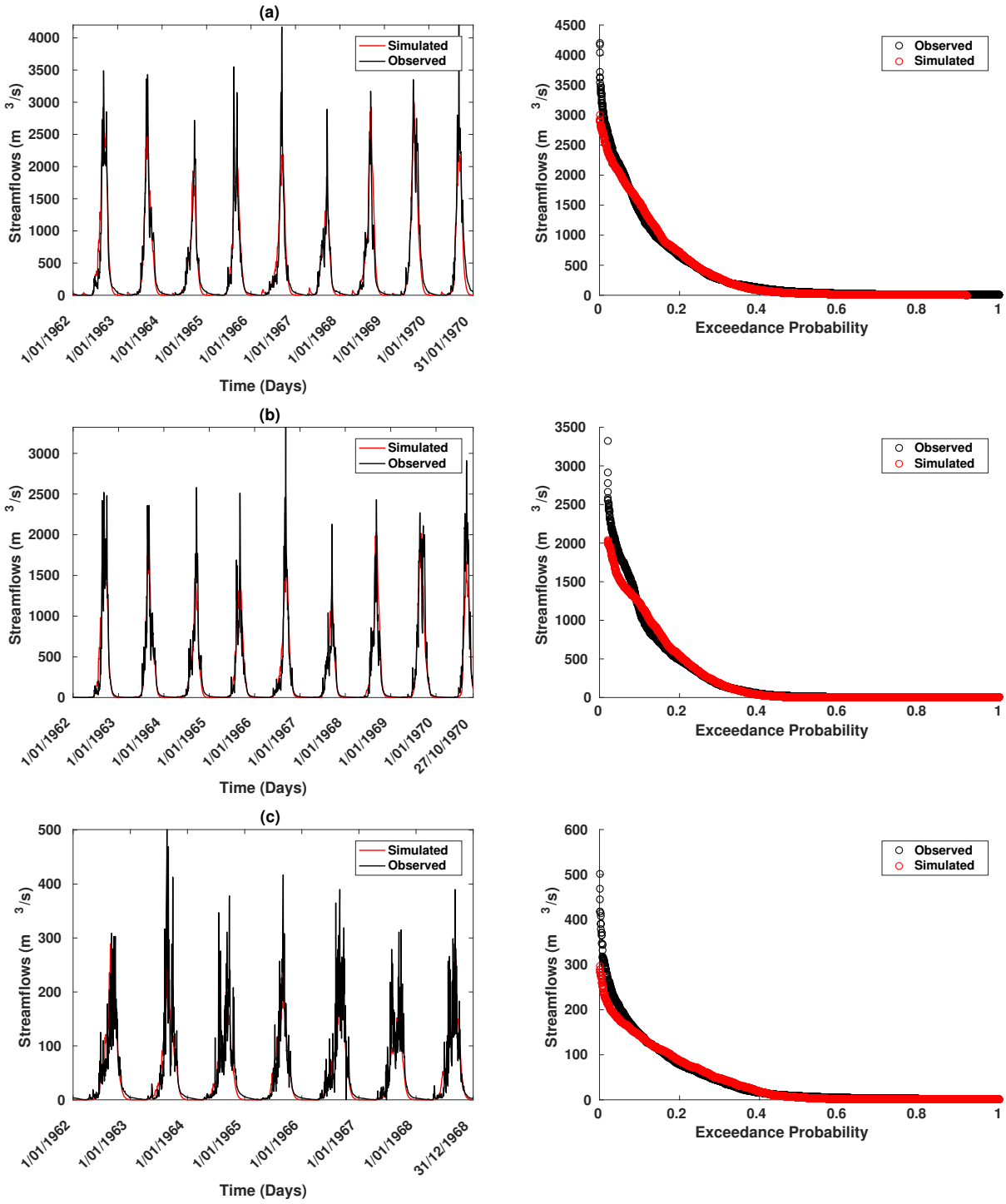

Figure 26: *Comparison between observed and simulated hydro graphs and flows duration curves in the HBRB during the calibration period: a) Garoua, b) Riao and c) Buffle Noir outlets respectively.*

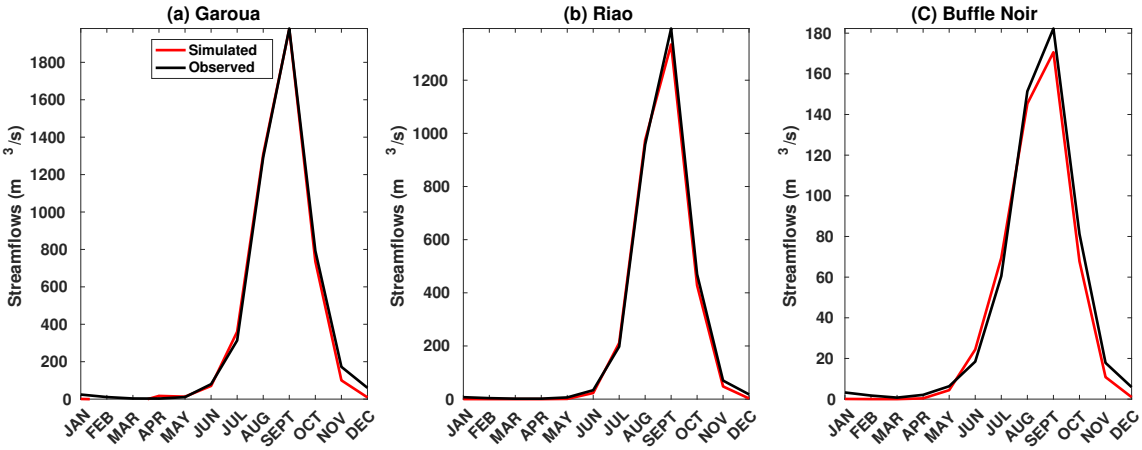

Figure 27: *Comparison between monthly average observed and simulated streamflow for the calibration period in different outlets.*

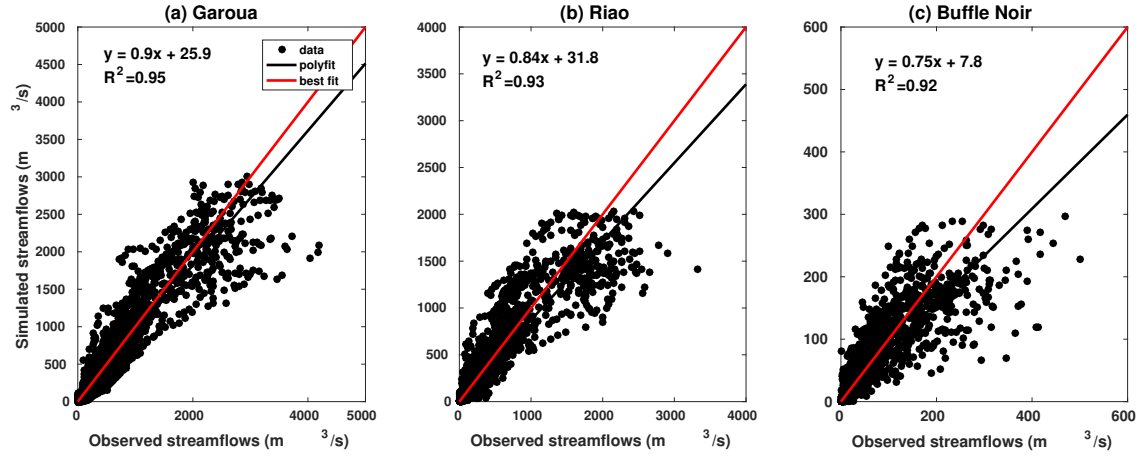

Figure 28: *Relationship between daily observed and simulated streamflow for the calibration period.*

3.1.4.3 Validation period

Figure 29 shows the validated daily streamflows at different control stations. The model reproduced the drought conditions in the basin; estimation of the observed streamflows was less better than the calibration period. Relationship between simulated and measured streamflows shows a strong correlation in the Garoua and Riao control stations (with $R^2 \geq 0.90$), otherwise in the Buffle Noir control station, he shows a less correlation ($R^2 = 0.82$) (Fig. 30). In general, the model exhibits good performance in reproducing the streamflows in all control stations, although some errors in computing high-flow series. In addition, average monthly streamflows for the validation period (Fig. 31) show an excellent model performance, with an exception in August and September where significant difference in magnitude is noted for all control stations.

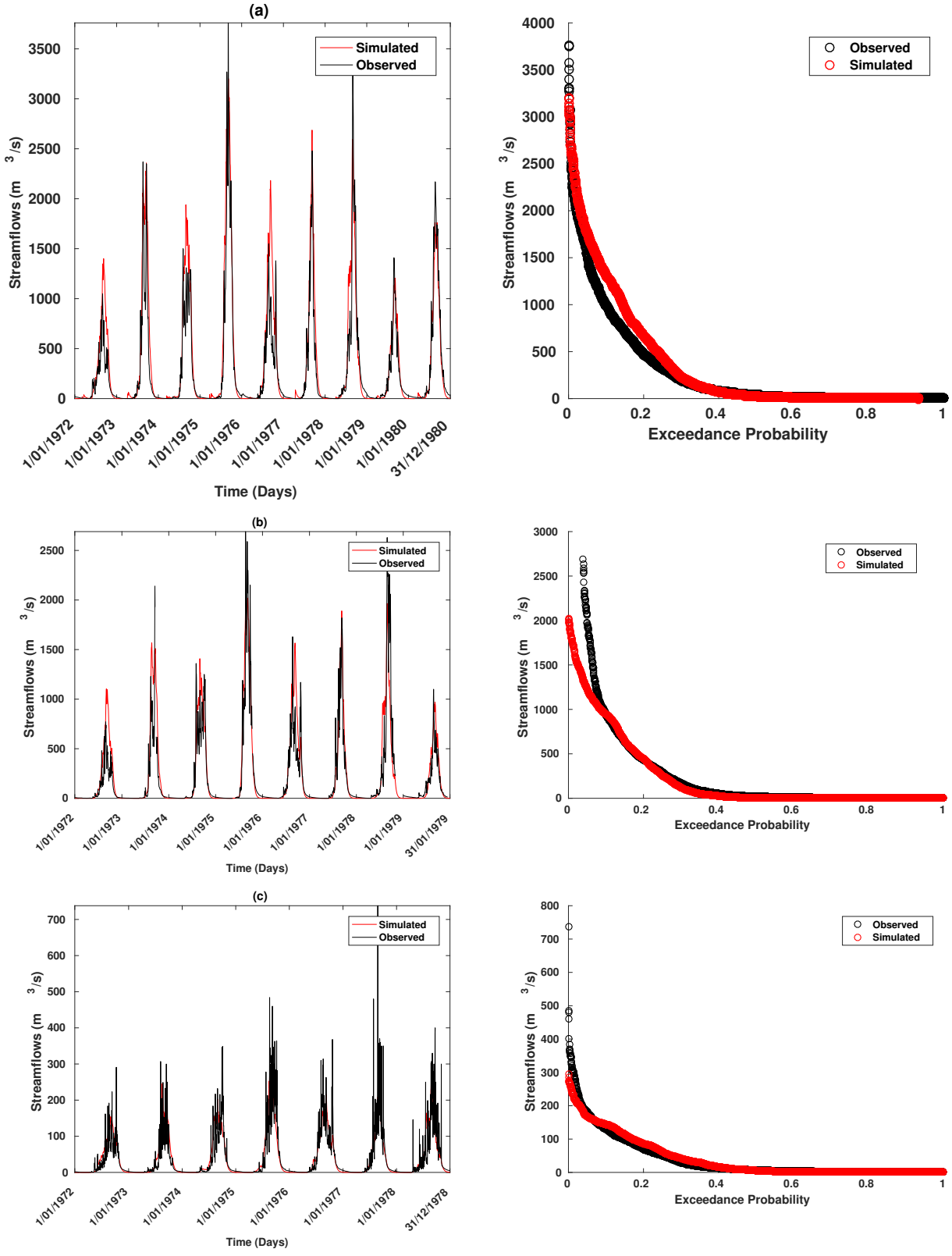

Figure 29: *Comparison between observed and simulated hydro graphs and flows duration curves in the HBRB during the validation period: a) Garoua, b) Riao and c) Buffle Noir outlets respectively.*

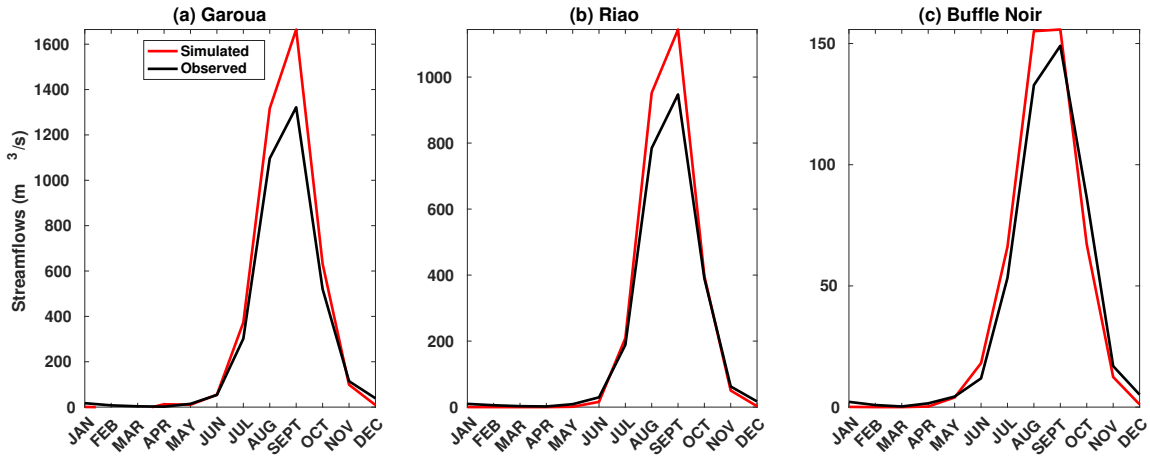

Figure 30: *Comparison between monthly average observed and simulated streamflow for the validation period in different outlets.*

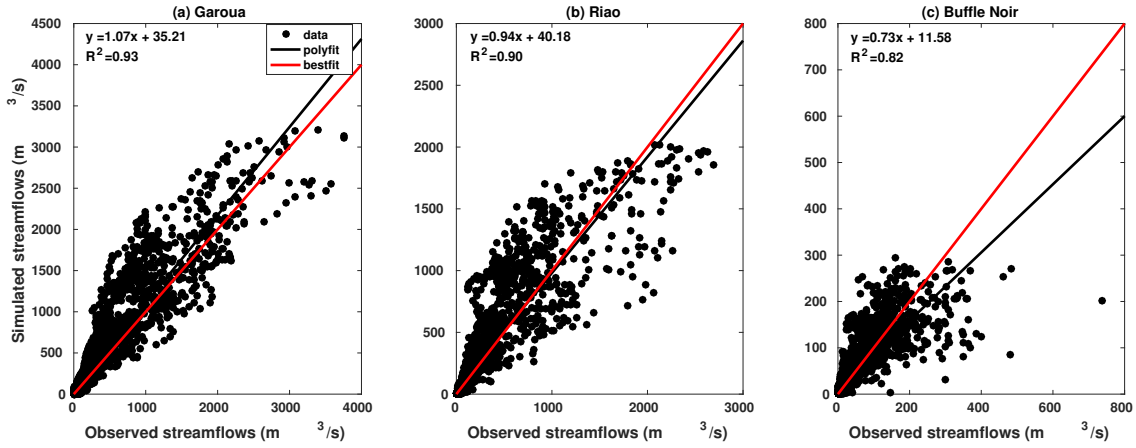

Figure 31: *Relationship between daily observed and simulated streamflow for the validation period.*

3.1.4.4 Statistical analysis

Table 13 gives a statistical summary of the model performance for the calibration and validation periods at all control stations. The model very few overestimates the total runoff volume during the calibration period with a small volume error (less than 8%), while there is an underestimation of the total runoff volume during the validation period at all gaging stations with the volume error relatively high (greater than 15%), except the Buffle Noir outlet. Likewise, Table 13 presents the Nash-Sutcliffe Efficiency (NSE) for daily streamflows ranging from 0.76-0.89 for the calibration period, and 0.66-0.81 for the validation period, indicating good model performance. Comparing to the Table 8, the model performance varies from good to very good. The worst and the best simulations are obtained in the Buffle Noir and Garoua stations respectively. This result was expected because at the Buffle Noir station, the basin has a very clear torrential character. The flow variations are very sudden; each tornado or heavy rainfall gives rise to a distinct flood peak, which can last less than a day. This is

the reason why the hydrograph of the flows in the Garoua and Riao stations during the rainy season is much less serrated than in the Buffle Noir (Figs 26 and 29). The ratio between Root mean square error and observed standard deviation (RSR) ranges from 0.33 to 0.49 and 0.43 to 0.58 for calibration and validation stages, respectively. This reinforced the greater ability of the model to simulate the hydrological characteristics of the basin. In general, the model better performed during the calibration stage than in the validation stage and also more accurate in reproducing the flows in downstream stations than upstream station, as shown by the NSE, RSR, and correlation coefficients. Despite the good performance of the model, errors could be attributed to the uncertainty in estimating of measured streamflows and the average climatology data used for the catchment, as well as the complex hydrological characteristics of the basin (topography and size of catchments).

Table 13: *Summary of statistical results for daily simulated and measured streamflows.*

outlet		**Period**	NSE	R^2	RSR	$PBIAS(\%)$
Garoua	**Calibration**	1961-1970	0.89	0.95	0.33	-3.69
	Validation	1971-1980	0.81	0.93	0.43	18.98
Riao	**Calibration**	1961-1970	0.86	0.93	0.38	-4.21
	Validation	1971-1979	0.78	0.90	0.47	15.01
Buffle Noir	**Calibration**	1961-1968	0.76	0.92	0.49	-7.03
	Validation	1971-1978	0.66	0.82	0.58	3.33

3.2 Sensitivity of hydrological model to PET input

This section presents the results of the sensitivity analysis of model parameters and efficiency due to the variation of the model input especially potential evapotranspiration (PET). Comparison between different PET estimation methods is performed and their impact to the model parameters and efficiency is assessed follow both dynamic and static approaches. Results show, despite the significant differences in PET computation methods, model performance is insensitive and little sensitive to PET input when we follow dynamic and static approaches respectively.

3.2.1 Difference between PET estimation methods

Table 14 shows a statistical summary of the performance of each PET estimation method compared to the Penman method. There is a large spread between PET methods employed. Some methods such as McGuinness-Bordne, Jensen-Haise, Schendel, and Blanney-Criddle methods systematically overestimate the PET (in comparison to the chosen reference given by the Penman formula) with the $PBIAS$ of $28.81\%, 22.20\%, 21.43\%$ and 18.06% respectively. While Abtew, Makkink and Trajkovic methods systematically under-estimate it with the $PBIAS$ of -35.84%, -24.45% and -18.12% respectively.

Table 14: *Performance evaluation of the 18 PET estimation methods at the HBRB.*

Methods name	$PBIAS$ (%)	$RMSE$ ($mm.day^{-1}$)	MB ($mm.day^{-1}$)	SEE ($mm.day^{-1}$)	MR (–)
Priestley-Taylor (PT)	-15.13	1.29	-0.83	0.63	0.86
Schendel (SCH)	21.43	1.51	1.17	0.74	1.24
Thornthwaite (TH)	7.93	2.08	-0.43	1.95	1.06
Hamon (HAM)	16.80	1.34	-0.94	0.58	0.85
Blaney-Criddle (BC)	18.06	1.92	0.99	1.63	1.18
Romanenko (RO)	18.24	1.68	1.00	1.32	1.19
Global Radiation (GR)	-14.04	1.23	-0.77	0.43	0.88
Net Radiation (NR)	-10.96	1.16	-0.60	0.45	0.91
Hargreaves (HAR)	-0.55	0.91	-0.03	0.63	1.02
Trajkovic (TRA)	-18.12	1.36	-0.99	0.46	0.84
Berti (BER)	-12.84	1.16	-0.70	0.56	0.89
Ravazzani (RAV)	-13.41	1.18	-0.73	0.55	0.88
Makkink (MA)	-24.45	1.67	-1.34	0.52	0.77
McGuinness-Bordne (MB)	28.81	1.92	1.58	0.74	1.33
Jensen-Haise (JH)	22.20	1.58	1.22	0.96	1.24
Turc (TU)	-15.32	1.29	-0.84	0.55	0.86
Abtew (AB)	-35.84	2.24	-1.97	0.45	0.66
Caprio (CA)	20.45	1.50	1.12	0.96	1.22

Multi-scale statistics evaluation shows that the Hargreaves-Samani method ($PBIAS = -0.55\%$; $MB = -0.03\ mm.day^{-1}$; $SEE = 0.63\ mm.day^{-1}$ and $MR = 1.02$) is among the eighteen considered methods the most similar to the chosen reference (Penman formula). Relationship between daily PET estimated using each method versus the daily Penman PET shows an acceptable correlation, indicating a good coherence among the various PET methods(with correlation greater than 0.5) (Fig. 32), although some important underestimation (Abtew, Makkink) and overestimation (Blaney-Criddle, Jensen-Haise) are noticed. Figure 33 shows the average monthly and annual PET estimated using different methods. These methods reasonably capture the seasonality of the PET in this area, which a peak is obtained in March with most methods and the minimum obtained during the rainy season specifically in August. The Hargreaves-Samani method also reasonably captures both the annual cycle and the inter-annual variability of the PET in this area compared to the Penman method. Thus it is the best method in computing daily, average monthly and annual PET in this area. This result is similar to those of (Allen et al., 1998) and (Sabziparvar and Tabari, 2010) who suggested the use of Hargreaves-Samani method to compute PET in data scarce contexts where only temperature is available, but contrary to those of (Djaman et al., 2015) who found that this method performed poorly under Sahelian conditions over the Senegal River Valley.

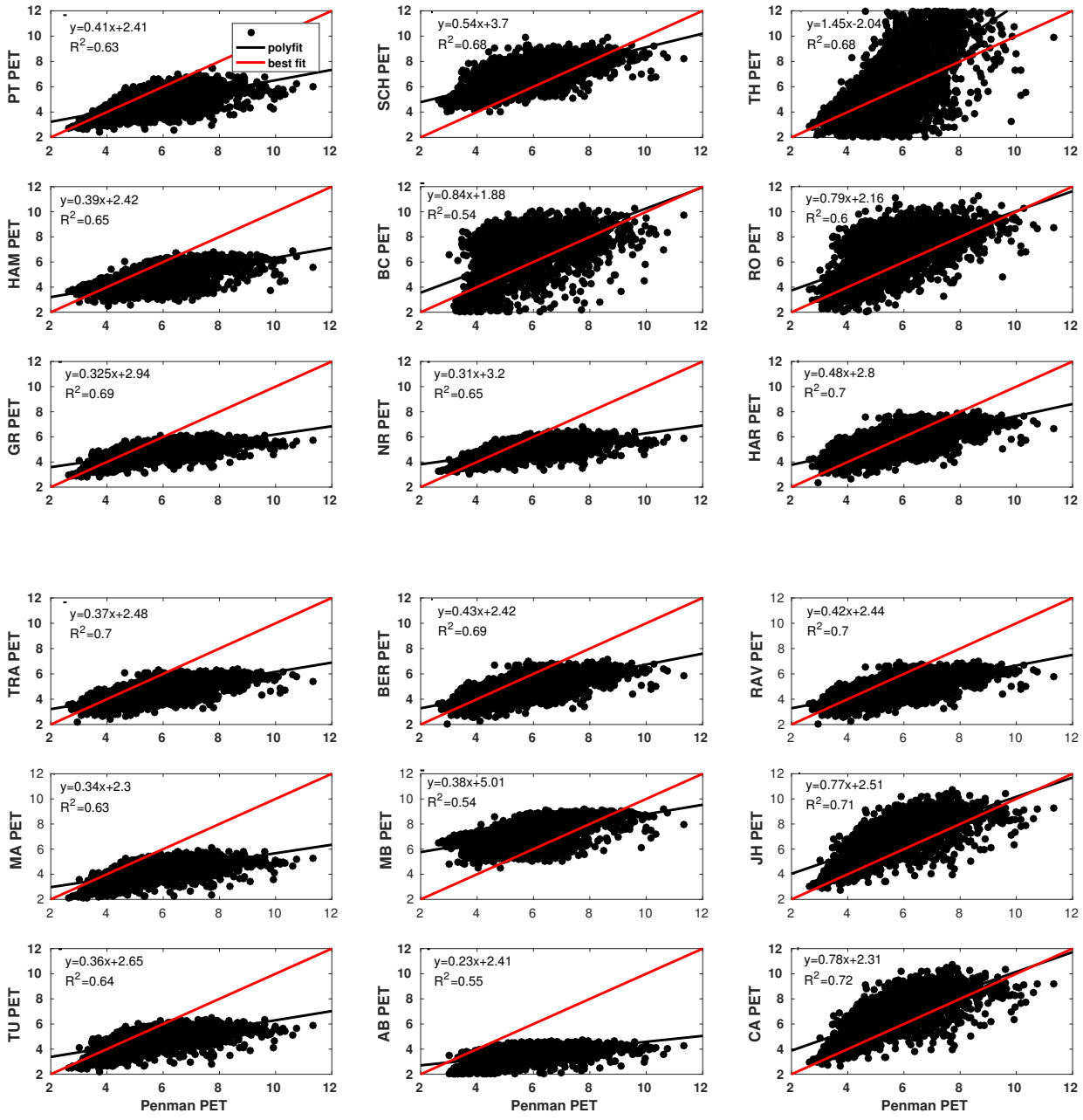

Figure 32: *Relationship between the daily potential evapotranspiration (PET) estimates of each method versus the Penman PET (mm.day^{-1}) over HBRB.*

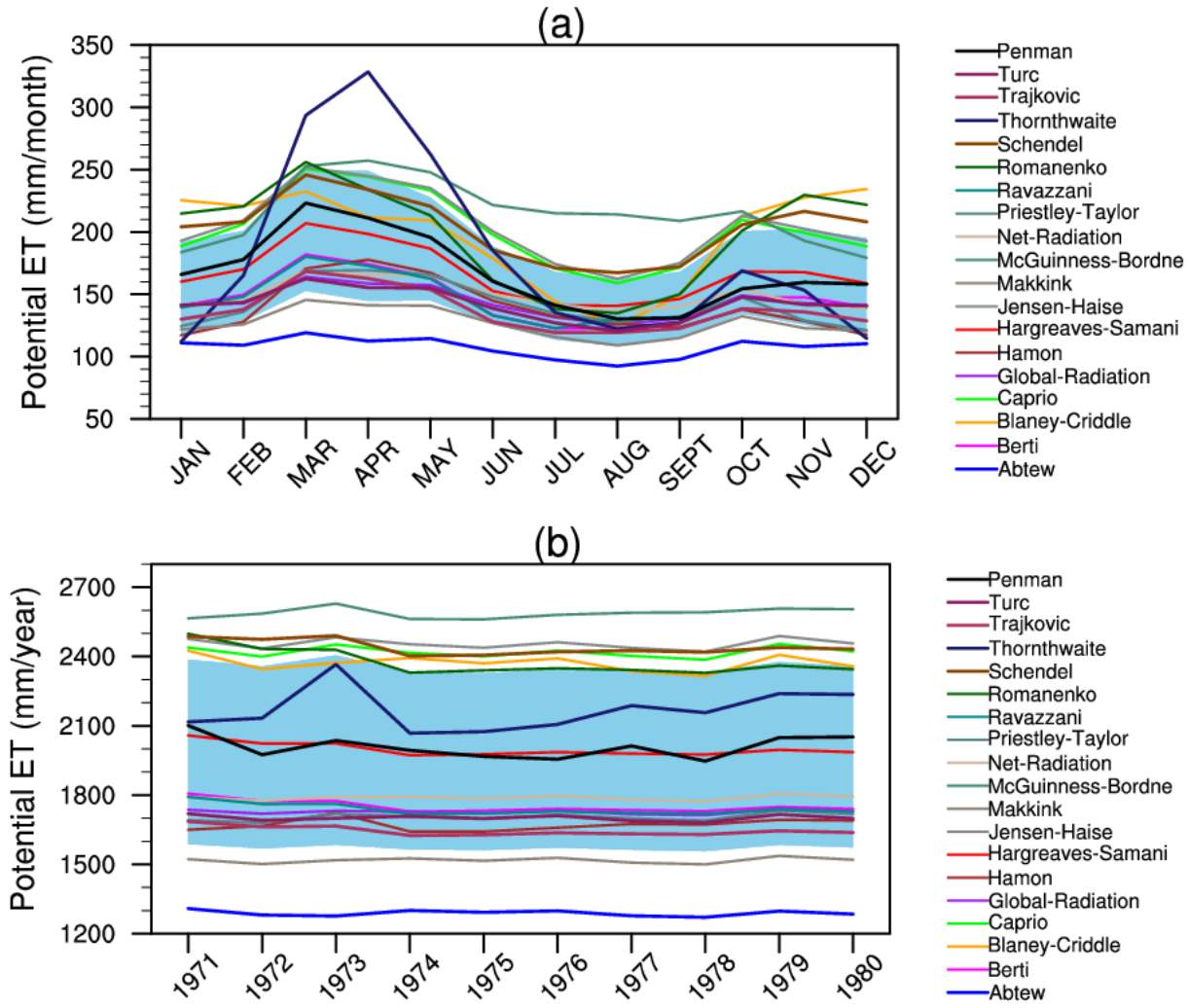

Figure 33: *Annual cycle (a) and inter-annual variability (b) of potential evapotranspiration estimates of each method. The sky Blue band represents simulating uncertainty (envelope of the standard deviation generated from the mean of the computed PET with different PET inputs)*

3.2.2 Effect of different PET inputs on optimized model parameters of the HBV-Light model

In this stage, the HBV-Light model was calibrated using each PET estimation method listed in Table 9 and the optimized model parameters set was obtained after 20,000 model runs by using Multi-objectives function. Figure 34 shows the marginal distribution of the optimized model parameter obtained using the different PET estimation methods, while Table Table 15 summarizes the statistics regarding median, mean, standard deviation (StD) and coefficient of variation (CV) of each parameter.

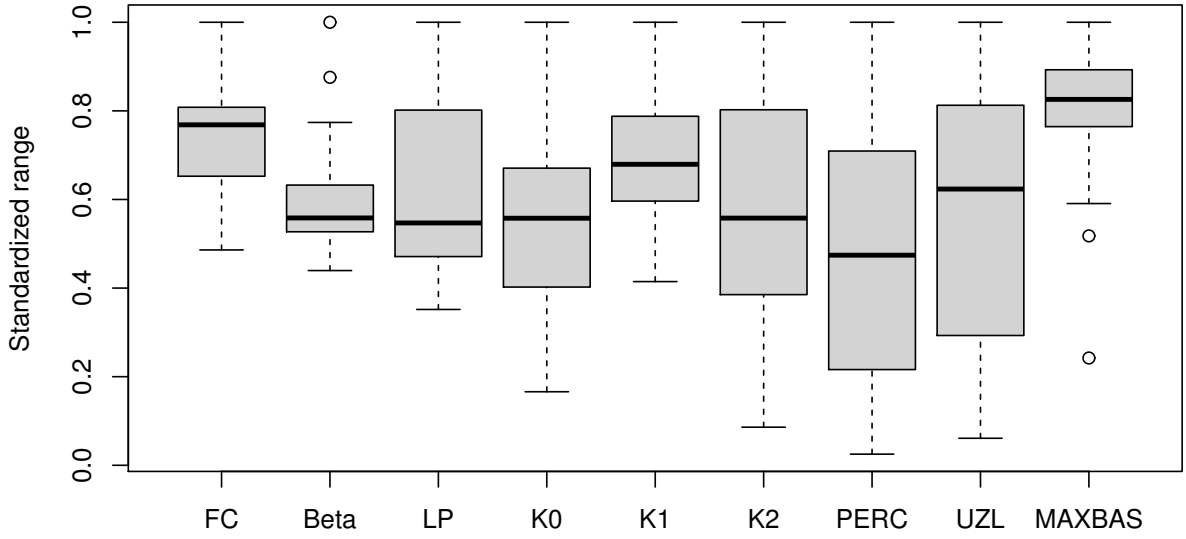

Figure 34: *Marginal distribution of the set of optimized parameters obtained by using 19 PET method. In all the box-and-whisker plots, the whiskers represent the minimum and maximum of each model parameter.*

Table 15: *Descriptive statistics of the variation of the optimized model parameters using 19 PET methods during the calibration.*

Methods name	$Min.$	$Max.$	25^{th} $Percentile$	$Median$	$Mean$	75^{th} $Percentile$	StD	$CV(\%)$
FC	240.5	494.8	322.8	380.2	371.1	399.8	69.40	18.70
LP	0.33	0.93	0.44	0.51	0.58	0.74	0.2	34.58
β	2.11	3.72	2.51	2.68	2.725	2.9	0.43	15.81
K_0	0.08	0.49	0.20	0.27	0.27	0.33	0.12	43.24
K_1	0.051	0.124	0.074	0.084	0.085	0.097	0.02	20.01
K_2	0.007	0.081	0.031	0.045	0.047	0.065	0.02	47.11
UZL	6.04	99.03	29.01	61.75	54.91	80.48	31.1	56.64
$PERC$	0.14	5.60	1.21	2.65	2.68	3.97	1.77	65.99
$MAXBAS$	2.94	4.97	3.845	4.17	4.175	4.44	0.52	12.42

The results show that the model parameters vary according to different PET input. Two parameters of the soil and evaporation routine (FC and β), the recession coefficient of subsurface runoff (K_1) and the transformation routine parameter ($MAXBAS$) are less sensitive to PET input. These parameters have been found to be well identifiable parameters in the HBV-Light model at this watershed. The response and groundwater routine parameters (K_0, K_2, $PERC$, UZL) are the most sensitive parameters to PET input. This can be explained by the fact that those parameters are found to be non-influential parameters for both total volume runoff and high-flow series in this watershed and each value taking in the initial ranges can perform well. In addition, a shape coefficient parameter (LP), which has been identified as less well-defined and more sensitive parameter for both

total volume runoff and high-flow series is most sensitive to PET. In the internal structure and formulation of the model, FC and LP are the parameters that control the soil moisture extraction function. LP is the fraction of maximum soil moisture capacity (FC) above which actual ET equals PET. When LP is close to 1, the actual ET will be higher, and vice versa. Thus, the over/under estimation of PET results in an increase/decrease of this parameter. For example, the McGuinness-Bordne method systematically over-estimated PET, has the higher value of LP ($LP = 0.93$), while the Abtew method which systematically underestimated the PET, gives the lower value of LP. This means that the over/under-estimation PET compared to the Penman method is compensated by the model parameter. This result suggests that, in this basin, the optimized model parameters are sensitive to PET estimation in a way similar to what has been found in other studies (Vazquez and Feyen, 2003; Andreassian et al., 2004; Oudin et al., 2006; Birhanu et al., 2018).

3.2.3 Effect of different PET inputs on the model efficiency of the HBV-Light model

3.2.3.1 Dynamic sensitivity approach

The best set of optimized model parameters obtained during the calibration period using each PET estimation method was used to simulate the streamflows in the validation period (1971–1980). The statistical criteria between observed and simulated streamflows were then computed to assess the impact of different PET inputs on the model performance. The results show that all the PET estimation methods used in this study reproduce the annual cycle of monthly streamflows well, although there is overestimation of monthly streamflows in August and September (Fig. 35a). The marginal distribution of each statistical criteria obtained using different PET formulation is presented in Fig.36, while the statistics of each criterion are summarized in Table 16. Each PET method simulated the daily streamflows well during the validation period with values of NSE ranging between 0.78 and 0.87. The CV for each statistical criterion is closer to relatively low values (less than 7%). This suggests that the rainfall-runoff model efficiency is insensitive to PET estimation methods, which is also reinforced by the narrow band of uncertainty in the model simulations by using different PET inputs (Fig. 35a). This means that the model adapts its parameters to the over- or under-estimation of the PET during the calibration period as found in the previous studies (Oudin et al., 2006; Bai et al., 2016; Birhanu et al., 2018). This also confirms that the best set of model parameters obtained from each PET estimation method are representative for basin scale hydrological simulation. Of the four statistical criteria used in this work, R^2 is the least sensitive, while RSR is the most sensitive. Therefore, the different PET inputs influence peak flows more than the streamflow volumes over the studied period.

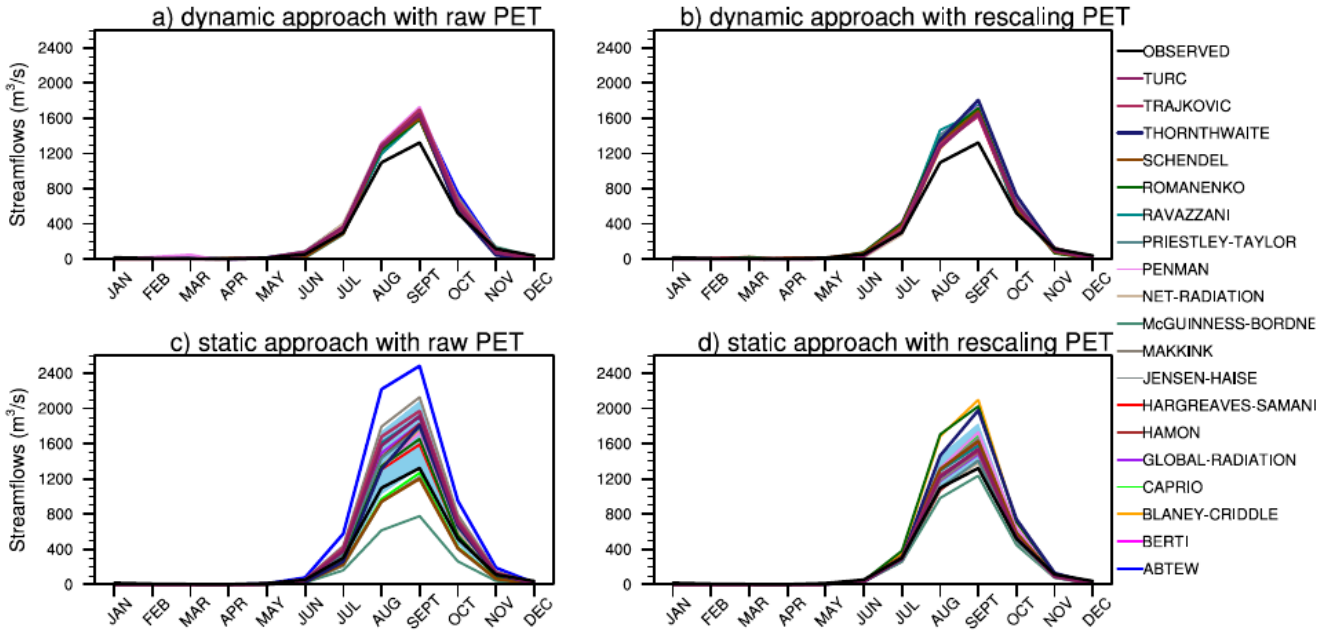

Figure 35: *Annual cycle of monthly streamflows simulated by using different PET inputs by follow the dynamic approach (first line of the panel) and the static approach (Second line of the pannel). The streamflows was simulated by using both raw (First column of the panel) and rescaling (Second column of the panel) PET inputs. The sky Blue band represents simulating uncertainty (envelope of the standard deviation generated from the mean of the simulated streamflows with different PET inputs).*

Table 16: *Descriptive statistics of the variation of the model efficiency using raw/rescaling PET inputs during the validation period.*

Methods name	*Min.*	*Max.*	25^{th} *Percentile*	*Median*	*Mean*	75^{th} *Percentile*	*StD*	*CV*(%)
				Dynamic sensitivity approach				
NSE	0.78/0.745	0.87/0.85	0.83/0.795	0.84/0.81	0.84/0.81	0.85/0.82	0.02/0.025	2.5/3.09
R^2	0.93/0.92	0.96/0.94	0.94/0.935	0.94/0.94	0.94/0.94	0.94/0.94	0.005/0.004	0.54/0.47
RSR	0.36/0.39	0.47/0.5	0.39/0.42	0.4/0.44	0.4/0.44	0.41/0.44	0.025/0.03	6.33/6.46
CB	0.78/0.74	0.91/0.86	0.82/0.78	0.845/0.81	0.85/0.80	0.87/0.83	0.04/0.03	4.42/3.95
				Static sensitivity approach				
NSE	0.66/0.81	0.87/0.88	0.71/0.85	0.79/0.87	0.79/0.86	0.84/0.88	0.07/0.02	8.45/2.44
R^2	0.93/0.935	0.94/0.94	0.94/0.94	0.94/0.94	0.94/0.94	0.94/0.94	0.003/0.001	0.36/0.16
RSR	0.36/0.34	0.58/0.435	0.4/0.35	0.46/0.36	0.46/0.37	0.53/0.385	0.07/0.03	15.74/7.38
CB	0.57/0.80	0.885/0.998	0.64/0.85	0.79/0.91	0.75/0.90	0.85/0.94	0.11/0.06	14.32/6.90

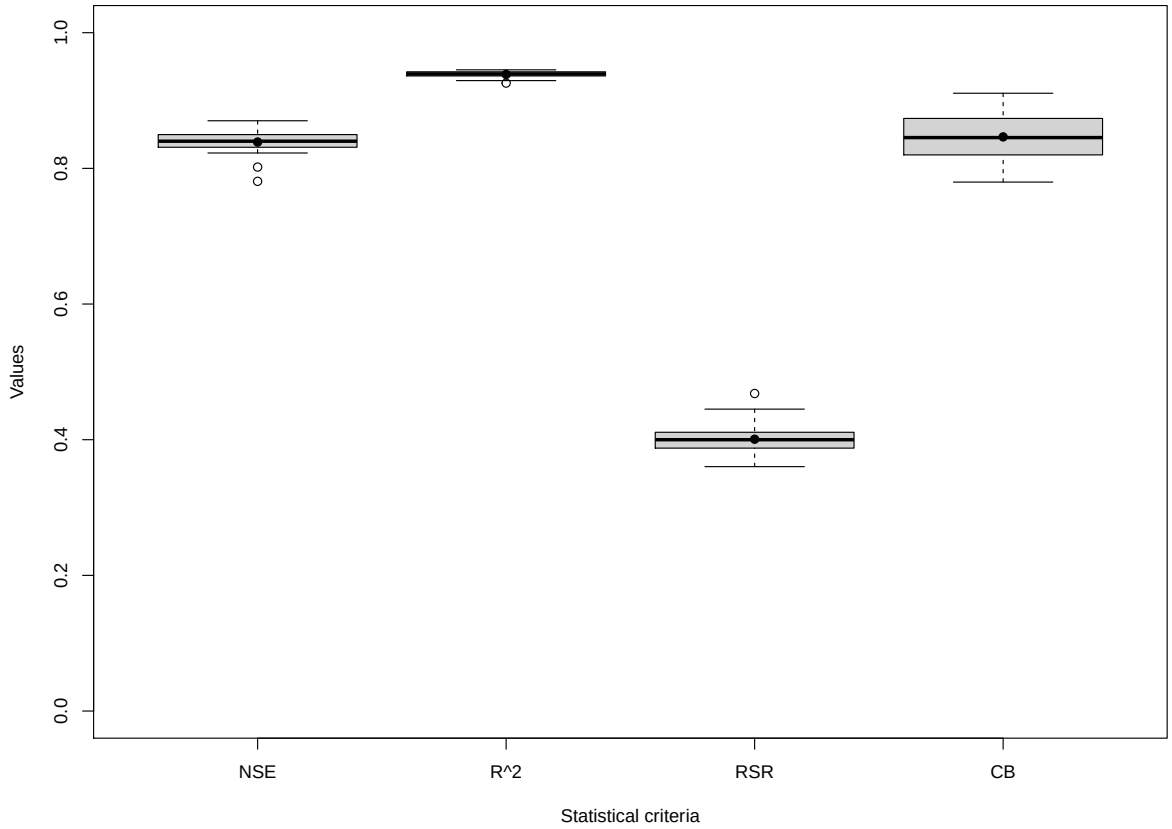

Figure 36: *Distribution of each statistical criterion obtained using different PET estimation methods followed the dynamic sensitivity approach. In all the box-and-whisker plots, the whiskers represent the minimum and maximum of each model performance criterion. The outer edges of the boxes and the horizontal lines within the boxes represent the 25th, 75th, and 50th (Median) percentiles of each model performance criterion. The filled circle represents the average value of each statistical criterion.*

3.2.3.2 Static sensitivity approach

Using the same set of optimized model parameters obtained during the calibration period with the Penman's PET, which we consider in this study, as the best PET method, the HBV-Light model

performance using each of the PET estimation methods was evaluated. Figure 37 represents the dispersion of each performance criteria obtained by using all 19 PET models. This highlights the presence of largest uncertainty rates in model performance. This can be explained by the fact that some PET inputs systematically over- or under-estimate the modeled streamflows and they are not within the large range of the model simulations (see Fig. 35c). The result is reinforced by a larger CV (greater than 8%) for all the model performance except the The coefficient of correlation R^2 (Table 16). Several differences are noted between the dynamic and static approaches. Firstly, the dynamic sensitivity approach reproduced streamflows simulations better than the static approach (Table 16). Secondly, in the static approach the PET method had a large impact on streamflow simulation (Fig. 35c) with the model performance generally affected. The result is not surprising because the over- or under estimation of PET impacts the river flow given that the optimized model parameters are unchanged. We conclude that the different PET input has moderated impact to the rainfall-runoff model efficiency and suggest that hydrological models compensate for the efficiency loss in the runoff simulation caused by different PET inputs through the model parameter calibration. Therefore, the dynamic approach is the best for hydrological studies.

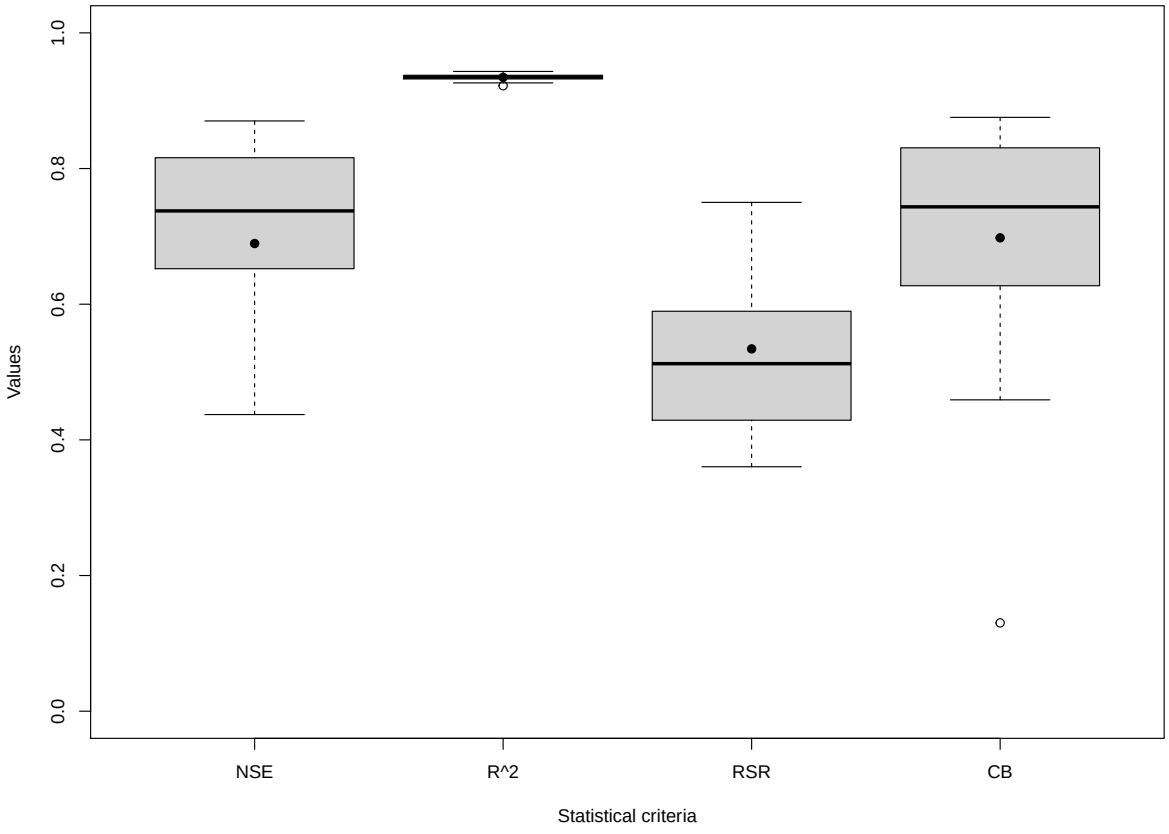

Figure 37: Same at figure 36 but for the static sensitivity approach.

3.2.4 What is the impact of the rescaling factor of PET methods on model efficiency?

The rescaling factor was applied to PET in the calibration, and validation periods. In the first step, the model was calibrated by using each rescaling PET and the set of optimized model parameters were obtained for each PET method. In the second step, the model was validated by using each rescaling PET and his corresponding set of optimized model parameters (dynamic approach). In the last step, the model was validated by using each rescaling PET and the set of optimized model parameters obtained with Penman's PET input. The dispersion of each model performance can be found in Fig. 38. The results reveal that in this basin, the rescaling factor of PET doesn't improve the performance of the model and the model remains insensitive to different rescaling PET inputs when following the dynamic approach (Fig. 35b) because the CV for each statistical criteria (NSE, RSR, CB and R^2) is less than 7% for both raw and rescaling PET inputs (Table 16). However, in the static approach, the model performance is systematically improved, and the rescaling PET input has a moderate impact on model simulations (Fig. 35d). For example, when we use the different raw PET inputs, the mean of NSE is 0.76 and his CV is 8.45%, while the use rescaling PET better performed the model simulations with the mean of NSE equals to 0.86, with a small dispersion (CV=2.4%). Therefore, the use of different PET methods without rescaling factor or recalibration, particularly when using a static sensitivity, can lead to a deterioration of model simulations and performance as reported in the previous studies (Oudin et al., 2005; Samains and Pauwels, 2013; Bai et al., 2016).

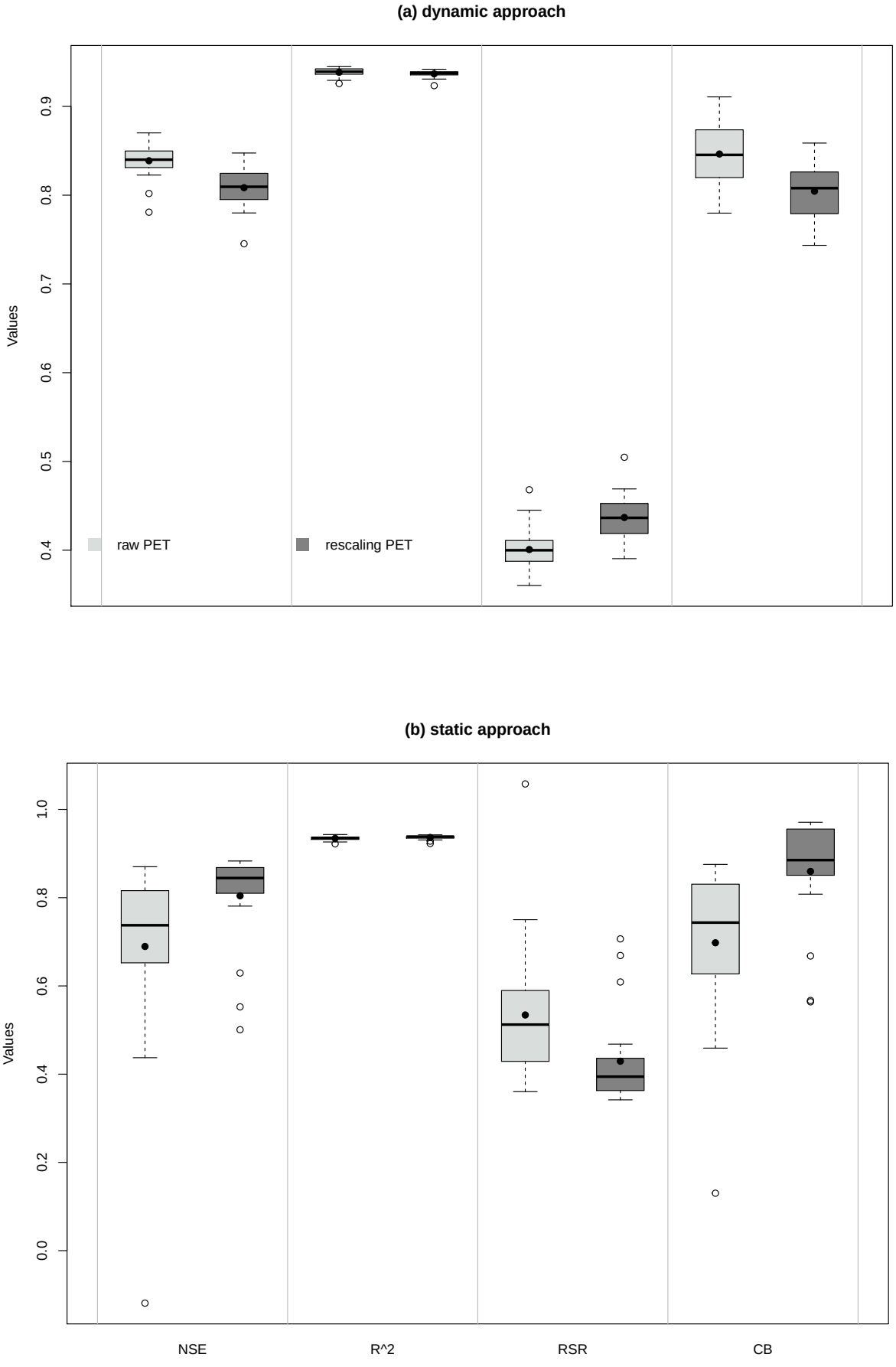

Figure 38: *Boxplot of each statistical criteria obtained using raw and rescaling PET inputs: dynamic approach (top) and static approach (bottom) [RF = Rescaling Factor].*

3.3 REMO model evaluation

This section describes the performance of the two outputs termed REMO–EC and REMO–MPI generated by the REMO model in simulating the present climate within the reference period 1983–2005. The annual cycle of precipitation, 2-m temperature, and estimated PET is shown in Figure 39, while Table 17 summarizes the values of the different statistical criteria used.

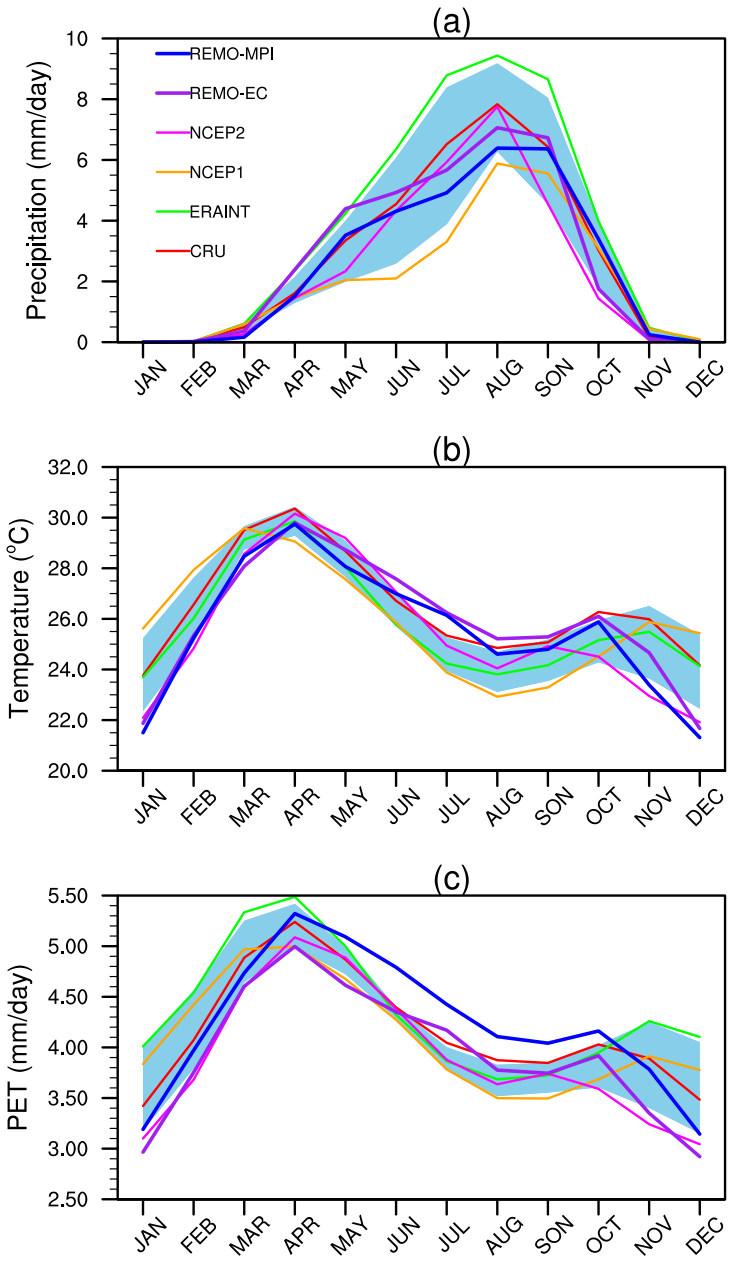

Figure 39: *Climatological annual cycle of mean monthly precipitation (a), 2-m temperature (b) and potential evapotranspiration (c) in all observational datasets (ERAI, CRU, NCEP1 and NCEP2) and the REMO model simulations (REMO-EC and REMO-MPI) over HBRB. The sky Blue band represents observational uncertainty (envelope of the standard deviation generated from the mean of the observation and reanalysis data).*

The reanalysis and observation data have similar variability of the annual cycle of monthly rainfall,

Table 17: Summary of statistical evaluation of monthly precipitation, 2-m temperature and potential evapotranspiration (REMO-EC and REMO-MPI) with the ERAINT, CRU, NCEP1 and NCEP2 data for the current 23-yr period (1983–2005) over the BRB.

	Precipitation											
	ERAINT			**CRU**			**NCEP1**			**NCEP2**		
	MB	R^2	$RMSE$	MB	R^2	$RMSE$	MB	R^2	$RMSE$	MB	R^2	$RMSE$
REMO-EC	0.96	0.97	1.48	0.05	0.97	0.64	-0.52	0.90	1.43	-0.43	0.95	0.95
REMO-MPI	1.17	0.98	1.72	0.26	0.98	0.65	-0.73	0.96	0.95	-0.22	0.93	0.98
	2-m temperature											
REMO-EC	1.95	0.54	3.03	0.88	0.88	2.18	0.86	0.57	2.34	-0.15	0.96	0.77
REMO-MPI	0.62	0.52	2.42	0.51	0.87	1.32	-0.47	0.54	2.26	-1.47	0.95	1.67
	Potential evapotranspiration											
REMO-EC	0.43	0.69	0.64	0.24	0.95	0.31	0.18	0.71	0.48	-0.03	0.97	0.17
REMO-MPI	0.13	0.66	0.53	-0.06	0.94	0.24	-0.06	0.69	0.24	-0.12	0.97	0.50

2-m temperature and PET over BRB, even though there exist some errors in time and magnitude. Most notable errors are found in the ERAINT and NCEP1 during the rainy season in which there are an over-estimation and under-estimation of rainfall respectively. When the magnitude of uncertainties in the observation and reanalysis data are taken into account, the REMO model represents the seasonality of temperature, PET and rainfall well with a unimodal character of rain (maximum obtained in August). Although the peak of rainfall intensity in all the two REMO simulations is lower compared with CRU and NCEP2 observation and reanalysis datasets, the REMO results sit within the spread of the combined reanalysis and CRU data. The annual cycle of 2-m temperature and PET do not exhibit a large variability between the different datasets (simulations and observations) as in case of mean monthly precipitation. In summer, the two REMO simulations overestimate the PET, while there is a stronger under-estimation of both 2-m temperature and PET during the September–October–November (SON) and December–January–February (DJF) seasons when compared to ERA and NCEP1.

These results are reinforced by recent studies (Fotso-Nguemo et al., 2016; Vondou and Haensler, 2017; Tamoffo et al., 2018), which demonstrated the ability of the REMO model to simulate well various aspects of the present climate such as daily, seasonal and annual cycle of precipitation over CA. In addition, Vondou and Haensler (2017) found that REMO model captures the variability in precipitation anomalies between different events associated with El Nino/Southern Oscillation, while Tamoffo et al. (2018) show that REMO adequately simulates the frequency of wet days, the threshold of extreme rainfall and the cumulative frequency of daily rainfall over CA.

3.4 Effect of climate change on the different climate and hydrological components in the HBRB

This section focuses on the potential changes of hydro-climatic conditions (precipitation, temperature, PET, AET, soil moisture and streamflow) by the near (2041–2065) and late (2071–2095) of the twenty-first century under RCPs 2.6, 4.5 and 8.5 relative to the baseline period (1981–2005).

3.4.1 Changes in monthly, seasonal and annual precipitation

The rainy season over the HBRB extends from May to October with a maximum in August (see Fig. 39). Under RCP2.6 and RCP4.5, rainfall changes for the months May–August is uncertain as results are both weakly positive and negative depending on the driving GCM and future period (Fig. 40). However, under the RCP8.5 scenario, decreases in rainfall are projected in both the near and late future for these months. During September, large decreases in rainfall are projected under all scenarios in both time periods. The signal is strongest in the REMO–EC combination under RCP2.6, although in RCP8.5 both models show a strong decrease. During October, large increases in rainfall are projected by the REMO–EC model combination especially in the far future under RCPs 4.5 and 8.5. However, the REMO–MPI model combination projects effectively no change to a small decrease in rainfall in October rainfall. The projected change in October rainfall is, therefore, more uncertain than in September. Under RCP2.6, the signal in August is uncertain during the far future as results are both weakly negative and positive depending on the driving GCM.

Seasonally, the signal changes with changing RCP. In RCP2.6 there is a projected decrease in MAM rainfall, an increase in JJA rainfall and a decrease in SON. In RCP4.5, there is a near-term increase but far-term decrease in MAM rainfall, smaller magnitudes in JJA changes than in RCP2.6 and a mixed signal of change in SON in both time slices. In RCP8.5, both near and far future show general decreases in rainfall in all seasons by most models. However, the SON season needs to be interpreted in the context of the monthly changes in September and October, particularly for the REMO–EC model combination that shows large, opposite signals in each respective month.

Although the decrease in annual rainfall increases with increased GHGs concentration scenario, the rainfall change under RCP2.6 is larger than that of RCP4.5 and RCP8.5 in the near future with the REMO-EC. We also notice an increase in annual rainfall in the far future under RCP2.6 with REMO-MPI and in the near future under RCP 4.5 with REMO-EC.

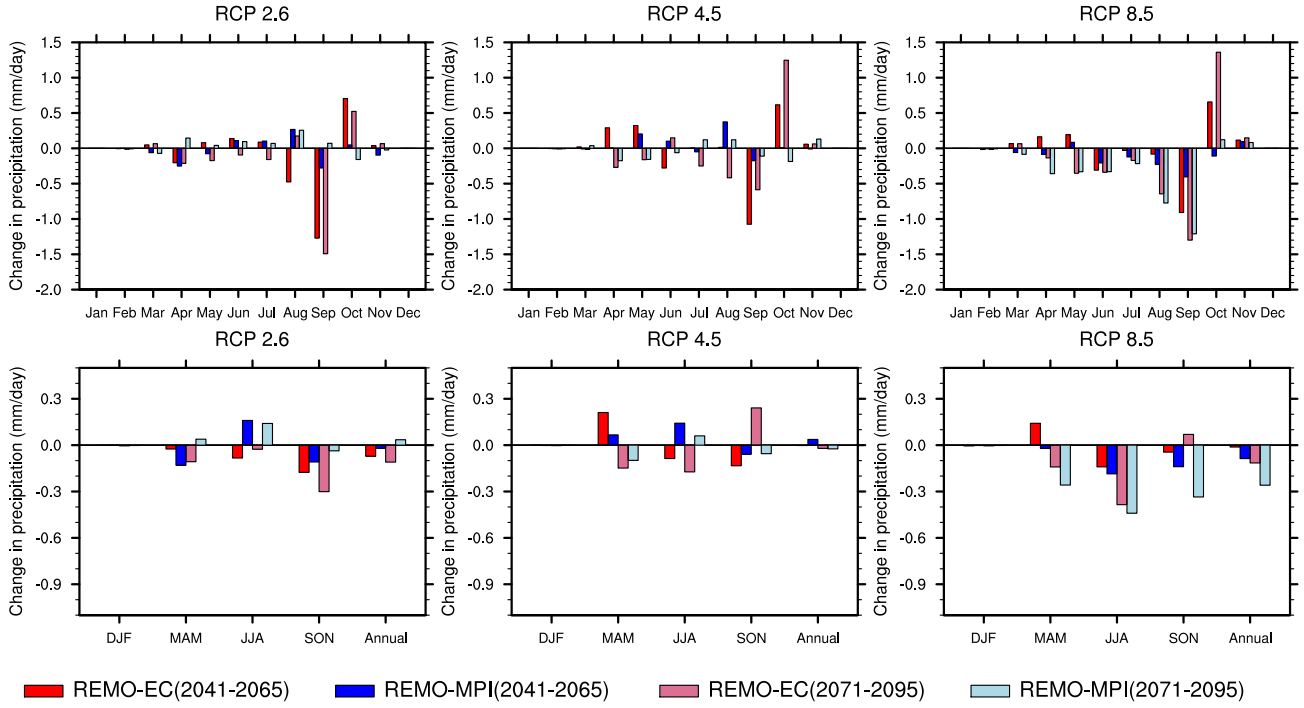

Figure 40: *Projected monthly (top), seasonal and annual (bottom) changes in precipitation over the HBRB under the three scenarios (RCP2.6, RCP4.5, RCP8.5) for the two future periods (2041-2065 and 2071-2095) relative to the baseline period (1981-2005).*

In summary, with increasing RCP, rainfall is projected to decrease during the rainy season with the largest impact during the key rainfall months of August and September under RCP8.5. The large projected increase in rainfall during October is only evident in one driving GCM (EC) so it should be interpreted with caution. A similar negative trend was reported by Mbaye et al. (2015) in the Upper Senegal Basin and Oguntunde and Abiodun (2013) in the NRB by using REMO and RegCM4 RCMs, respectively. These results are also consistent with future dry conditions previously projected over CA (Fotso-Nguemo et al., 2016, 2017; Sonkoué et al., 2018; Mba et al., 2018; Tamoffo et al., 2019, 2018).

3.4.2 Changes in monthly, seasonal and annual temperature

Projected monthly, seasonal and annual temperature changes over HBRB for the near and late twenty-first century under RCP2.6, RCP4.5 and RCP8.5 scenarios simulated with REMO-EC and REMO-MPI are presented in Figure 41. In general, the temperature was predicted to increase in all months and seasons under scenarios, models and future periods. In particular, under RCP2.6, the increase is low than under RCP4.5 and RCP8.5, while RCP8.5 gave high value (up to $5°C$), as expected in higher equivalent CO_2 concentrations. The late of the twenty-first century predicted a high increase under RCP4.5 and RCP8.5 with all data while under RCP2.6 the highest value was predicted in the near

future with REMO-EC data. This feature is common to all multi-model ensembles studies performed in this region (Mkankam, 2001; Oguntunde and Abiodun, 2013; Fotso-Nguemo et al., 2017; Mba et al., 2018).

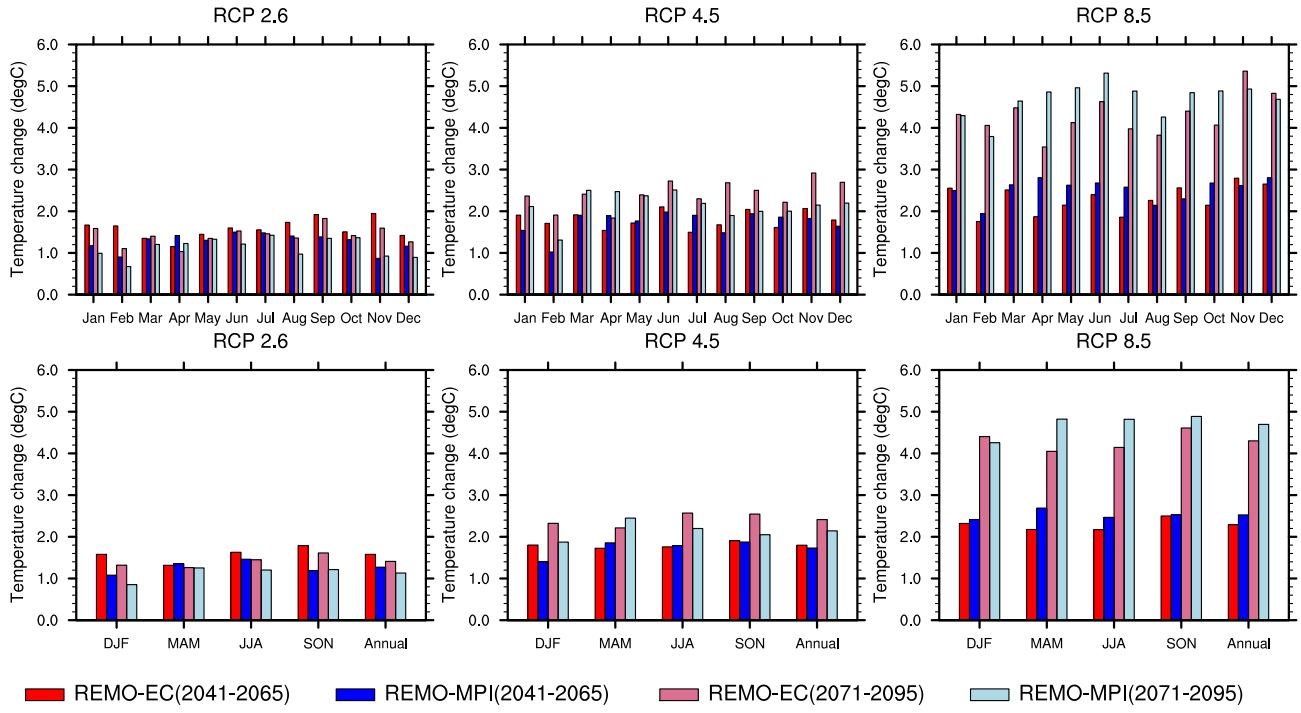

Figure 41: *Projected monthly (top), seasonal and annual (bottom) changes in temperature over the BRB under the three scenarios (RCP2.6, RCP4.5, RCP8.5) for the two future periods (2041-2065 and 2071-2095) relative to the baseline period (1981-2005).*

3.4.3 Changes in monthly, seasonal and annual PET

Projected monthly, seasonal and annual changes in potential evapotranspiration (PET) derived from REMO-EC and REMO-MPI in the study area are shown in Figure 42. The impact of climate change on PET is similar to the pattern of changes in temperature with potential increase among scenarios, models and future periods. This result was expected given that temperature and PET are strongly correlated (Mkankam, 2001). The increase is more important for RCP8.5 scenario ranges between 0.5-1.8 mm/day, while the RCP2.6 scenario gives the lower increase in PET less than 0.5 mm/day. We also notice that the maximum increase of monthly, seasonal and annual PET will be observed in the far future under RCP4.5 and RCP8.5 scenarios with all models, while the maximum increase will be predicted in the near future under RCP2.6. The REMO-EC data predict the maximum increase of monthly, seasonal and annual PET under RCP2.6 scenario while the maximum increase of monthly, seasonal and annual PET will be predicted by REMO-MPI data under RCP4.5 and RCP8.5.

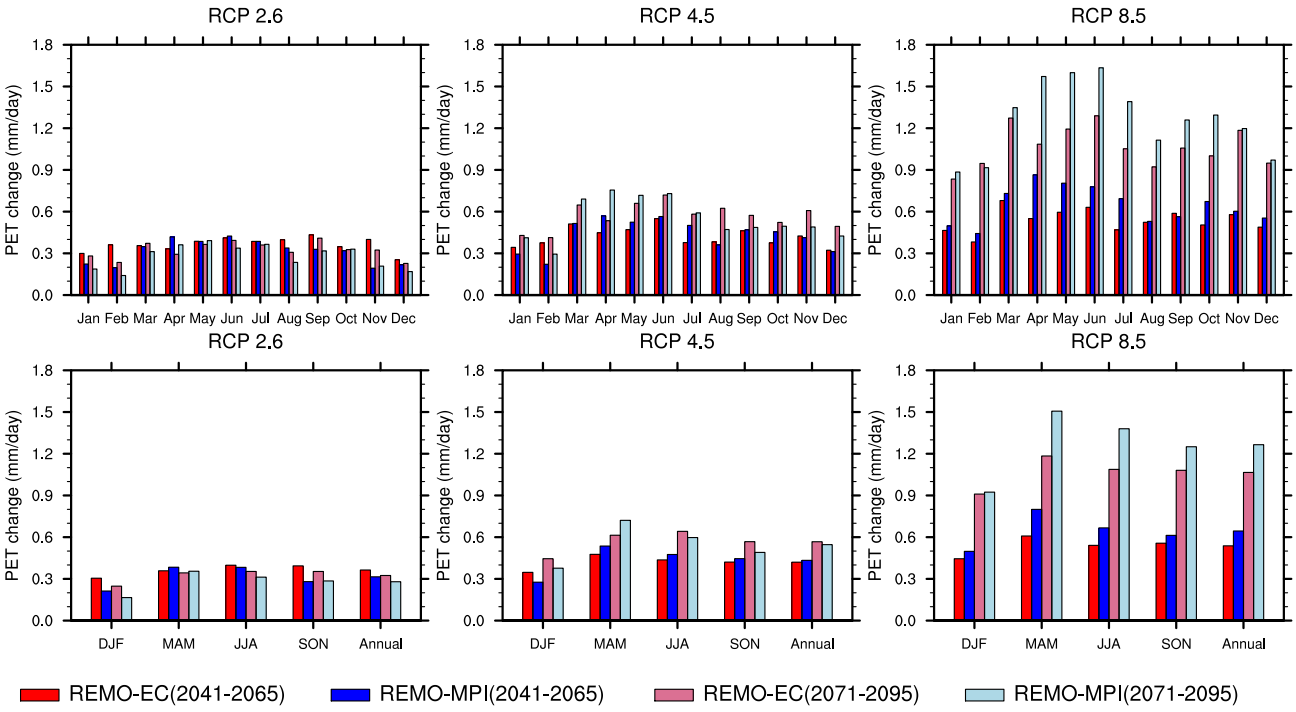

Figure 42: *Projected monthly (top), seasonal and annual (bottom) changes in potential evapotranspiration (PET) over the BRB under the three scenarios (RCP2.6, RCP4.5, RCP8.5) for the two future periods (2041-2065 and 2071-2095) relative to the baseline period (1981-2005).*

3.4.4 Changes in monthly, seasonal and annual AET

The monthly, seasonal and annual change of actual evapotranspiration presented in Figure 43 shows a small decrease of AET during very hot dry months (January-April), while there is an increase during the important wet months (June-October) and November. Under RCP2.6, the change signal in May is uncertain as results are both weakly positive and negative depending of the driving GCM. This is also true for scenarios RCP4.5 and 8.5 where a contrasting runs' signal is observed in January, April and May under both time periods and models (RCP4.5), and in May and December during the late of twenty-first century (RCP8.5) respectively. The possible explanation of the decrease and increase of AET during the dry months and wet months respectively will be due to the fact evapotranspiration is influenced by the available water and energy. During the dry months, the water is unavailable and there is an increase available energy (increase temperature), thus result in a decrease AET. Or, during the wet months, both water and energy are available, then result in an increase AET.

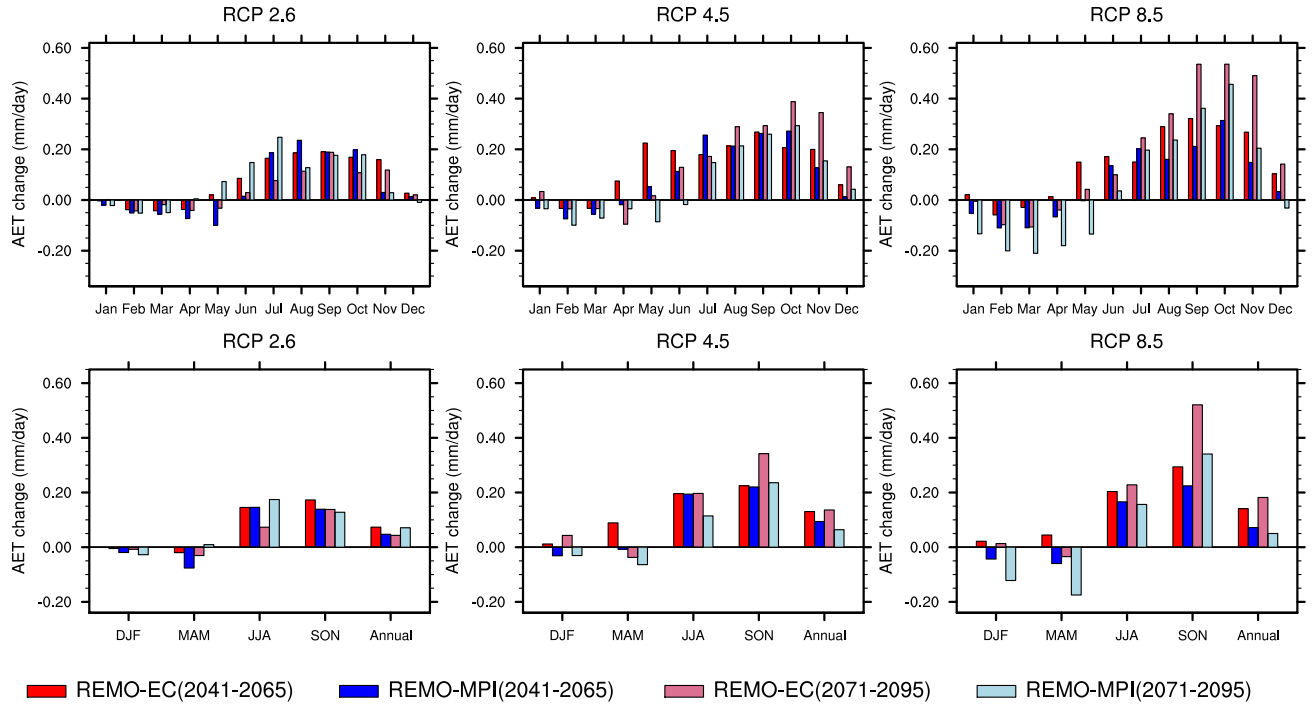

Figure 43: *Projected monthly (top), seasonal and annual (bottom) changes in actual evapotranspiration (AET) over the BRB under the three scenarios (RCP2.6, RCP4.5, RCP8.5) for the two future periods (2041-2065 and 2071-2095) relative to the baseline period (1981-2005).*

Seasonally, there is an increase of AET in Summer (JJA) and Autumn (SON) under the scenarios, models and time periods. Under RCP8.5, the increase is maximum due the maximum increase of temperature under the same scenario as shown in Figure 41. During DJF and MAM seasons, the change signal is uncertain under RCP4.5 and 8.5, while there is a decrease in RCP2.6.

In general, the change in average annual AET is projected to decrease under the scenarios, models and time periods. In particular, under RCP4.5, the change signal in the REMO-EC is large during the late of twenty-first century than that during in the near twenty first century. Or, with REMO-MPI, there is a contradiction.

3.4.5 Changes in monthly, seasonal and annual soil moisture

Figure 44 shows relative change in monthly, seasonal and annual soil moisture under the scenarios, models and time periods. In general, the average monthly, seasonal and annual soil moisture is projected to decrease under the scenarios, models and time periods. In particular, the maximum decrease of monthly, seasonal and annual soil moisture will be observed under RCP8.5 in the two future periods. This will the result of the combination of the maximum decrease of rainfall and maximum increase of PET and AET under the same scenario. Additionally, under RCP8.5, the change signal in the REMO-MPI combination is larger than that of the REMO-EC, while we note a

contradiction under RCP2.6.

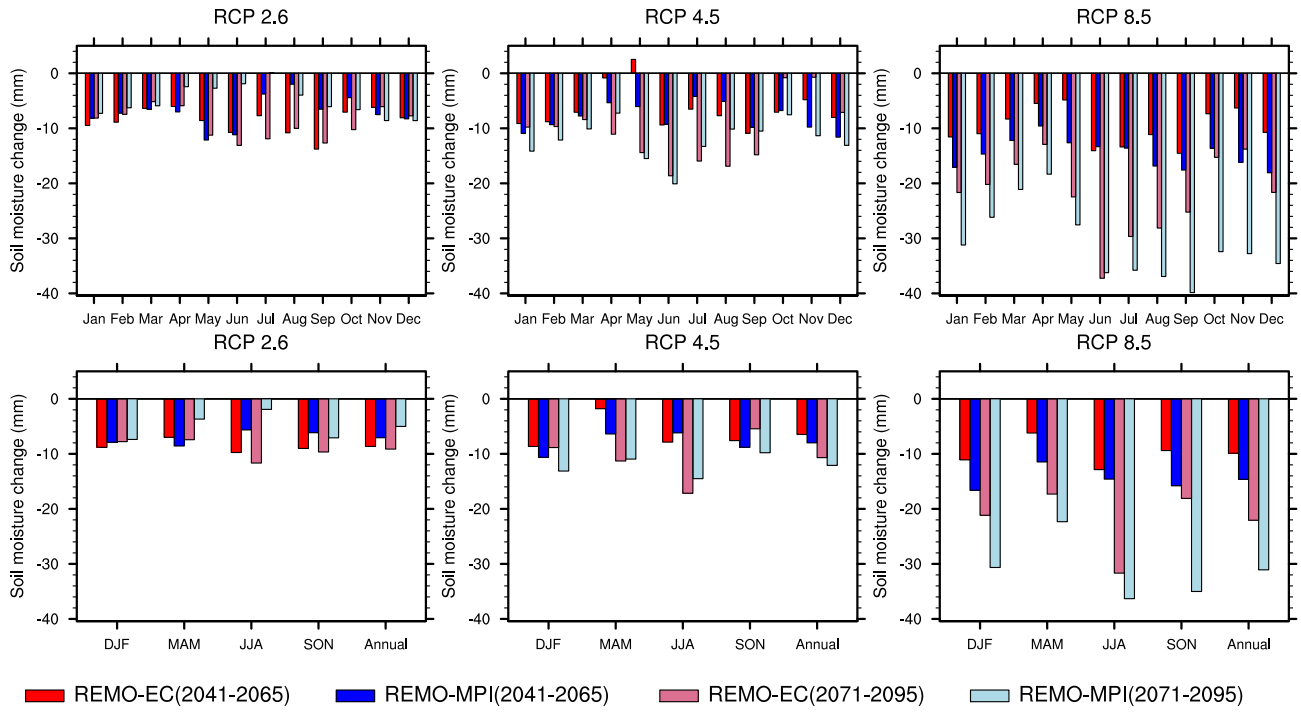

Figure 44: *Projected monthly (top), seasonal and annual (bottom) changes in soil moisture over the BRB under the three scenarios (RCP2.6, RCP4.5, RCP8.5) for the two future periods (2041-2065 and 2071-2095) relative to the baseline period (1981-2005).*

3.4.6 Changes in monthly, seasonal and annual streamflow

Figure 45 shows relative changes in monthly, seasonal and annual streamflow under the scenarios, models and time periods. Although there were some differences between scenarios, models and future periods, in general, streamflows are projected to decrease. During September, large decreases in streamflows are projected under all scenarios, models and future periods. The signal is strong in the REMO–MPI combination under RCP8.5 during the late of the twenty-first century. The dry months (November–April) do not exhibit a change signal which can be explained by the absence of rainfall during the period.

Seasonally, the sensitivity of streamflows to CC differed between the wet and dry seasons. In particular, a considerable decrease in streamflows is found in SON. Under those scenarios, seasons and time periods, the streamflow change is larger in the REMO–EC combination than that of the REMO–MPI combination, except under RCP8.5, which REMO–MPI predicted a larger streamflows change in SON. This can be explained since REMO–MPI projects a large change in rainfall than does REMO–EC in the same season (SON). The ranges of relative changes in annual streamflow are smaller than those in seasonal streamflow.

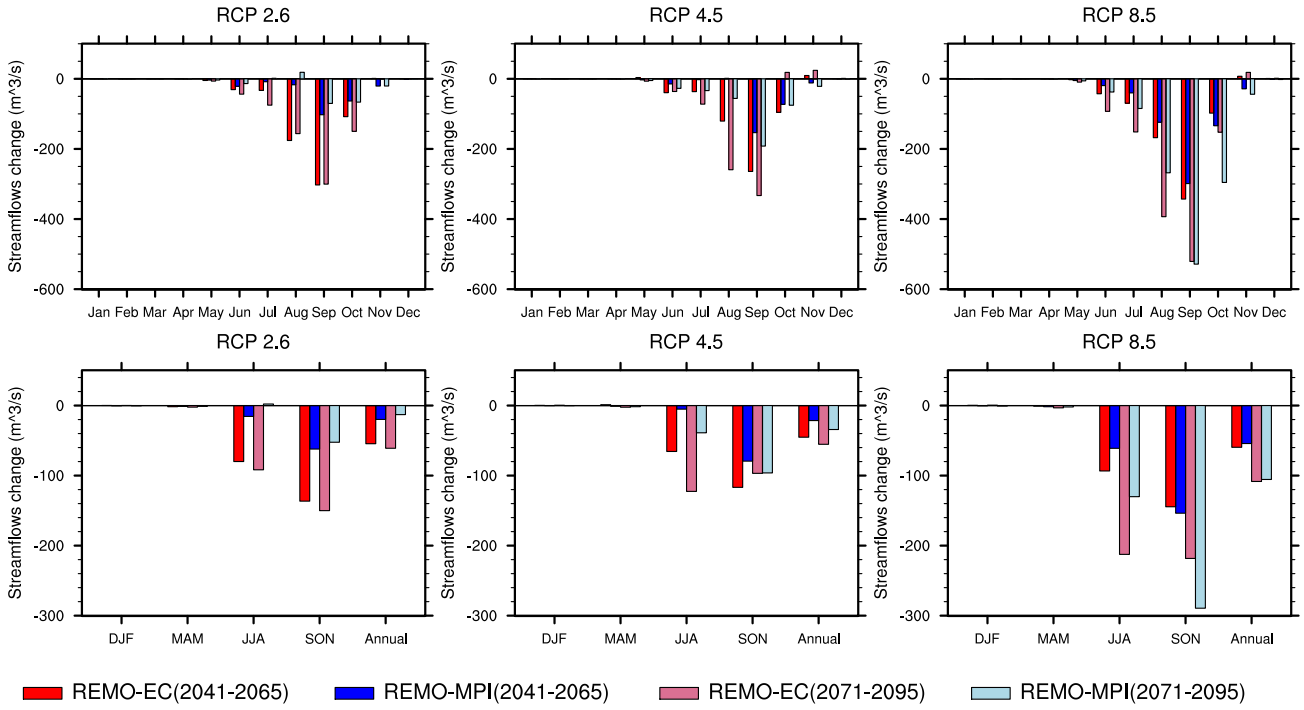

Figure 45: *Projected monthly (top), seasonal and annual (bottom) changes in streamflow over the BRB under the three scenarios (RCP2.6, RCP4.5, RCP8.5) for the two future periods (2041-2065 and 2071-2095) relative to the baseline period (1981-2005).*

Although the decrease in annual streamflows increases with increased GHGs concentration scenario, the streamflow change under RCP2.6 is larger than that of RCP4.5 with REMO–EC in the two time periods. This result was expected because streamflow is usually very sensitive to changes in precipitation (as shown in Fig. 46) and the rainfall change under RCP2.6 is larger than the change under RCP4.5 with the same model. The results also reveal that the relative change in annual streamflows in the two time periods are relatively larger with REMO–EC under RCP2.6 and RCP4.5 than that of REMO–MPI, while under RCP8.5, the maximum annual decrease in streamflows is obtained with REMO–MPI simulations (Table 18). The projected late twenty-first century change in annual streamflows is larger than that in the mid twenty-first century under all scenarios and models except REMO–MPI under RCP2.6. This can be explained by the increase of precipitation in the near future with REMO–MPI under the same scenario and the change in streamflow is strongly correlated with the change in PET (Fig. 46) with the same model under the same scenario.

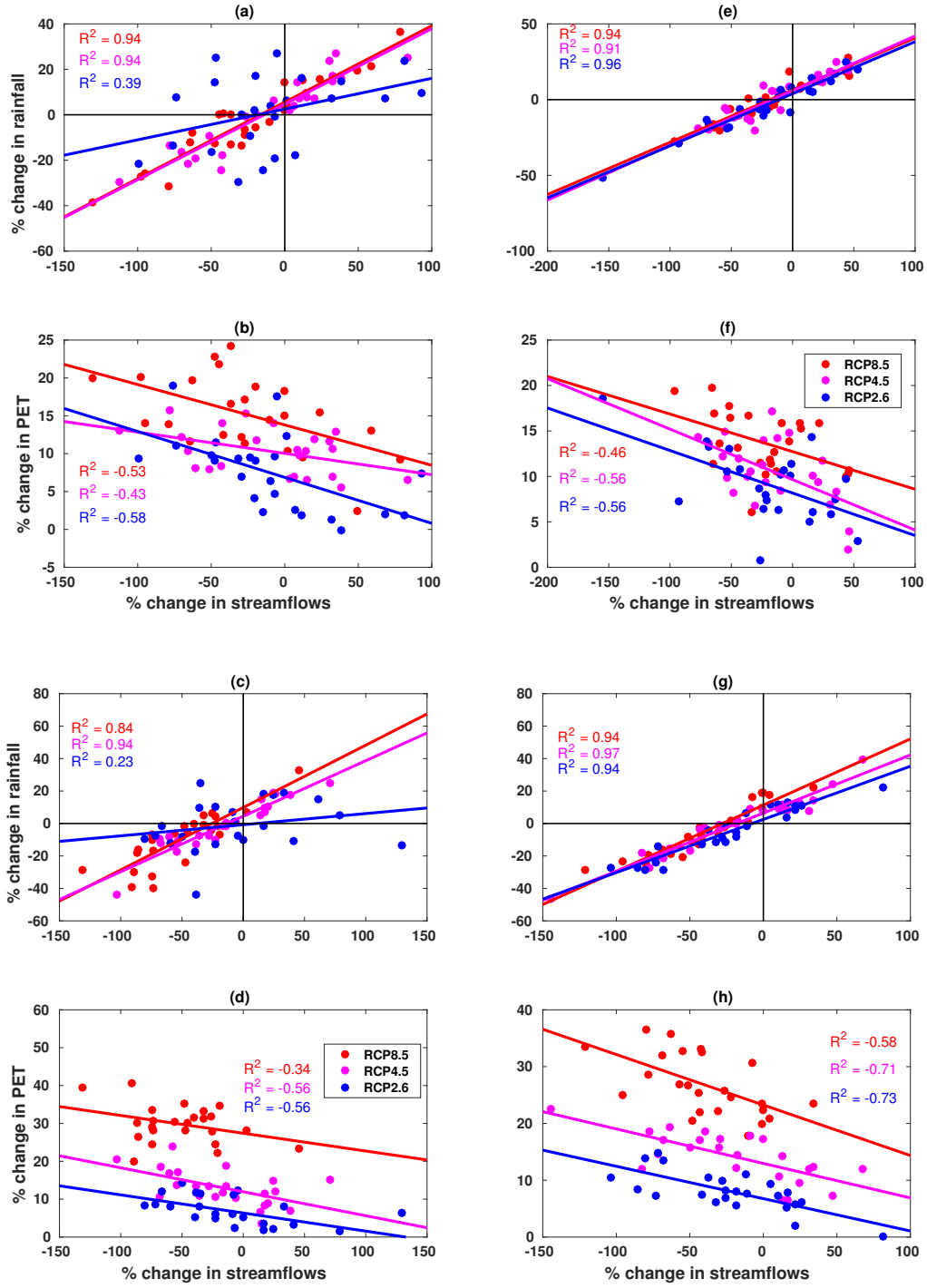

Figure 46: *Change in the inter-annual streamflow as a response to precipitation and potential evapotranspiration change under emission scenarios RCP2.6, RCP4.5 and RCP8.5. Projected precipitation, potential evapotranspiration, and streamflow changes are calculated comparing period 1981–2005 to periods 2041-2065 (first and second line of the pannel) and 2071–2095 (third and fourth lines of the pannel). REMO-MPI [first column of the pannel (a, b, c, d)] and REMO-EC [second column of the pannel (e, f, g, h)].*

Table 18: Mean annual water balance components and percent change per RCM–GCM for the historical (1981–2005) and projected (2041–2065 and 2071-2095) periods under RCP2.6, RCP4.5 and RCP8.5 scenarios.

	near future (2041-2065)													
	REMO-EC							**REMO-MPI**						
Water balance		**RCP2.6**		**RCP4.5**		**RCP8.5**			**RCP2.6**		**RCP4.5**		**RCP8.5**	
components	Baseline	value	%	value	%	value	%	Baseline	value	%	value	%	value	%
Precipitation (mm/year)	1020.5	995.26	-2.48	1020.6	00	1016.9	-0.35	952.7	945.87	-0.71	966.55	1.45	920.98	-3.33
PET (mm/year)	1456.9	1586.6	8.90	1610.2	10.53	1653.5	13.49	1567	1682.2	7.37	1725.5	10.11	1802.6	15.04
AET (mm/year)	738.71	765.70	3.65	786.56	6.48	790.51	7.01	733.88	751.43	2.39	768.55	4.72	760.51	3.62
Soil moisture (mm/day)	158.99	150.35	-5.43	152.53	-4.06	149.11	-6.21	147.88	140.82	-4.77	139.9	-5.39	133.25	-9.89
Streamflow (m^3/s)	273.16	218.53	-19.99	227.87	-16.58	213.44	-21.86	207.39	187.58	-9.55	186.03	-10.3	153.07	-26.19
Hydropower (MW)	67.33	53.56	-20.01	56.16	-16.58	52.61	-21.86	51.11	46.23	-9.55	45.85	-10.3	37.73	-26.19
Late twenty First century (2071-2095)														
Precipitation (mm/year)	1020.5	981.41	-3.83	1013.4	-0.69	979.25	-4.04	952.7	965.45	1.33	944.05	-0.9	858.18	-9.92
PET (mm/year)	1456.9	1575.5	8.14	1664.2	14.23	1845.8	26.69	1567	1669.3	6.52	1766.9	12.76	2029.2	29.49
AET (mm/year)	738.71	754.62	2.15	788.76	6.78	805.58	9.05	733.88	760.08	3.57	757.60	3.23	752.70	2.56
Soil moisture (mm/day)	158.99	149.84	-5.75	148.30	-6.72	136.91	-13.88	147.88	142.87	-3.38	135.79	-8.17	116.27	-21.03
Streamflow (m^3/s)	273.16	211.94	-22.41	217.71	-20.3	164.33	-39.84	207.39	194.49	-6.22	173.17	-16.5	101.49	-51.06
Hydropower (MW)	67.33	52.24	-22.41	53.66	-20.3	40.50	-39.84	51.11	48.38	-6.22	42.68	-16.5	25.02	-51.06

In summary, with increasing RCP, streamflow is projected to decrease during the rainy season with the largest impact during the key high flow month of September. The similar negative trend of streamflow was also found in several studies using the REMO model in Upper Senegal, Térou and Ouémé catchments, respectively, by Mbaye et al. (2015), Cornelissen et al. (2013) and Bossa et al. (2014).

Compared to previous studies of the BRB (Mkankam, 2001; Sighomnou, 2004), we produced opposite results. This can be explained given that streamflow can strongly relate to the combined change in precipitation and PET (Fig. 46). Mkankam (2001) and Sighomnou (2004) found the increase of precipitation in the BRB by using HadCM2 and ECHAM4/OPYC3, and HadCM3 GCMs respectively, which naturally predict the increase of streamflows.

These findings demonstrate the importance of forcing hydrological models with higher resolution climate data for impact studies, and the need for regional climate information over Africa (Lennard et al., 2018), because Fotso-Nguemo et al. (2017) found that GCMs (EC-Earth and MPI-ESM-LR) predict an increase of rainfall over CA, while the REMO model forced by those GCMs predict a decrease. A similar result was also reported by Oguntunde and Abiodun (2013) when comparing RegCM3 RCM with ECHAM5 GCM.

3.5 Changes in monthly, seasonal and annual hydropower potential of the Lagdo Dam

This section presents the results of the potential impacts of climate change on hydropower potential of the Lagdo dam under different scenarios. The hydropower potential was computed based on the modeled streamflows under both scenarios and time periods. Figure 47 shows relative changes in monthly, seasonal and annual hydropower potential under the scenarios, models and time periods. The impact of climate change on hydropower potential is similar to the pattern of changes in streamflows. In general, hydropower potential of the Lagdo dam is projected to decrease. During September, the signal is strong under all scenarios, models and time periods, with the maximum decrease observed in the REMO-MPI combination during the late of the twenty-first century. The dry months do not exhibit a change signal which can be explained by absence of rainfall, thus very few streamflow. Under RCP2.6, the signal in August is uncertain during the late of the twenty-first century as results are both weakly positive and negative depending on the driving GCM. This is also true for scenarios RCP4.5 and 8.5 where an uncertain signal is observed in October and November for the two future periods (RCP4.5), and in November during the end of the century (RCP8.5) respectively.

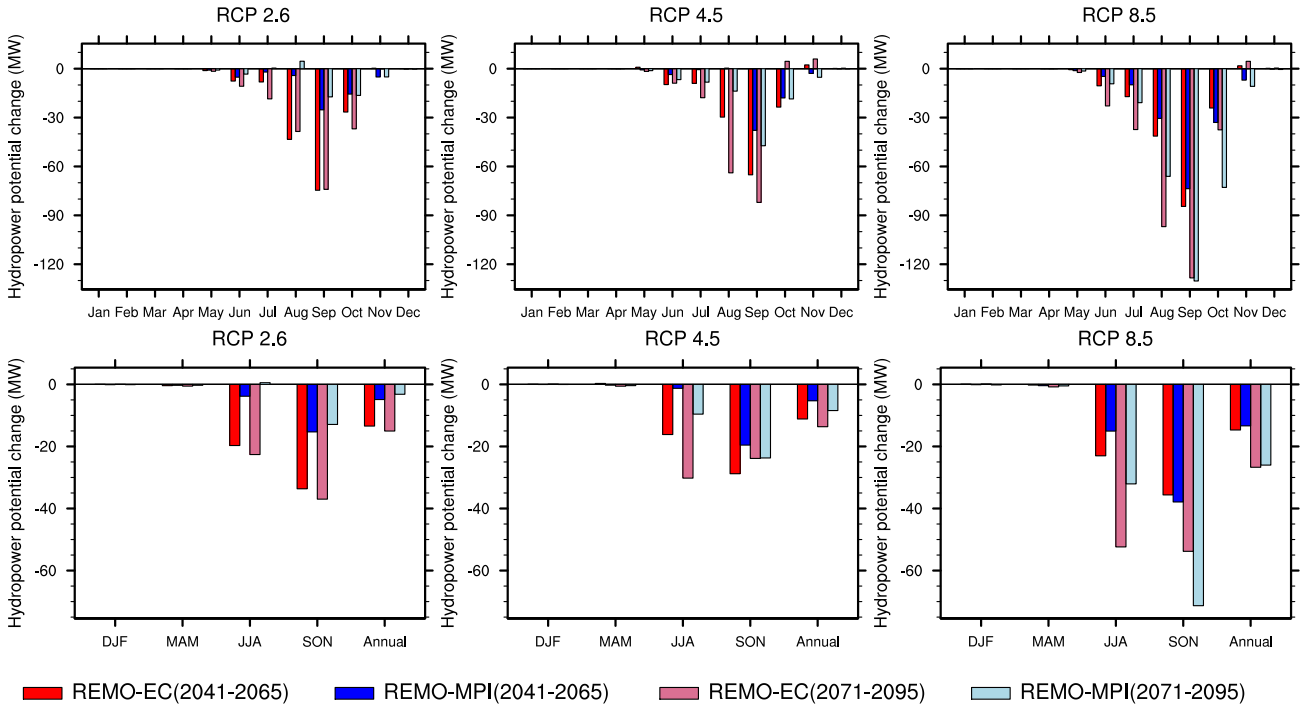

Figure 47: *Projected monthly (top), seasonal and annual (bottom) changes in hydropower potential of the Lagdo dam under the three scenarios (RCP2.6, RCP4.5, RCP8.5) for the two future periods (2041-2065 and 2071-2095) relative to the baseline period (1981-2005).*

Seasonally, the December-January-February (DJF) and March-April-May (MAM) seasons do not exhibit a change signal, while the June-July-August (JJA) and September-October-November (SON) seasons exhibit a clear decrease on hydropower potential. This can be explained by a combination of reduced precipitation, increased of both potential and actual evapotranspiration and reduced soil moisture, that result in a decrease in streamflows and thus hydropower potential in summer (JJA) and autumn (SON). The results also reveal that the relative change in seasonal as well as in annual hydropower potential are relatively larger with REMO–EC than that of REMO–MPI under both scenarios and time periods, except in SON under RCP8.5, where the signal is relatively large with REMO-MPI than that of REMO-EC in the two time periods. These seasonal and annual changes in hydropower potential are similar than those in streamflows. This can be explained by the fact that the streamflows and head are the main drivers of hydropower potential, and head is a constant, thus any change of streamflows characteristics will significantly impact the hydropower potential in the same direction. Relationship between change in inter-annual streamflows and in hydropower potential shows a strong and significant correlation ($R^2 = 1$) (see Fig. 48).

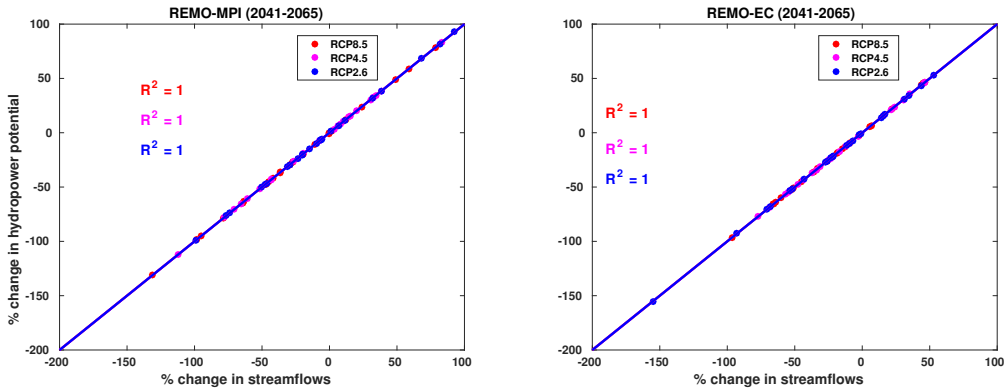

Figure 48: *Relationship between change in inter-annual streamflow and hydropower potential change under emission scenarios RCP2.6, RCP4.5 and RCP8.5.*

In summary, the seasonal and annual hydropower potential will decrease under both scenarios and time periods. The magnitude of the signal should vary according to the scenarios and time periods. This finding is consistent with that of Grijsen (2014). He used 15 GCMs runs from phase 3 of the Coupled Model Intercomparison Project (CMIP3) under A1B emission scenario and the Turc-Pike rainfall runoff model to study the potential impact of climate change on hydro-energy in different watersheds in Cameroon and found that hydro-energy generated at Lagdo dam in the Benue basin may suffer a significant decrease due to climate change.

3.6 Ecohydrological status of the watershed

This section presents the results of the Ecohydrological status of the HBRB determined by plotting the unused water (P_{ex}) versus unused energy (E_{ex}) in order to test the validity in assessing the interaction between increase PET and precipitation change as projected by the RCM-GCM. Figure 49 shows the ecohydrological status of the HBRB under scenarios, models and time periods. The results reveal a clear change signal under scenarios, models and time periods. The direction of the shift relative to the baseline period implies the drier environmental conditions in the watershed (water stress) due to a decrease in excess water (precipitation) and an increase in evaporative demand (according to Fig. 15). This led to a decrease of streamflow in the watershed and denotes an increase in PET higher than the increase in AET as reported in Table 18. According to Tomer and Schilling (2009), the change signal is not associated with a change in land use but rather with a change in climate.

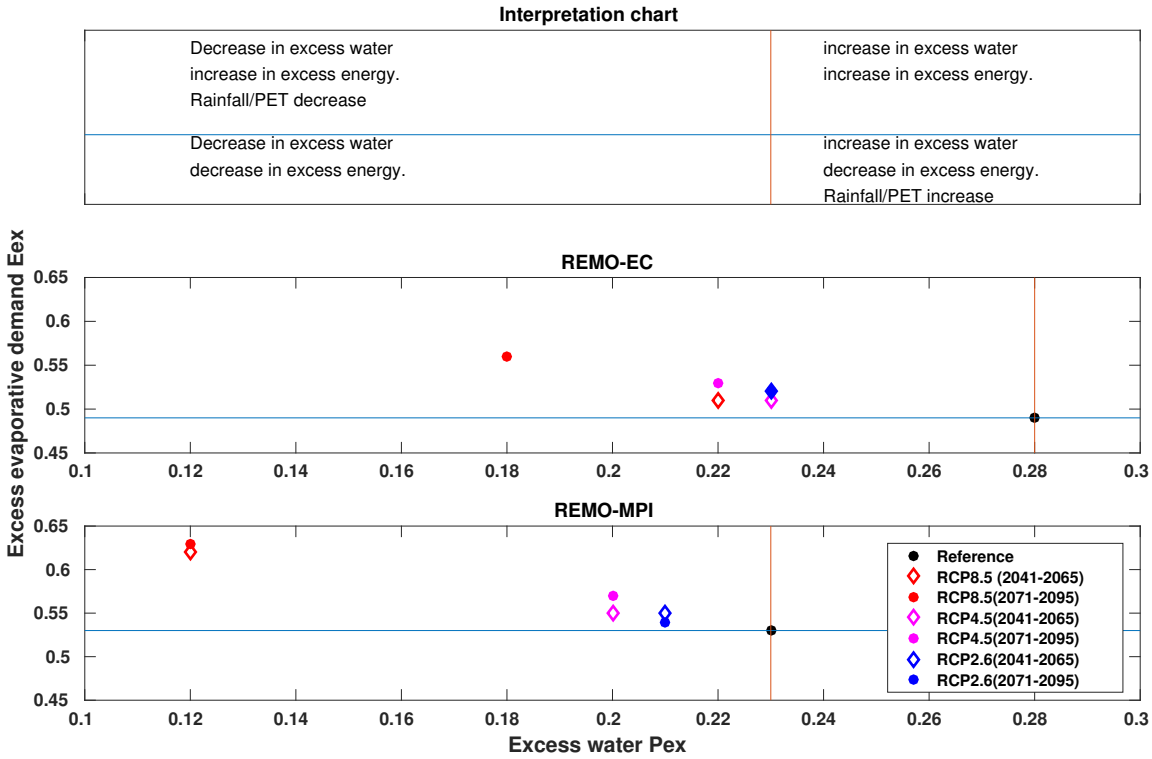

Figure 49: *Plot of excess precipitation (P_{ex}) V_s. evaporative demand (E_{ex}) for the reference period (1981–2005) and emission scenarios RCP2.6, RCP4.5 and RCP8.5 [2041–2065 (diamond) and 2071-2095 (filled circle)] for the REMO-MPI and REMO-EC. The shift in RCP dots compared to the reference period's dot indicates the effects of climate change on the catchment hydrology. P_{ex} and E_{ex} for each period are calculated from the annual average rainfall, potential evapotranspiration, and actual evapotranspiration.*

Drier environmental conditions of the watershed will be more evident under the RCP8.5 scenario than under the RCP4.5 and RCP2.6 scenarios, respectively. This can explain the important decrease of streamflow and hydropower potential under the RCP8.5 scenario as shown in Table 18. The result also reveals that the REMO–MPI projects an extreme drier environmental condition than REMO–EC under RCP8.5. The same result was reported by Fotso-Nguemo et al. (2016) over the CA region.

In summary, in the future, the HBRB will be move to a water stress. This result can be reinforced by those found by Guenang and Mkankam (2014) and Oguntunde et al. (2018). Guenang and Mkankam (2014) have assessed the drought occurrences in Cameroon over recent decades and found that the drought magnitude and duration increased with time for both short and long timescales in the North of Cameroon, as a response of a reduction in precipitation due to CC. Oguntunde et al. (2018) have studied the impacts of climate variability and change on drought characteristics in the NRB and found an increase in drought intensity and frequency over the NRB as a result of statistically significant correlation between runoff and drought indices.

Conclusion

In this chapter, we have analyzed the performance of the HBV-Light hydrological model to simulate the measured streamflows and the capacity of REMO model forced at it's lateral and surface boundary by two GCMs (EC-Earth and MPI-ESM) to simulate present climate in the HBRB. The impacts of climate change on hydro-climatic variables and hydropower potential were analyzed during the two future periods (2041–2065 and 2071–2095) relative to the baseline period (1981-2005) under RCP2.6, 4.5 and 8.5 scenarios.

The HBV-Light hydrological model performed well in the HBRB. It simulated the annual cycle of streamflows, low and high flows well although some bias. The uncertainties arising from the problem of identifying and optimizing model parameters insignificant impact on model predictions, while the model outputs are found to be significantly or not impacted by different PET inputs when we followed the static or dynamic sensitivity approaches respectively. The REMO model was found to reproduce the annual cycle of rainfall, 2-m temperature and PET well, although some relative low biases still exist. Under RCPs scenarios and time periods, the region will move to an extreme environmental drier conditions with the decrease of rainfall, increase of PET and temperature. This will negatively impact the streamflows and the hydropower potential of the Lagdo dam.

General conclusion and outlook

1 General conclusion

In the area where rainfed agriculture is the most important socioeconomic activity and where hydropower is the major source of electricity production, impact studies of future water resources are highly important for adaptation, or for inclusion in the design of new systems purpose. The main focus of this research was to evaluate the influence of the projected temperature and precipitation change on water resources and hydropower potential in the HBRB, Northern Cameroon. Streamflow used to compute the hydropower potential was produced by coupling dynamically downscaled precipitation and temperature from the REMO regional climate model (RCM) forced by the boundary conditions data of the Europe-wide Consortium Earth System Model (EC-ESM) and the Max Planck Institute-Earth System Model (MPI-ESM) general circulation models (GCMs) and the HBV-Light hydrological model under three (GHGs) concentration scenarios (RCP2.6, RCP4.5, and RCP8.5) during the future and baseline periods.

The successful application of hydrological models for water resource management of the catchment mostly depends on the quantification and reduction of uncertainties arising from model structure and model parameters. Identification of influential and non-influential model parameters that controlling the model outputs variations, as well as the parameter identifiability are valuable tools for reducing the model parameter dimension and limiting prediction uncertainty while maintaining a high quality solution for model calibration. The first stage of this study focused on the optimization and the performance evaluation of the HBV-Light hydrological model in the HBRB. For this task, a detailed analysis of the model parameter sensitivity and uncertainty to the model response was performed by using the Monte-Carlo procedure and multiple objective functions. The results showed that the soil and evaporation routine parameters (FC, β and LP) in addition with the recession coefficient (K_1) and the transformation routine parameter ($MAXBAS$) are the most or less influential parameters of the HBV-Light model to the volume error and high-flow series in the HBRB. Thus other parameters (K_0, K_2, $PERC$ and UZL) can be kept constant during the calibration of the model. The most or less influential parameters to the model response are also found to be more or less well-defined parameters in the model structure. The recalibration of the model based on the lower and upper limits

of the confidence interval showed that the optimized model parameters high performed the model in the HBRB during the calibration and validation stages, although some errors in simulating peak flows. The model predictions uncertainties revealed that the best simulation as well as the measured streamflows lie inside the 95% uncertainty band of model predictions, indicating the insignificant implications of the model parameters uncertainties to the model predictions and giving the merit to the Monte-Carlo procedure in calibrating and predicting uncertainties in model. Therefore, the HBV-Light hydrological model, with his set of optimized model parameters can be used as a tool by the decision-makers, water planners and scientific community to better manage the water resources in the HBRB, to predict extreme events such as floods and droughts and to address the future challenge on water resources and hydropower potential under climate change scenarios.

Unlike rain, direct measurement of evapotranspiration (ET) is hard, time consuming and costly because ET is depended on a number of factors that may vary both spatially and/or temporally. In practice, estimation of actual ET is often made by using information about Potential evapotranspiration (PET) and soil moisture. Several methods exist to estimate PET, ranging from using a single climate variable to combination methods. However, developed initially for agricultural applications, this approximation at the watershed scale is either unproven or inappropriate. There are advantages in using PET in the hydrological modeling as this considerably simplifies the representation of evaporation processes in a watershed but can considerably impact the model simulations and the optimized model parameters. In the second stage of this study, nineteen (19) PET estimation methods of different data requirements were applied in order to assess their effect on model performance, optimized parameters, and robustness of the HBV-Light hydrological model. The Monte-Carlo procedure was implemented to calibrate the HBV-Light model for each PET input while considering similar objective functions and dynamic and static sensitivity analysis approaches were used. The results revealed that, although significant differences between PET estimation methods, the hydrological model performance was satisfactory for each PET input in the calibration and validation periods. The model simulations and resultant efficiency are insensitive to PET inputs when we follow the dynamic approach. However, when using the static sensitivity approach the model simulations and efficiency are influenced by the PET inputs. This means that the over and under-estimation of PET is compensated by the model parameter during the calibration period. The hydrological model parameters were found to be sensitive to the 19 PET inputs. The ill defined model parameters are significantly affected by the PET inputs than the well defined parameters except the soil moisture threshold for reduction of ET parameter (LP) which is the most sensitive of well defined parameters to the PET inputs. In addition, the hydrological model performance was found to be insensitive to the rescaling PET inputs for both dynamic and static approaches. We also noted that, by following the static SA approach, the model performance is systematically improved when the rescaling factor of PET is used. Hargreaves method was also found to be best in computing PET in the HBRB and

therefore can be for agricultural applications when the data is not available in sufficient quantity over the study time period. This analysis provides a plausible explanation of the conflicting results obtained in the previous sensitivity analysis studies and now that we understand this we can suggest to the global hydrological modeling community the dynamic approach for impact assessment studies and for sensitivity of discharge projections to potential evapotranspiration estimation. This approach is the more reliable approach in simulating discharge because during the model recalibration, hydrological model has the potential to adapt its model parameters to the influence of both random and systematic errors in input data. However, if static sensitivity approach is used, then rescaling of input data should be done to avoid poor model results.

In the last stage of this research, the ability of the REMO model to simulate the present climate was evaluated prior to future climate change impact assessment. The REMO model was found to reproduce the annual cycle of rainfall, 2-m temperature and PET well, although some relative low biases still exist (MB less than 1 mm/day). The correlation coefficient between the REMO model and reanalysis (ERAINT, NCEP1, NCEP2) and observation (CRU) datasets are around 0.95 for precipitation, thus a strong correlation. Annual temperature and PET are projected to consistently increase under all scenarios, models and future periods. Although there is some uncertainty, annual precipitation is generally projected to decrease in the HBRB up to 10% under the RCP8.5 scenario in the late twenty-first century. This potential increase of both temperature and PET and a decrease of precipitation may lead to a decrease in the soil moisture and the increase of water stress of the plants. The agricultural production is likely to decline and with the decline of vegetation cover, the amplification of desertification in this area will increase. The combination of reduced precipitation increased PET and reduced soil moisture, resulting in a decrease in streamflow in the HBRB. This important decrease of streamflow will also negatively affect the hydropower potential of the Lagdo Dam, water irrigation and navigation in both future periods and importantly will move the region into a drier environmental conditions as shown by (E_{ex})–(P_{ex}) plot.

The results of this research might be useful for decision makers and planners in better managing the water resources and in developing adaptation strategies so as to limit the risks associated with global warming.

2 Outlook

One major caveat of this study is that only one RCM has been used. Likewise, results indicate that rainfall change in October is uncertain with contrasting runs' signal. Therefore, further works with a multi-model ensemble from CORDEX-Africa matrix are needed to quantify the range of uncertainty in this signal. Despite the fact that this study highlights the importance of using RCMs instead of GCMs for impact studies, both RCMs and GCMs are still biased, therefore, bias-correction

techniques needed to be performed for impact studies. We also found that the hydrological model efficiency is slightly sensitive to different PET inputs, it will be also much interesting to assess the impact of different PET inputs on the climate change impact signal. Until Lumped and conceptual hydrological model better performed in this catchment, the use of the semi-distributed or distributed hydrological models will be envisage-able in other to take into account the land use and land cover change in the impact studies.

References

Abebe, N.A., F.L. Ogden, and N.R. Pradhan, 2010: Sensitivity and uncertainty analysis of the conceptual HBV rainfall–runoff model: Implications for parameter estimation. *J. Hydrol.*, **389**, 301 – 310, doi: 10.1016/j.jhydrol.2010.06.007.

Abrate, T., P. Hubert, and D. Sighomnou, 2013: A study on hydrological series of the Niger River. *Hydrol. Sci. J.*, **58**, 271–279, doi: 10.1080/02626667.2012.752575.

Aghakouchak, A., and E. Habib, 2010: Application of a conceptual hydrologic model in teaching hydrologic processes. *Int. J. Eng. Educ.*, **26**, 963–973.

Aghakouchak, A., N. Nakhjiri, and E. Habib, 2013: Ensemble streamflow simulation and uncertainty analysis. *Hydrol. Earth Syst. Sci.*, **17**, 445–452, doi: doi:10.5194/hess–17–445–2013.

Allen, R.G., L.S. Pereira, D. Raes, and M. Smith, 1998: Crop evapotranspiration - Guidelines for computing crop water requirements. *FAO Irrigation and drainage paper 56, FAO, Rome, 300.*

Amougou, J.A., 2018: Chapitre 2: Changements climatiques au Cameroun–Manifestations, Vulnérabilités, Impacts et Réponses. *Science, Economics and Politics of Climate Change: A guide for policymakers in Cameroon*, 5.

Andreassian, V., C. Perrin, and C. Michel, 2004: Impact of imperfect potential evapotranspiration knowledge on the efficiency and parameters of watershed models. *J. Hydrol.*, **286(1-4)**, 19–35, doi: 10.1016/j.jhydrol.2003.09.030.

Angel, D.P., S. Attoh, D. Kromm, J. Dehart, R. Slocum, and S. White, 1998: The drivers of greenhouse gas emissions: What do we learn from local case studies? *Local Environ.*, **3**, 263–277, doi: 10.1080/13549839808725565.

Arétouyap, Z., N.P. Njandjock, D. Bisso, R. Nouayou, B. Lengué, and T.A. Lepatio, 2014: Climate Variability and its Possible Interactions with Water Resources in Central Africa. *J. Applied Sci.*, **14**, 2219–2233, doi: 10.3923/jas.2014.2219.2233.

ASCE, 1993: Criteria for evaluation of watershed models. *J. Irrig. Drain. Eng*, **119**, 429–442.

Bai, P., X. Liu, T. Yang, F. Li, K. Liang, S. Hu, and C. Liu, 2016: Assessment of the Influences of Different Potential Evapotranspiration Inputs on the Performance of Monthly Hydrological Models under Different Climatic Conditions. *J. Hydrometeor.*, **17**, 2259–2274, doi:10.1175/JHM–D–15–0202.1.

Bergström, S., 1976: *Development and Application of a Conceptual Runoff Model for Scandinavian*

Catchments. A: Bulletin series. Department of Water Resources Engineering, Lund Institute of Technology, University of Lund, 134.

Bergström, S., 1992: The HBV model - its structure and applications. *SMHI Reports*, **No. 4**, Norrköping, 44.

Bergström, S., 2006: Experience from applications of the HBV hydrological model from the perspective of prediction in ungauged basins. *IAHS Pub.*, **307**, 97.

Bergström, S., and A. Forman, 1973: Development of a conceptual deterministic rainfall-runoff model. *Nordic Hydrol.*, **4**, 147–170.

Beven, K., 2005: On the concept of model structural error. *Water Sci. Technol.*, **52**, 167–175, doi: 10.2166/wst.2005.0165.

Beven, K.J., 2001: Rainfall-runoff modelling, the primer. *John Wiley & Sons Ltd*, 360.

Birhanu, D., H. Kim, C. Jang, and S. Park, 2018: Does the complexity of evapotranspiration and hydrological models enhance robustness? *Sustainability*, **10**, 28–37, doi:10.3390/su10082837.

Blanco, G., R. Gerlagh, S. Suh, J. Barrett, H.C. de Coninck, C.F. Diaz Morejon, R. Mathur, N. Nakicenovic, A. Ofosu Ahenkora, J. Pan, H. Pathak, R. Rice, J.and Richels, S.J. Smith, D.I. Stern, F.L. Toth, and P. Zhou, 2014: Drivers, Trends and Mitigation. In: Climate Change 2014: Mitigation of Climate Change. Contribution of Working Group III to the AR5 of the IPCC [Edenhofer, O., R. Pichs-Madruga, Y. Sokona, E. Farahani, S. Kadner, K. Seyboth, A. Adler, I. Baum, S. Brunner, P. Eickemeier, B. Kriemann, J. Savolainen, S. Schlömer, C. von Stechow, T. Zwickel and J.C. Minx (eds.)]. *Cambridge University Press, Cambridge, United Kingdom and New York, NY, USA*, 62.

Blanco, I.M., 2011: *Modeling Climate Change Impacts on Hydrology and Water Resources: Case Study Rio Conchos Basin*. PhD Dissertation, University of Texas at Austin, 214p.

Blasone, R.S., 2007: *Parameter estimation and uncertainty assessment in hydrological modelling.* PhD thesis, Technical University of Denmark, 71.

Bossa, A.Y., B. Diekkrüger, and E.K. Agbossou, 2014: Scenario-Based Impacts of Land Use and Climate Change on Land and Water Degradation from the Meso to Regional Scale. *Water*, **6**, 3152–3181, doi: 10.3390/w6103152.

Boyer, J.F., C. Dieulin, N. Rouche, A. CRES, E. Servat, J.E. Paturel, and G. Mahé, 2006: SIEREM : an environmental information system for water resources. *5th World FRIEND Conference, La Havana–Cuba, November 2006 in Climate Variability and Change–Hydrological Impacts IAHS Publ.*, **308**, 19–25.

Boyle, D.P., H.V. Gupta, and S. Sorooshian, 2000: Toward improved calibration of hydrologic models: Combining the strengths of manual and automatic methods. *Water Resour. Res.*, **36**, 3663–3674, doi: 10.1029/2000WR900207.

Brovkin, V., L. Boysen, T. Raddatz, V. Gayler, A. Loew, and M. Claussen, 2013: Evaluation of

vegetation cover and land-surface albedo in MPI-ESM CMIP5 simulations. *J. Adv. Model. Earth Syst.*, **5**, 48–57.

Busuioc, A., F. Giorgi, X. Bi, and M. Ionita, 2006: Comparison of regional climate model and statistical downscaling simulations of different winter precipitation change scenarios over Romania. *Theor.Appl. Climatol.*, **86**, 101–123, doi: 10.1007/s00704–005–0210–8.

Callaway, J., 2004: Adaptation benefits and costs: Are they important in the global policy picture and how can we estimate them? *Global Environ. Change - Human Policy Dimens.*, **14**, 273–282, doi: 10.1016/j.gloenvcha.2004.04.002.

Carson, R.T., 2009: The Environmental Kuznets Curve: Seeking Empirical Regularity and Theoretical Structure. *Rev. Environ. Econ. Policy.*, **4**, 3–23, doi: 10.1093/reep/rep021.

Cheo, A.E., H.J. Voigt, and R.L. Mbua, 2013: Vulnerability of water resources in northern Cameroon in the context of climate change. *Environ. Earth Sci.*, **70**, 1211–1217, doi: 10.1007/s12665–012–2207–9.

Cherie, N.Z., 2013: *Downscaling and modeling the effects of climate change on hydrology and water resources in the upper Blue Nile river basin, Ethiopia.* PhD thesis, Universitäts bibliothek Kassel, 329p.

Chou, S.C., A. Lyra, C. Mourão, C. Dereczynski, I. Pilotto, J. Gomes, J. Bustamante, P. Tavares, A. Silva, D. Rodrigues, D. Campos, D. Chagas, G. Sueiro, G. Siqueira, and J. Marengo, 2014: Assessment of climate change over South America under RCP4.5 and 8.5 downscaling scenarios. *Am. J. Clim. Change*, **3(5)**, 512–525.

Chow, T.V., D.R. Maidment, and L.W. Mays, 1988: Applied hydrology. *Water Resources Handbook; McGraw-Hill: New York, NY, USA*, 294.

Christensen, J.H., B. Hewitson, A. Busuioc, A. Chen, X. Gao, R. Held, R. Jones, R.K. Kolli, W. Kwon, R. Laprise, V. Magana Rueda, L. Mearns, C. Menendez, J. Räisänen, A. Rinke, A. Sarr, P. Whetton, R. Arritt, R. Benestad, M. Beniston, D. Bromwich, D. Caya, J. Comiso, R. de Elia, and K. Dethloff, 2007: Regional climate projections. *Climate Change, 2007: The Physical Science Basis. Contribution of Working group I to the AR4 of the IPCC, University Press, Cambridge, Chapter 11, ISBN: 978-0-521-88009-1, pp 847–940.*

Cornelissen, T., B. Diekkrüger, and S. Giertz, 2013: A comparison of hydrological models for assessing the impact of land use and climate change on discharge in a tropical catchment. *J. Hydrol.*, **498**, 221 – 236.

Dassou, E., A. Ombolo, S. Chouto, G. Mboudou, J. Essi, and E. Bineli, 2016: Trends and Geostatistical Interpolation of Spatio-Temporal Variability of Precipitation in Northern Cameroon. *Am. J. Clim. Change*, **5**, 229–244, doi: 10.4236/ajcc.2016.52020.

Dassou, E.F., 2019: *Impact de la variabilité climatique sur la réponse hydrologique du bassin versant supérieur de la Bénoué (Nord-Cameroun).* Thèse de Doctorat/PhD, Université de Maroua, 332.

de Oliveira, V.A., C.R. de Mello, M.R. Viola, and R. Srinivasan, 2017: Assessment of climate change impacts on streamflow and hydropower potential in the headwater region of the Grande river basin, Southeastern Brazil. *Int. J. Climatol.*, **37**, 5005–5023, doi: 10.1002/joc.5138.

Deb, D., J. Butcher, and R. Srinivasan, 2015: Projected Hydrologic Changes Under Mid-21st Century Climatic Conditions in a Sub-arctic Watershed. *Water Resour. Manag.*, **29**, 1467–1487, doi: 10.1007/s11269–014–0887–5.

Dee, D.P., S.M. Uppala, A.J. Simmons, P. Berrisford, P. Poli, S. Kobayashi, U. Andrae, M.A. Balmaseda, G. Balsamo, P. Bauer, P. Bechtold, A.C.M. Beljaars, L. van de Berg, J. Bidlot, N. Bormann, C. Delsol, R. Dragani, M. Fuentes, A.J. Geer, L. Haimberger, S.B. Healy, H. Hersbach, E.V. Hólm, L. Isaksen, P. Kållberg, M. Köhler, M. Matricardi, A.P. McNally, B.M. Monge-Sanz, J.J. Morcrette, B.K. Park, C. Peubey, P. de Rosnay, C. Tavolato, J.N. Thépaut, and F. Vitart, 2011: The era-interim reanalysis: configuration and performance of the data assimilation system. *Q. J. R. Meteorol. Soc.*, **137**, 553–597. doi:10.1002/qj.828.

Djaman, K., A.B. Balde, A. Sow, B. Muller, S. Irmak, M.K. N'Diaye, B. Manneh, Y.D. Moukoumbi, K. Futakuchi, and K. Saito, 2015: Evaluation of sixteen reference evapotranspiration methods under sahelian conditions in the Senegal River Valley. *J. Hydrol.: Reg. Stud.*, **3**, 139–159, doi:10.1016/j.ejrh.2015.02.002.

Djaman, K., M. O'Neill, L. Diop, A. Bodian, S. Allen, K. Koudahe, and K. Lombard, 2019: Evaluation of the Penman-Monteith and other 34 reference evapotranspiration equations under limited data in a semiarid dry climate. *Theor. Appl. Climatol.*, **137**, 729–743, doi: 10.1007/s00704–018–2624–0.

Donfack, F.C., A. Lenouo, and C. Tchawoua, 2018: Water Requirements for Corn Yields in the Northern Regions of Cameroon Using AquaCrop Model. *J. agric. ecol. res. int.*, **16**, 1–11, doi: 10.9734/JAERI/2018/44993.

Doorenbos, J., and W.O. Pruitt, 1977: *Guidelines for Predicting Crop Water Requirements.* FAO Irrigation and Drainage. Paper No. 24. FAO, Rome, Italy.

Dzana, J.G., J.R.N. Ngoupayou, and P. Tchawa, 2011: The Sanaga discharge at the Edea Catchment outlet (Cameroon): An example of hydrologic responses of a tropical rain-fed river system to changes in precipitation and groundwater inputs and to flow regulation. *River Res. Appl.*, **27**, 754–771, doi: 10.1002/rra.1392.

FAOSTAT, 2012: United Nations Food and Agriculture Organization. *Available online: http://faostat.fao.org/site/291/default.aspx.*

Federer, C.A., C. Vorosmarty, and B. Fekete, 1996: Intercomparison of methods for calculating potential evaporation in regional and global water balance models. *Water Resour. Res.*, **32(7)**, 2315–2321.

FISRWG, 1998: *Stream corridor restoration: Principles, processes, and practices.* National Technical

Info Svc, 637.

Flato, G., J. Marotzke, B. Abiodun, P. Braconnot, SChou, W. Collins, P. Cox, F. Driouech, S. Emori, V. Eyring, C. Forest, P. Gleckler, E. Guilyardi, C. Jakob, V. Kattsov, C. Reason, and M. Rummukainen, 2014: Evaluation of climate models. In: *Climate change 2013: the physical science basis. Contribution of Working Group I to the Fifth Assessment Report of the Intergovernmental Panel on Climate Change*, pp. 741–866. Cambridge University Press.

Flato, G.M., 2011: Earth system models: an overview. *WIREs Climate Change*, **2**, 783–800, doi: 10.1002/wcc.148.

Fotso-Nguemo, T.C., 2018: *Évaluation et analyse de la valeur ajoutée du modèle climatique régional REMO en Afrique Centrale dans le contexte des changements climatiques.* Thèse de Doctorat/PhD, Université de Yaoundé 1, 138.

Fotso-Nguemo, T.C., D.A. Vondou, W.M. Pokam, Z.Y. Djomou, I. Diallo, A. Haensler, L.A.D. Tchotchou, P.H. Kamsu-Tamo, A.T. Gaye, and C. Tchawoua, 2017: On the added value of the regional climate model REMO in the assessment of climate change signal over Central Africa. *Clim. Dyn.*, **49**, 3813–3838, doi: 10.1007/s00382–017–3547–7.

Fotso-Nguemo, T.C., D.A. Vondou, C. Tchawoua, and A. Haensler, 2016: Assessment of simulated rainfall and temperature from the regional climate model REMO and future changes over Central Africa. *Clim. Dyn.*, **48**, 3685–3705, doi: 10.1007/s00382–016–3294–1.

Fowler, H.J., S. Blenkinsop, and C. Tebaldi, 2007: Linking climate change modelling to impacts studies: recent advances in downscaling techniques for hydrological modelling. *Int. J. Climatol.*, **27**, 1547–1578, doi: 10.1002/joc.1556.

Freer, J., K. Beven, and B. Ambroise, 1996: Bayesian Estimation of Uncertainty in Runoff Prediction and the Value of Data: An Application of the GLUE Approach. *Water Resour. Res.*, **32**, 2161–2173, doi: 10.1029/95WR03723.

Gachon, P., and Y. Dibike, 2007: Temperature change signals in Northern Canada: convergence of statistical downscaling results using two driving GCMs. *Int. J. Climatol.*, **27**, 1623–1641, doi: 10.1002/joc.1582.

Gao, H., T.J. Bohn, E. Podest, K.C. McDonald, and D.P. Lettenmaier, 2011: On the causes of the shrinking of lake chad. *Environ. Res. Lett.*, **6**, 034021, http://stacks.iop.org/1748–9326/6/i=3/a=034021.

Geist, H.J., and E.F. Lambin, 2002: Proximate Causes and Underlying Driving Forces of Tropical Deforestation: Tropical forests are disappearing as the result of many pressures, both local and regional, acting in various combinations in different geographical locations. *Bioscience*, **52**, 143–150, doi: 10.1641/0006–3568(2002)052[0143:PCAUDF]2.0.CO;2.

Giorgetta, M.A., J. Jungclaus, C.H. Reick, S. Legutke, J. Bader, M. Böttinger, V. Brovkin, T. Crueger, M. Esch, K. Fieg, K. Glushak, V. Gayler, H. Haak, H.D. Hollweg, T. Ilyina,

S. Kinne, L. Kornblueh, D. Matei, T. Mauritsen, U. Mikolajewicz, W. Mueller, D. Notz, F. Pithan, T. Raddatz, S. Rast, R. Redler, E. Roeckner, H. Schmidt, R. Schnur, J. Segschneider, K.D. Six, M. Stockhause, C. Timmreck, J. Wegner, H. Widmann, K.H. Wieners, M. Claussen, J. Marotzke, and B. Stevens, 2013: Climate and carbon cycle changes from 1850 to 2100 in MPI-ESM simulations for the Coupled Model Intercomparison Project phase 5. *J. Adv. Model. Earth Syst.*, **5**, 572–597, doi:10.1002/jame.20038.

Giorgi, F., C. Jones, and G.R. Asrar, 2009: Addressing climate information needs at the regional level: the CORDEX framework. *World Meteorol. Org. (WMO) Bull.*, **58**, 175.

Goosse, H., P.Y. Barriat, M.F. Loutre, and V. Zunz, 2010: *Introduction to climate dynamics and climate modeling*. Centre de recherche sur la Terre et le climat Georges Lemaître-UCLouvain, 36.

Grijsen, J., 2014: Understanding the impact of climate change on hydropower: the case of Cameroon. *Report No. 87913 ,World Bank, Washington, DC*, 166.

Guenang, G.M., and F.K. Mkankam, 2014: Computation of the Standardized Precipitation Index (SPI) and Its Use to Assess Drought Occurrences in Cameroon over Recent Decades. *J. Appl. Meteorol. Climatol.*, **53**, 2310–2324, doi: 10.1175/JAMC–D–14–0032.1.

Guenang, G.M., and K.F. Mkankam, 2012: Onset, retreat and length of the rainy season over Cameroon. *Atmos. Sci. Lett.*, **13**, 120–127, doi: 10.1002/asl.371.

Gupta, H.V., S. Sorooshian, and P.O. Yapo, 1999: Status of automatic calibration for hydrologic models: Comparison with multilevel expert calibration. *J. Hydrol. Eng.*, **4**, 135–143.

Haensler, A., F. Saeed, and D. Jacob, 2013: Assessing the robustness of projected precipitation changes over Central Africa on the basis of a multitude of global and regional climate projections. *Clim. Change*, **121**, 349–363, doi: 10.1007/s10584–013–0863–8.

Hagemann, S., 2002: An improved land surface parameter dataset for global and regional climate models. *Report / Max-Planck-Institut für Meteorologie, 336.*

Hakala, K., N. Addor, C. Teutschbein, M. Vis, H. Dahklaoui, and J. Seibert, 2019: Hydrological modeling of climate change impacts. In: *Encyclopedia of Water: Science, Technology, and Society, 20.*

Harris, I., P. Jones, T. Osborn, and D. Lister, 2014: Updated high-resolution grids of monthly climatic observations–the CRUTS3.10 dataset. *Int. J. Climatol.*, **34**, 623–642, doi: 10.1002/joc.3711.

Haylock, M.R., G.C. Cawley, C. Harpham, R.L. Wilby, and C.M. Goodess, 2006: Downscaling heavy precipitation over the United Kingdom: a comparison of dynamical and statistical methods and their future scenarios. *Int. J. Climatol.*, **26**, 1397–1415, doi: 10.1002/joc.1318.

Hertwich, E.G., and G.P. Peters, 2009: Carbon Footprint of Nations: A Global, Trade-Linked Analysis. *Environ. Sci. Technol.*, **43**, 6414–6420, doi: 10.1021/es803496a.

Hewitson, B.C., and R.G. Crane, 2006: Consensus between GCM climate change projections with

empirical downscaling: precipitation downscaling over South Africa. *Int. J. Climatol.*, **26**, 1315–1337, doi: 10.1002/joc.1314.

Hijioka, Y., Y. Matsuoka, H. Nishimoto, T. Masui, and M. Kainuma, 2008: Global GHG emission scenarios under GHG concentration stabilization targets. *J. Glob. Environ. Eng.*, **13**, 97–108, https://ci.nii.ac.jp/naid/10021137422/en/.

Hurtt, G.C., L.P. Chini, S. Frolking, R. Betts, J. Feddema, G. Fischer, J. Fisk, K. Hibbard, R. Houghton, A. Janetos, C. Jones, G. Kindermann, T. Kinoshita, K.K. Goldewijk, K. Riahi, E. Shevliakova, S. Smith, E. Stehfest, A. Thomson, P. Thornton, D. van Vuuren, and Y. Wang, 2011: Harmonization of land-use scenarios for the period 1500–2100: 600 years of global gridded annual land-use transitions, wood harvest, and resulting secondary lands. *Clim. Change*, **109**, 117–161, doi:10.1007/s10584–011–0153–2.

Ilyina, T., K.D. Six, J. Segschneider, E. Maier-Reimer, H. Li, and I. Núñez-Riboni, 2013: Global ocean biogeochemistry model HAMOCC: Model architecture and performance as component of the MPI-Earth system model in different CMIP5 experimental realizations. *J. Adv. Model. Earth Syst.*, **5**, 287–315.

IPCC, 2001: Climate Change 2001: The Scientific Basis, Technical Summary of the Working Group I Report [Houghton, J.T., Y. Ding, D.J. Griggs, M. Noguer, P.J. van der Linden, X. Dai, K. Maskell, and C.A. Johnson (eds.)]. *Cambridge University Press, Cambridge, United Kingdom and New York, NY, USA, 893.*

IPCC, 2007: Climate Change 2007: The Physical Science Basis. Contribution of Working Group I to the Fourth Assessment Report of the Intergovernmental Panel on Climate Change [Solomon, S., D. Qin, M. Manning, Z. Chen, M. Marquis, K.B. Averyt, M.Tignor and H.L. Miller (eds.)]. *Cambridge University Press, Cambridge, United Kingdom and New York, NY, USA, 43.*

IPCC, 2013: Climate Change 2013: The Physical Scientific Basis, IPCC Contribution of Working Group I to the AR5 of the IPCC [Stocker, T.F., D. Qin, G.-K. Plattner, M. Tignor, S.K. Allen, J. Boschung, A. Nauels, Y. Xia, V. Bex and P.M. Midgley (eds.)]. *Cambridge University Press, Cambridge, United Kingdom and New York, NY, USA, 222.*

IRAP, 2015: Hydropower in Africa: African Dams Briefing. *1250 Pretorius street, Suite G9 Ground Floor, East wing Pro Equity Court, Hatfiled 00083, Pretoria, 181.*

Irmak, S., T. Howell, R. Allen, J. Payero, and D. Martin, 2005: Standardized ASCE-Penman–Monteith: Impact of sum-of-hourly vs. 24-hr-timestep computations at reference weather station sites. *Trans. ASABE*, **48(3)**, 1063–1077, doi: 10.13031/2013.18517.

Irmak, S., A. Irmak, R.G. Allen, and J.W. Jones, 2003: Solar and Net Radiation-Based Equations to Estimate Reference Evapotranspiration in Humid Climates. *J. Irrig. Drain. Eng.*, **123**, 336–347.

Jacob, C., 2001a: The representation of cloud cover in atmospheric general circulation models. *PhD thesis, Ludwig-Maximilians-Universitaet Muenchen*, pp. 193.

Jacob, D., 2001b: A note to the simulation of the annual and inter-annual variability of the water budget over the Baltic Sea drainage basin. *Meteorol. Atmos. Phys.*, **77**, 61–73, doi: 10.1007/s007030170017.

Jacob, D., A. Elizalde, A. Haensler, S. Hagemann, P. Kumar, R. Podzun, D. Rechid, A.R. Remedio, F. Saeed, K. Sieck, C. Teichmann, and C. Wilhelm, 2012: Assessing the Transferability of the Regional Climate Model REMO to Different COordinated Regional Climate Downscaling EXperiment (CORDEX) Regions. *Atmosphere*, **3**, 181–199, doi: 10.3390/atmos3010181.

Jakob, M., R. Marschinski, and M. Hübler, 2013: Between a Rock and a Hard Place: A Trade-Theory Analysis of Leakage Under Production and Consumption-Based Policies. *Environ. Resour. Econ.*, **56**, 47–72, doi: 10.1007/s10640–013–9638–y.

Jensen, M.E., R.D. Burman, and R.G. Allen, 1990: Evapotranspiration and water requirements. *ASCE Manual 70, New York, USA, 332pp.*

Jørgensen, S.E., and G. Bendoricchio, 2001: *Fundamentals of ecological modelling*, Volume 21. Elsevier, 523.

Jubb, I., P. Canadell, and M. Dix, 2013: Representative concentration pathways (RCPs). *Australian Government, Department of the Environment, 3.*

Jung, C., D. Lee, and J. Moon, 2014: Comparison of the Penman Monteith and regional calibration of Hargreaves equation for actual evapotranspiration using SWAT stimulated results in Seolma-Cheon watershed. *Hydrol. Sci. J.*, **61**, 1–16.

Jungclaus, J., N. Fischer, H. Haak, K. Lohmann, J. Marotzke, D. Matei, U. Mikolajewicz, D. Notz, and J. Von Storch, 2013: Characteristics of the ocean simulations in the max planck institute ocean model (mpiom) the ocean component of the mpi-earth system model. *J. Adv. Model. Earth Syst.*, **5**, 422–446.

Kalnay, E., M. Kanamitsu, R. Kistler, W. Collins, D. Deaven, L. Gandin, M. Iredell, S. Saha, G. White, J. Woollen, Y. Zhu, M. Chelliah, W. Ebisuzaki, W. Higgins, J. Janowiak, K.C. Mo, C. Ropelewski, J. Wang, A. Leetmaa, R. Reynolds, R. Jenne, and D. Joseph, 1996: The NCEP/NCAR 40-Year Reanalysis Project. *Bull. Am. Meteorol. Soc.*, **77**, 437–472, doi: 10.1175/1520–0477(1996)077<0437:TNYRP>2.0.CO;2.

Kanamitsu, M., W. Ebisuzaki, J. Woollen, S.K. Yang, J.J. Hnilo, M. Fiorino, and G.L. Potter, 2002: NCEP–DOE AMIP-II Reanalysis (R-2). *Bull. Am. Meteorol. Soc.*, **83**, 1631–1644, doi: 10.1175/BAMS–83–11–1631.

Khan, M.Y.A., S. Daityari, and G.J. Chakrapani, 2016: Factors responsible for temporal and spatial variations in water and sediment discharge in Ramganga River, Ganga Basin, India. *Environ. Earth Sci.*, **75**, 283, doi:10.1007/s12665–015–5148–2.

Kiehl, J.T., and K.E. Trenberth, 1997: Earth's Annual Global Mean Energy Budget. *Bull. Am. Meteorol. Soc.*, **78**, 197–208, doi: 10.1175/1520–0477(1997)078<0197:EAGMEB>2.0.CO;2.

Klemeš, V., 1986: Operational testing of hydrologic simulation models. *Hydrol. Sci. J.*, **31(1)**, 13–24.

Klepper, O., H. Scholten, and J.P.G.D. Van Kamer, 1991: Prediction uncertainty in an ecological model of the oosterschelde estuary. *J. Forecast.*, **10**, 191–209, doi: 10.1002/for.3980100111.

Kostinakis, K., F. Xystrakis, K. Theodoropoulos, D. Stathis, and E. Eleftheriadou, 2011: Estimation of reference potential evapotranspiration with focus on vegetation science - the EmPEst software. *J. Irrig. Drain. Eng. - ASCE*, **137(9)**, 616–619.

Kwakye, S.O., and A. Bárdossy, 2020: Hydrological modelling in data-scarce catchments: Black Volta basin in West Africa. *SN Appl. Sci.*, **2**, 1–19. https://doi.org/10.1007/s42452–020–2454–4.

Legates, D.R., and G.J. McCabe, 1999: Evaluating the use of "goodness-of-fit" measures in hydrologic and hydroclimatic model validation. *Water Resour. Res.*, **135(1)**, 233–241, doi: 10.1029/1998WR900018.

Lennard, C.J., G. Nikulin, A. Dosio, and W. Moufouma-Okia, 2018: On the need for regional climate information over Africa under varying levels of global warming. *Environ. Res. Lett.*, **13**, 060401, doi: 10.1088/1748–9326/aab2b4.

Li, L., I. Diallo, C.Y. Xu, and F. Stordal, 2015: Hydrological projections under climate change in the near future by RegCM4 in Southern Africa using a large-scale hydrological model. *J. Hydrol.*, **528**, 1 – 16, doi: 10.1016/j.jhydrol.2015.05.028.

Lienou, G., 2013: Integrated Future Needs and Climate Change on the River Niger Water Availability. *J. Water Resource. Prot.*, **5(9)**, 887–893, doi: 10.4236/jwarp.2013.59090.

Liénou, G., G. Mahé, J.E. Paturel, E. Servat, D. Sighomnou, and L. Sigha-Nkamdjou, 2008: Impact de la variabilité climatique en zone équatoriale: exemple de modification de cycle hydrologique des rivières du sud-Cameroun. *13th IWRA World Water Congress, Montpellier, France.*

Lim, H.J., S.H. Yoo, and S.J. Kwak, 2009: Industrial CO2 emissions from energy use in Korea: A structural decomposition analysis. *Energ. Policy*, **37**, 686 – 698, doi: 10.1016/j.enpol.2008.10.025.

Liu, Y., and H.V. Gupta, 2007: Uncertainty in hydrologic modeling: Toward an integrated data assimilation framework. *Water Resour. Res.*, **43**, doi: 10.1029/2006WR005756.

Lohmann, U., and E. Roeckner, 1996: Design and performance of a new cloud microphysics scheme developed for the ECHAM general circulation model. *Clim. Dyn.*, **12**, 557–572, doi: 10.1007/BF00207939.

Louis, J.F., 1979: A parametric model of vertical eddy fluxes in the atmosphere. *Bound-Layer Meteorol.*, **17**, 187–202, doi: 10.1007/BF00117978.

Madsen, H., 2003: Parameter estimation in distributed hydrological catchment modelling using automatic calibration with multiple objectives. *Adv. Water Resour.*, **26**, 205 – 216, doi: 10.1016/S0309–1708(02)00092–1.

Madsen, H., G. Wilson, and H.C. Ammentorp, 2002: Comparison of different automated strategies for calibration of rainfall-runoff models. *J. Hydrol.*, **261(1–4)**, 48—-59.

Mafany, G., W. Fantong, and G. Nkeng, 2006: Groundwater quality in Cameroon and its vulnerability to pollution. In: *Groundwater pollution in Africa*, pp. 61–70. CRC Press.

Magrin, G., 2007: L'Afrique sub-saharienne face aux famines énergétiques. *EchoGéo*, doi:10.4000/echogeo.1976.

Mahé, G., and J.E. Paturel, 2009: Sahelian annual rainfall variability and runoff increase of Sahelian Rivers. *Geosc.*, **341**, 538–546.

Malla, S., 2009: CO2 emissions from electricity generation in seven Asia-Pacific and North American countries: A decomposition analysis. *Energ. Policy*, **37**, 1 – 9, doi: 10.1016/j.enpol.2008.08.010.

Matulla, C., N. Groll, H. Kromp-Kolb, H. Scheifinger, M. Lexer, and M. Widmann, 2002: Climate change scenarios at Austrian National Forest Inventory sites. *Clim. Res.*, **22**, 161–173, doi: 10.3354/cr022161.

Mba, W.P., G.N.T. Longandjo, W. Moufouma-Okia, J.P. Bell, R. James, D.A. Vondou, A. Haensler, T.C. Fotso-Nguemo, G.M. Guenang, A.L.D. Tchotchou, P.H. Kamsu-Tamo, R.R. Takong, G. Nikulin, C.J. Lennard, and A. Dosio, 2018: Consequences of 1.5^oC and 2^oC global warming levels for temperature and precipitation changes over Central Africa. *Environ. Res. Lett.*, **13**, 055011, doi: 10.1088/1748–9326/aab048.

Mbaye, M.L., S. Hagemann, A. Haensler, T. Stacke, A.T. Gaye, and A. Afouda, 2015: Assessment of Climate Change Impact on Water Resources in the Upper Senegal Basin (West Africa). *Am. J. Clim. Change*, **4**, 77–93, doi: doi:10.4236/ajcc.2015.41008.

Melching, C.S., 1995: Reliability estimation. *Computer Models of Watershed Hydrology, Water Resour. Pub. https://ci.nii.ac.jp/naid/10021137804/en/.*

Milne, B.T., V.K. Gupta, and C. Restrepo, 2002: A scale invariant coupling of plants, water, energy, and terrain. *Écoscience*, **9**, 191–199.

, MINEE, and GWP. Plan d'Action Nationale de Gestion Intégrée des Ressources en Eau (PANGIRE): État des lieux du secteur - Connaissance et usages des ressources en eau. pp. 219.

MINEP, and UNDP, 2012: Évaluation des risques, de la vulnérabilité et adaptations aux changements climatiques Cameroun. *Final report*, 256p.

Mishra, S., 2009: Uncertainty and sensitivity analysis techniques for hydrologic modeling. *J. Hydroinform.*, **11**, 282–296, doi: 10.2166/hydro.2009.048.

Mishra, S., N.E. Deeds, and B.S. RamaRao, 2003: Application of classification trees in the sensitivity analysis of probabilistic model results. *Reliab. Eng. Syst. Safety*, **79**, 123 – 129, doi: 10.1016/S0951–8320(02)00222–3.

Mkankam, F.K., 2001: Impact of greenhouse gas induced climate change on the runoff of the Upper Benue River (Cameroon). *J. Hydrol.*, **252**, 145 – 156, doi: 10.1016/S0022–1694(01)00445–0.

Molua, E.L., and C.M. Lambi, 2006: Climate, hydrology and water resources in Cameroon. *CEEPA, Pretoria*, 37.

Moradkhani, H., K.L. Hsu, H. Gupta, and S. Sorooshian, 2005: Uncertainty assessment of hydrologic model states and parameters: Sequential data assimilation using the particle filter. *Water Resour. Res.*, **41**, doi: 10.1029/2004WR003604.

Morcrette, J.J., 1991: Radiation of cloud radiative properties in the european centre for medium range weather forecasts forecasting system. *J. Geophys. Res.*, **96(5)**, 9121–9132.

Moriasi, D.N., J.G. Arnold, M.W. Van Liew, R.L. Bingner, R.D. Harmel, and T.L. Veith, 2007: Model evaluation guidelines for systematic quantification of accuracy in watershed simulations. *Trans. ASABE*, **50**, 885–900.

Moss, R., W. Babiker, S. Brinkman, E. Calvo, T. Carter, J. Edmonds, I. Elgizouli, S. Emori, L. Erda, K. Hibbard, R. Jones, M. Kainuma, J. Kelleher, J.F. Lamarque, M. Manning, B. Matthews, J. Meehl, L. Meyer, J. Mitchell, N. Nakicenovic, B. ONeill, R. Pichs, K. Riahi, S. Rose, R. Stouffer, D. van Vuuren, J. Weyant, T. Wilbanks, J.P. vanYpersele, and M. Zurek, 2008: Towards new scenarios for the analysis of emissions: Climate change, impacts and response strategies. *IPCC, Geneva, Switzerland.*

Moss, R., J.A. Edmonds, K.A. Hibbard, M.R. Manning, S.K. Rose, D.P. van Vuuren, T.R. Carter, S. Emori, M. Kainuma, T. Kram, G.A. Meehl, J.F.B. Mitchell, N. Nakicenovic, K. Riahi, S.J. Smith, R.J. Stouffer, A.M. Thomson, J.P. Weyant, and T.J. Wilbanks, 2010: The next generation of scenarios for climate change research and assessment. *Nature*, **463**, 747–756.

Moussa, R., 2008: Significance of the Nash-Sutcliffe efficiency measure for linear rise and exponential recession in event based flood modelling. In: *Geophysical Research Abstracts*, Volume 10, pp. 1–2.

Munang, M., 2010: Climate change impacts on the hydroelectricity potentials of the Sanaga basin: past and future trends. *MSc thesis, University of Buea.*

Nakicenovic, N., J. Alcamo, A. Grubler, K. Riahi, R. Roehrl, H.H. Rogner, and N. Victor, 2000: *Special report on emissions scenarios (SRES), a special report of Working Group III of the intergovernmental panel on climate change.* Cambridge University Press, 608.

Nansai, K., S. Kagawa, S. Suh, M. Fujii, R. Inaba, and S. Hashimoto, 2009: Material and Energy Dependence of Services and Its Implications for Climate Change. *Environ. Sci. Technol.*, **43**, 4241–4246, doi: 10.1021/es8025775.

Nash, J.E., and J.V. Sutcliffe, 1970: River flow forecasting through conceptual models. Part I - a discussion of principles. *J. Hydrol.*, **10**, 282–290, doi: 10.1016/0022–1694(70)90255–6.

Neba, A., 1987: *Modern Geography of the Republic of Cameroon.* Neba Pub., 204.

Nicholson, S.E., B. Some, and B. Kone, 2000: An Analysis of Recent Rainfall Conditions in West Africa, Including the Rainy Seasons of the 1997 El Niño and the 1998 La Niña Years. *J.*

Climate, **13**, 2628–2640, doi:10.1175/1520–0442(2000)013<2628:AAORRC>2.0.CO;2.

Nonki, R.M., 2014: Impact de la formulation de l'évapotranspiration potentielle (ETP) sur le modèle pluie-débit HBV-Light modifié: cas du bassin versant de la Bénoué à Garoua (Nord-Cameroon). *Mémoire de Master, Université de Yaoundé 1, 66.*

Nonki, R.M., A. Lenouo, C.J. Lennard, and C. Tchawoua, 2019: Assessing climate change impacts on water resources in the Benue River Basin, Northern Cameroon. *Environ. Earth Sci.*, **78**, 606, doi: 10.1007/s12665–019–8614–4.

Ogilvie, A., G. Mahé, J. Ward, G. Serpantié, J. Lemoalle, P. Morand, B. Barbier, A.T. Diop, A. Caron, R. Namarra, D. Kaczan, A. Lukasiewicz, J.E. Paturel, G. Liénou, and J.C. Clanet, 2010: Water, agriculture and poverty in the Niger River basin. *Water International*, **35**, 594–622, doi:10.1080/02508060.2010.515545.

Oguntunde, P.G., and B.J. Abiodun, 2013: The impact of climate change on the Niger River Basin hydroclimatology, West Africa. *Clim. Dyn.*, **40**, 81–94, doi: 10.1007/s00382–012–1498–6.

Oguntunde, P.G., G. Lischeid, and B.J. Abiodun, 2018: Impacts of climate variability and change on drought characteristics in the Niger River Basin, West Africa. *Stoch. Environ. Res. Risk Assess.*, **32**, 1017–1034, doi: 10.1007/s00477–017–1484–y.

Okolle, J., P. Oumarou, A. Almeck, F. Ntam, B. Ngane, C. Suh, P. Mounjouenpou, J. Akoa Etoa, E. Mfoumou, A. Ngatchou, P. Mveng, A. Ngome, M. Meliko, D. Pompidou, G. Nyambi, and N. Woin, 2016: Status of Agricultural Innovations, Innovation Platforms, and Innovations Investment. *2015 PARI project country report: Republic of Cameroon*, 103.

Oloruntade, A.J., 2017: *Modeling the impacts of Climate Change on Hydrology and Water Resources in the Niger-South sub-catchment of the Niger River Basin, Nigeria.* PhD Dissertation, Universiti Putra Malaysia, 245p.

Olsson, J., C. Uvo, and K. Jinno, 2001: Statistical atmospheric downscaling of short-term extreme rainfall by neural networks. *Phys. Chem. Earth, Part B: Hydrology, Oceans and Atmosphere*, **26**, 695 – 700, doi: 10.1016/S1464–1909(01)00071–5.

O'Neill, B.C., M. Dalton, R. Fuchs, L. Jiang, S. Pachauri, and K. Zigova, 2010: Global demographic trends and future carbon emissions. *Proc. Natl. Acad. Sci.*, **107**, 17521–17526, doi:10.1073/pnas.1004581107.

Oudin, L., F. Hervieu, C. Michel, C. Perrin, V. Andreassian, F. Anctil, and C. Loumagne, 2005: Which potential evapotranspiration input for a lumped rainfall-runoff model? -Part 2:Towards a simple and efficient potential evapotranspiration model for rainfall-runoff modelling. *J. Hydrol.*, **303**, 290–306, doi:10.1016/j.jhydrol.2004.08.026.

Oudin, L., C. Perrin, T. Mathevet, V. Andreassian, and C. Michel, 2006: Impact of biased and randomly corrupted inputs on the efficiency and the parameters of watershed models. *J. Hydrol.*, **320**, 62–83, doi:10.1016/j.jhydrol.2005.07.016.

Pal, I., and A. Al-Tabbaa, 2011: Regional changes of the severities of meteorological droughts and floods in India. *J. Geogr. Sci.*, **21**, 195, doi:10.1007/s11442–011–0838–5.

Penlap, K.E., C. Matulla, H.V. Storch, and K.F. Mkankam, 2004: Downscaling of GCM scenarios to assess precipitation changes in the little rainy season (March–June) in Cameroon. *Clim. Res.*, **26**, 85–96.

Penman, H.L., 1948: Natural evaporation from open water, bare soil and grass. *Proc. Roy. Soc. A–Math. Phys.*, **193**, 120–145, doi.org/10.1098/rspa.1948.0037.

Pianosi, F., K. Beven, J. Freer, J.W. Hall, J. Rougier, D.B. Stephenson, and T. Wagener, 2016: Sensitivity analysis of environmental models: A systematic review with practical workflow. *Environ. Model. Softw.*, **79**, 214 – 232, https://doi.org/10.1016/j.envsoft.2016.02.008.

Poméon, T., D. Jackisch, and B. Diekkrüger, 2017: Evaluating the performance of remotely sensed and reanalysed precipitation data over West Africa using HBV light. *J. Hydrol.*, **547**, 222–235. https://doi.org/10.1016/j.jhydrol.2017.01.055.

Rakhecha, P., and V.P. Singh, 2009: *Applied hydrometeorology*. Springer Science and Business Media.

Refsgaard, J.C., J.P. van der Sluijs, J. Brown, and P. van der Keur, 2006: A framework for dealing with uncertainty due to model structure error. *Adv. Water Resour.*, **29**, 1586 – 1597, doi: 10.1016/j.advwatres.2005.11.013.

Refsgaard, J.C., J.P. van der Sluijs, A.L. Højberg, and P.A. Vanrolleghem, 2007: Uncertainty in the environmental modelling process – a framework and guidance. *Environ. Model. Softw.*, **22**, 1543 – 1556, https://doi.org/10.1016/j.envsoft.2007.02.004.

Riahi, K., S. Rao, V. Krey, C. Cho, V. Chirkov, G. Fischer, G. Kindermann, N. Nakicenovic, and P. Rafaj, 2011: RCP 8.5—A scenario of comparatively high greenhouse gas emissions. *Clim. Change*, **109**, 33, doi: 10.1007/s10584–011–0149–y.

Robert, C., and G. Casella, 2013: *Monte Carlo statistical methods*. Springer Science & Business Media, 445.

Roeckner, E., K. Arpe, L. Bengtsson, M. Christoph, M. Claussen, L. Dmenil, , M. Esch, M. Giorgetta, U. Schlese, and U. Schulzweida, 1996: The atmospheric general circulation model ECHAM–4: model description and simulation of present–day climate. *MPI Technical Report No 218, Max-Planck-Institute for Meteorology, Hamburg, 94*.

Rosbjerg, D., and H. Madsen, 2006: *Concepts of Hydrologic Modeling*, Chapter 10, pp. doi: 10.1002/0470848944.hsa009. American Cancer Society.

Rosen, C., 2000: *World Resources 2000-2001: People and ecosystems: The fraying web of life*. Elsevier Science, 389.

Rusli, S.R., D. Yudianto, and J. tao Liu, 2015: Effects of temporal variability on HBV model calibration. *Water Sci. Eng.*, **8**, 291–300. https://doi.org/10.1016/j.wse.2015.12.002.

Sabziparvar, A.A., and H. Tabari, 2010: Regional estimation of reference evapotranspiration in arid

and semi-arid regions. *J. Irrig. Drain. Eng. ASCE*, **136(10)**, 724–731.

Sakho, S., J.P. Dupont, M.T. Cisse, and S. Loum, 2017: Hydrological responses to rainfall variability and dam construction: a case study of the upper Senegal River basin. *Environ. Earth Sci.*, **76**, 253, doi:10.1007/s12665–017–6570–4.

Saltelli, A., M. Ratto, S. Tarantola, and F. Campolongo, 2006: Sensitivity analysis practices: Strategies for model-based inference. *Reliab. Eng. Syst. Saf.*, **91**, 1109 – 1125, https://doi.org/10.1016/j.ress.2005.11.014.

Samains, B., and V.R.N. Pauwels, 2013: Impact of potential and (scintillometer–based) actual evapotranspiration estimates on the performance of a lumped rainfall–runoff model. *Hydrol. Earth Syst. Sci.*, **17**, 4525–4540, doi:10.5194/hess–17–4525–2013.

Seibert, J., 1997: Estimation of parameter uncertainty in the HBV-model. *Nordic Hydrol.*, **28(415)**, 247–262.

Seibert, J., 2005: HBV light version 2, user's manual. *Stockholm University, 32.*

Seibert, J., and M.J. Vis, 2012: Teaching hydrological modeling with a user-friendly catchment-runoff-model software package. *Hydrol Earth Syst. Sci.*, **16**, 3315–3325, doi: 10.5194/hess–16–3315–2012.

Shin, M.J., J.H. Guillaume, B.F. Croke, and A.J. Jakeman, 2015: A review of foundational methods for checking the structural identifiability of models: Results for rainfall-runoff. *J. Hydrol.*, **520**, 1 – 16, https://doi.org/10.1016/j.jhydrol.2014.11.040.

Shuttleworth, W.J., 1993: Evaporation. Chapter 4 in Handbook of hydrology, D.R. Maidment (Editor). *McGraw–Hill Inc., New York San Francisco Washington, D.C., 4.1-4.53.*

Sighomnou, D., 2004: *Analyse et redéfinition des régimes climatiques et hydrologiques du Cameroun : perspectives d'évolution des ressources en eau.* Thèse de Doctorat d'Etat, Université de Yaoundé 1, 289.

Sighomnou, D., L. Descroix, P. Genthon, G. Mahé, B.I. Moussa, E. Gautier, I. Mamadou, J.P. Vandervaere, T. Bachir, B. Coulibaly, J.L. Rajot, M.O. Issa, M.M. Abdou, N. Dessay, E. Delaitre, F.O. Maiga, A. Diedhiou, G. Panthou, T. Vischel, H. Yacouba, H. Karambiri, J.E. Paturel, P. Diello, E. Mougin, L. Kergoat, and P. Hiernaux, 2013: The Niger River Niamey flood of 2012: The paroxysm of the Sahelian paradox? *Science et changements planétaires/Sécheresse*, **24**, 3–13, doi:10.1684/sec.2013.0370.

Sighomnou, D., L. Sigha Nkamdjou, G. Liénou, A. Dezetter, G. Mahé, E. Servat, J.E. Paturel, J.C. Olivry, F. Tchoua, and G.E. Ekodeck, 2007: Impacts des fluctuations climatiques sur le régime des écoulements du fleuve Sanaga au Cameroun, prospectives pour le XXIème siècle. *Technical Document in Hydrology*, **80**, 173–182.

Singh, V.P., and D.A. Woolhiser, 2002: Mathematical Modeling of Watershed Hydrology. *J. Hydrol. Eng.*, **7**, 270–292, doi: 10.1061/(ASCE)1084–0699(2002)7:4(270).

Sobol, I.M., 2001: Global sensitivity indices for nonlinear mathematical models and their Monte Carlo estimates. *Math. Comput. Simul.*, **55**, 271–280, doi: 10.1016/S0378–4754(00)00270–6.

Solomon, S., D. Qin, M. Manning, Z. Chen, M. Marquis, K.B. Averyt, M. Tignor, and H.L. Miller, 2007: *Climate change 2007: Synthesis Report. Contribution of Working Group I, II and III to the AR4 of the IPCC. Summary for Policymakers.* Intergovernmental Panel on Climate Change (IPCC).

Sonkoué, D., D. Monkam, T.C. Fotso-Nguemo, Z.D. Yepdo, and D.A. Vondou, 2018: Evaluation and projected changes in daily rainfall characteristics over Central Africa based on a multi-model ensemble mean of CMIP5 simulations. *Theor. Appl. Climatol.*, doi: 10.1007/s00704–018–2729–5.

Spies, R.R., K.J. Franz, T.S. Hogue, and A.L. Bowman, 2015: Distributed hydrologic modeling using satellite-derived potential evapotranspiration. *J. Hydrometeor.*, **16**, 129–146, doi:10.1175/JHM–D–14–0047.1.

Steele-Dunne, S.C., P. Lynch, R. McGrath, T. Semmler, S. Wang, J. Hanafin, and P. Nolan, 2008: The impacts of climate change on hydrology in Ireland. *J. Hydrol.*, **356**, 28–45, doi: 10.1016/j.jhydrol.2008.03.025.

Stevens, B., M. Giorgetta, M. Esch, T. Mauritsen, T. Crueger, S. Rast, M. Salzmann, H. Schmidt, J. Bader, K. Block, R. Brokopf, I. Fast, S. Kinne, L. Kornblueh, U. Lohmann, R. Pincus, T. Reichler, and E. Roeckner, 2013: Atmospheric component of the MPI-M Earth System Model: ECHAM6. *J. Adv. Model. Earth Syst.*, **5**, 146–172. https://doi.org/10.1002/jame.20015.

Tamoffo, A.T., W. Moufouma-Okia, A. Dosio, R. James, W.M. Pokam, D.A. Vondou, T.C. Fotso-Nguemo, G.M. Guenang, P.H. Kamsu-Tamo, G. Nikulin, G.N. Longandjo, C.J. Lennard, J.P. Bell, R.R. Takong, A. Haensler, L.A.D. Tchotchou, and R. Nouayou, 2019: Process-oriented assessment of RCA4 regional climate model projections over the Congo Basin under 1.5^oC and 2^oC global warming levels: influence of regional moisture fluxes. *Clim. Dyn.*, **53**, 1911–1935, doi:10.1007/s00382–019–04751–y.

Tamoffo, A.T., D.A. Vondou, W.M. Pokam, A. Haensler, Z.D. Yepdo, T.C. Fotso-Nguemo, L.A.D. Tchotchou, and R. Nouayou, 2018: Daily characteristics of Central African rainfall in the REMO model. *Theor. Appl. Climatol.*, doi: 10.1007/s00704–018–2745–5.

Tarhule, A., Z. Saley-Bana, and P.J. Lamb, 2009: Rainwatch. *Bull. Amer. Meteor. Soc.*, **90**, 1607–1614, doi:10.1175/2009BAMS2697.1.

Tarhule, A., J.T. Zume, J. Grijsen, A. Talbi-Jordan, A. Guero, R.Y. Dessouassi, H. Doffou, S. Kone, B. Coulibaly, and N.R. Harshadeep, 2015: Exploring temporal hydroclimatic variability in the Niger Basin (1901–2006) using observed and gridded data. *Int. J. Climatol.*, **35**, 520–539.

Taylor, K.E., R.J. Stouffer, and G.A. Meehl, 2012: An overview of CMIP5 and the experiment design. *Bull. Amer. Meteor. Soc.*, **93**, 485–498.

Teichmann, C., B. Eggert, A. Elizalde, A. Haensler, D. Jacob, P. Kumar, C. Moseley, S. Pfeifer,

D. Rechid, A.R. Remedio, H. Ries, J. Petersen, S. Preuschmann, T. Raub, F. Saeed, K. Sieck, and T. Weber, 2013: How Does a Regional Climate Model Modify the Projected Climate Change Signal of the Driving GCM: A Study over Different CORDEX Regions Using REMO. *Atmosphere*, **4**, 214–236, doi: 10.3390/atmos4020214.

Thiemann, M., M. Trosset, H. Gupta, and S. Sorooshian, 2001: Bayesian recursive parameter estimation for hydrologic models. *Water Resour. Res.*, **37**, 2521–2535, doi: 10.1029/2000WR900405.

Thomson, A.M., K.V. Calvin, S.J. Smith, G.P. Kyle, A. Volke, P. Patel, S. Delgado-Arias, B. Bond-Lamberty, M.A. Wise, L.E. Clarke, and J.A. Edmonds, 2011: RCP4.5: a pathway for stabilization of radiative forcing by 2100. *Clim. Change*, **109**, 77, doi: 10.1007/s10584–011–0151–4.

Tiedtke, M., 1989: A Comprehensive Mass Flux Scheme for Cumulus Parameterization in Large-Scale Models. *Mon. Weather Rev.*, **117**, 1779–1800, doi: 10.1175/1520–0493(1989)117<1779:ACMFSF>2.0.CO;2.

Tiedtke, M., 1993: Representation of clouds in large-scale models. *Mon. Weather Rev.*, **121**, 3040–3061.

Tomer, M.D., and K.E. Schilling, 2009: A simple approach to distinguish land-use and climate-change effects on watershed hydrology. *J. Hydrol.*, **376**, 24 – 33, doi: 10.1016/j.jhydrol.2009.07.029.

Toro, S.M., 1997: Post-Construction Effects of the Cameroonian Lagdo Dam on the River Benue. *Water Environ. J.*, **11**, 109–113, doi: 10.1111/j.1747–6593.1997.tb00100.x.

Tramblay, Y., D. Ruelland, S. Somot, R. Bouaicha, and E. Servat, 2013: High-resolution Med-CORDEX regional climate model simulations for hydrological impact studies: a first evaluation of the ALADIN-Climate model in Morocco. *Hydrol. Earth Syst. Sci.*, **17**, 3721–3739, doi: doi:10.5194/hess–17–3721–2013.

Trzaska, S., and E. Schnarr, 2014: A review of downscaling methods for climate change projections. *United States Agency for International Development by Tetra Tech ARD*, 1–42.

Tsai, C.W., and S. Franceschini, 2005: Evaluation of Probabilistic Point Estimate Methods in Uncertainty Analysis for Environmental Engineering Applications. *J. Environ. Eng.*, **131**, 387–395, doi: 10.1061/(ASCE)0733–9372(2005)131:3(387).

Tshimanga, R.M., 2012: *Hydrological uncertainty analysis and scenario-based streamflow modelling for the Congo River Basin.* PhD thesis, Rhodes University, 324p.

Tshimanga, R.M., and D.A. Hughes, 2012: Climate change and impacts on the hydrology of the Congo Basin: The case of the northern sub-basins of the Oubangui and Sangha Rivers. *Phys. Chem. Earth, Parts A/B/C*, **50-52**, 72 – 83, doi: 10.1016/j.pce.2012.08.002.

Tshimanga, R.M., and D.A. Hughes, 2014: Basin–scale performance of a semidistributed rainfall–runoff model for hydrological predictions and water resources assessment of large rivers: The Congo River. *Water Resour. Res.*, **50**, 1174–1188, doi:10.1002/2013WR014310.

Uhlenbrook, S., J. Seibert, C. Leibundgut, and A. Rodhe, 1999: Prediction uncertainty of concep-

tual rainfall-runoff models caused by problems in identifying model parameters and structure. *Hydrol. Sci. J.*, **44**, 779–797, https://doi.org/10.1080/02626669909492273.

UNFCCC, 2007: United Nations Climate Change Conference, Nusa Dua, Bali, Indonesia, 3rd- 5th December, 2007.

van Liew, M.W., T.L. Veith, D.D. Bosch, and J.G. Arnold, 2007: Suitability of SWAT for the conservation effects assessment project: A comparison on USDA-ARS experimental watersheds. *J. Hydrologic Eng.*, **12(2)**, 173–189, doi: 10.1061/(ASCE)1084–0699(2007)12:2(173).

van Straten, G.T., and K.J. Keesman, 1991: Uncertainty propagation and speculation in projective forecasts of environmental change: A lake-eutrophication example. *J. Forecast.*, **10**, 163–190, doi: 10.1002/for.3980100110.

van Vuuren, D.P., J. Edmonds, M. Kainuma, K. Riahi, A. Thomson, K. Hibbard, G.C. Hurtt, T. Kram, V. Krey, J.F. Lamarque, T. Masui, M. Meinshausen, N. Nakicenovic, S.J. Smith, and S.K. Rose, 2011: The representative concentration pathways: an overview. *Clim. Change*, **109**, 5.

Vazquez, R.F., and J. Feyen, 2003: Effect of potential evapotranspiration estimates on effective parameters and performance of the MIKE SHE-code applied to a medium-size catchment. *J. Hydrol.*, **270**, 309–327.

Vecchia, A.V., and R.L. Cooley, 1987: Simultaneous confidence and prediction intervals for nonlinear regression models with application to a groundwater flow model. *Water Resour. Res.*, **23**, 1237–1250, doi: 10.1029/WR023i007p01237.

Viner, D., 2000: *Modelling Climate Change*. Chapter 8, University of East Anglia, UK, 3p. www.cru.uea.ac.uk/modelling-climate-change.

von Storch, H., E. Zorita, and U. Cubasch, 1993: Downscaling of Global Climate Change Estimates to Regional Scales: An Application to Iberian Rainfall in Wintertime. *J. Clim.*, **6**, 1161–1171, doi: 10.1175/1520–0442(1993)006<1161:DOGCCE>2.0.CO;2.

Vondou, D.A., and A. Haensler, 2017: Evaluation of simulations with the regional climate model REMO over Central Africa and the effect of increased spatial resolution. *Int. J. Climatol.*, **37**, 741–760, doi: 10.1002/joc.5035.

Vrugt, J.A., C.G.H. Diks, H.V. Gupta, W. Bouten, and J.M. Verstraten, 2005: Improved treatment of uncertainty in hydrologic modeling: Combining the strengths of global optimization and data assimilation. *Water Resour. Res.*, **41**, doi: 10.1029/2004WR003059.

Vrugt, J.A., H.V. Gupta, W. Bouten, and S. Sorooshian, 2003: A Shuffled Complex Evolution Metropolis algorithm for optimization and uncertainty assessment of hydrologic model parameters. *Water Resour. Res.*, **39**, doi: 10.1029/2002WR001642.

Wagener, T., M. Sivapalan, P. Troch, and R. Woods, 2007: Catchment Classification and Hydrologic Similarity. *Geogr. Compass.*, **1**, 901–931, doi: 10.1111/j.1749–8198.2007.00039.x.

Wagener, T., H.S. Wheater, and H.V. Gupta, 2004: *Rainfall-runoff modelling in gauged and ungauged catchments*. Imperial College Press, London, UK, 332pp. https://doi.org/10.1142/p335.

Wang, X., A.M. Melesse, and W. Yang, 2006: Influences of Potential Evapotranspiration Estimation Methods on SWAT's Hydrologic Simulation in a Northwestern Minnesota Watershed. *Trans. ASABE*, **49(6)**, 1755–1771.

Wilby, R., C. Dawson, and E. Barrow, 2002: SDSM: a decision support tool for the assessment of regional climate change impacts. *Environ. Model. Soft.*, **17**, 145 – 157, doi: 10.1016/S1364–8152(01)00060–3.

Wilby, R.L., J. Troni, Y. Biot, L. Tedd, B.C. Hewitson, D.M. Smith, and R.T. Sutton, 2009: A review of climate risk information for adaptation and development planning. *Int. J. Climatol.*, **29**, 1193–1215, doi: 10.1002/joc.1839.

Wu, Y., S. Liu, and A.L. Gallant, 2012: Predicting impacts of increased CO2 and climate change on the water cycle and water quality in the semiarid James River Basin of the Midwestern USA. *Sci. Total Environ.*, **430**, 150 – 160, doi: 10.1016/j.scitotenv.2012.04.058.

Xu, C.Y., and V.P. Singh, 2002: Intercomparison of methods for calculating potential evaporation in regional and global water balance models. *Water Resour. Manag.*, **16**, 197–219.

Yapo, P.O., H.V. Gupta, and S. Sorooshian, 1998: Multi-objective global optimization for hydrologic models. *J. Hydrol.*, **204**, 83 – 97, doi: 10.1016/S0022–1694(97)00107–8.

Yira, Y., B. Diekkrüger, G. Steup, and A.Y. Bossa, 2017: Impact of climate change on hydrological conditions in a tropical West African catchment using an ensemble of climate simulations. *Hydrol. Earth Syst. Sci.*, **21**, 2143–2161, doi: 10.5194/hess–21–2143–2017.

Zelelew, M.B., and K. Alfredsen, 2012: Sensitivity-guided evaluation of the HBV hydrological model parameterization. *J. Hydroinform.*, **15**, 967–990, doi: 10.2166/hydro.2012.011.

Zhao, L., J. Xia, C.Y. Xu, Z. Wang, and L. Sobkowiak, 2013: Evapotranspiration estimation methods in hydrological models. *J. Geogr. Sci.*, **23(2)**, 359–369.

List of publications and conferences

A Published article

1. **Rodric M. Nonki**, André Lenouo, Christopher J. Lennard and Clément Tchawoua (2019): **Assessing climate change impacts on water resources in the Benue River Basin, Northern Cameroon**. *Environmental Earth Sciences, Springer-Verlag GmbH Germany.* **78, 606**. DOI: 10.1007/s12665-019-8614-4.

B Posters presentation

1. **Rodric M. Nonki**, André Lenouo and Clément Tchawoua: **Assessing the impacts of climate change on hydrological parameters in the Garoua Benue River Basin (Central Africa) using Regional Climate Model REMO.** *Poster presented in the* ***Fourth Workshop on Water Resources in Developing Countries***, *organised by* ***ICTP (International Centre for Theoretical Physics)***, *on the topic:* **Hydroclimate Modelling and Analysis Tools**, *taken place from 12–23 June 2017 at ICTP Adriatico Guest House, Trieste, Italy.*

C Oral presentations

1. **Rodric M. Nonki**, André Lenouo, Raphaël M. Tshimanga and Clément Tchawoua: **Parameter uncertainty analysis, optimal calibration and evaluation of the lumped hydrological model in the Upper Benue River Basin, Northern Cameroon.** *Oral presentation did in the* ***International Conference Bangui 2019***, *on the topic:* **Water resources quality and uses in Central and Eastern Africa: the impacts over ecosystems and health**, *taken place from 21-26 OCtober 2019 at the CEMAC Palace, Bangui, Central Africa Republic.*

2. **Rodric M. Nonki**: **Processing NetCDF files using Climate Data Operators (CDO) software.** *Oral presentation did in the* ***Regional Workshop FRIEND AOC 2019***, *on the topic:* **Use and valorization of spatial hydrometeorological data**, *taken place from*

23-27 April 2019 at the Scientific and Innovation Cluster, Félix Houphouët-Boigny University, Bingerville, Ivory Coast.

3. **Rodric M. Nonki**, André Lenouo, Christopher J. Lennard and Clément Tchawoua: **Hydrologic effects of climate change in the Benue River Basin, Northern Cameroon.** *Oral presentation did in the* ***8th Global FRIEND-Water Conference****, on the topic:* **Hydrological Processes and Water Security in a Changing World**, *taken place from 6-9 November 2018 at the MARCO POLO PARKSIDE hotel, Beijing, China.*

4. **Rodric M. Nonki**, André Lenouo and Clément Tchawoua: **Assessing climate change impacts on hydrological parameters in the Benue River Basin (Central Africa) using an ensemble of CORDEX RCMs.** *Oral presentation did in the* ***CORDEX-Africa Vulnerability-Impacts-Adaptation (VIA) Workshop****, on the topic:* **Develop a coordinated strategy to quantify the impacts of climate change in the sectors of hydrology, agriculture, biodiversity and health over Africa**, *taken place from 12 – 16 February 2018 at the Southern Sun Hotel in Newlands, Cape Town, South Africa.*

5. **Rodric M. Nonki**, Oluwalani Adebanji: **Capacity of CHYM model to reproduce flow discharge in the Sanaga River Basin (Cameroon).** *Oral presentation did in the* ***Fourth Workshop on Water Resources in Developing Countries****, on the topic:* **Hydroclimate Modelling and Analysis Tools**, *taken place from 12–23 June 2017 at the International Centre for Theoretical Physics (ICTP) Adriatico Guest House, Trieste, Italy.*

D Conferences

1. *Attendance at the International Conference Bangui 2019, organised by the* ***UNESCO IHP FRIEND Program for West and Central Africa (FRIEND-AOC)****, on the subject of:* **Water resources quality and uses in Central and Eastern Africa: the impacts over ecosystems and health**, *from 22 to 23 October 2019 at the CEMAC Palace, Bangui, Central Africa Republic.*

2. *Attendance at the 8th Global FRIEND-Water Conference, organised by the* ***UNESCO IHP FRIEND Program****, on the subject of:* **Hydrological Processes and Water Security in a Changing World**, *from 6 to 9 November 2018 at the MARCO POLO PARKSIDE hotel, Beijing, China.*

E Workshops and summer schools

1. *Attendance at the training of trainers workshop, organized by the* ***Global Monitoring for Environment and Security in Africa Program (GMES-Africa)****, on the subject of:*

Space observation applications for water resources management in the Congo Basin and Central Africa, *from 24 to 26 October 2019 at the CEMAC Palace, Bangui, Central Africa Republic.*

2. *Attendance as trainer at the Regional Workshop FRIEND-AOC 2019, organized by:* ***UNESCO IHP FRIEND Program for West and Central Africa (FRIEND-AOC)***, *on the subject of:* **Use and valorization of spatial hydrometeorological data**, *from 23 to 27 April 2019 at the Scientific and Innovation Cluster, Félix Houphouët-Boigny University, Bingerville, Ivory Coast.*

3. *Attendance as Hydrology and water resources expert at the second CORDEX-Africa Vulnerability-Impacts-Adaptation (VIA) Workshop, organized by:* ***CORDEX (COordinated Regional Climate Downscaling EXperiment)***, *on the subject of:* **Develop a coordinated strategy to quantify the impacts of climate change in the sectors of hydrology, agriculture, biodiversity and health over Africa**, *from 12 to 16 February 2018 at the Southern Sun Hotel in Newlands, Cape Town, South Africa.*

4. *Attendance as Hydrology and water resources expert at the first CORDEX-Africa Vulnerability-Impacts-Adaptation (VIA) Workshop, organized by:* ***CORDEX (COordinated Regional Climate Downscaling EXperiment)***, *on the subject of:* **Develop a coordinated strategy to quantify the impacts of climate change in the sectors of hydrology, agriculture, biodiversity and health over Africa**, *from 15 to 17 February 2017 at the Southern Sun Hotel in Newlands, Cape Town, South Africa.*

5. *Attendance at the Fourth Workshop on Water Resources in Developing Countries, organized by:* ***ICTP***, *on the subject of:* **Hydroclimate Modelling and Analysis Tools**, *from 12 to 23 June 2017 at Adriatico Guest House Laboratory, Trieste, Italy.*

Environmental Earth Sciences (2019) 78:606
https://doi.org/10.1007/s12665-019-8614-4

ORIGINAL ARTICLE

Assessing climate change impacts on water resources in the Benue River Basin, Northern Cameroon

Rodric M. Nonki[1] · André Lenouo[2] · Christopher J. Lennard[3] · Clément Tchawoua[4]

Received: 28 November 2018 / Accepted: 23 September 2019

Abstract

The Benue River Basin (BRB) is a major tributary of the Niger River Basin (NRB) and the second-largest river in Cameroon. It serves many water resource functions including irrigation, hydroelectricity production and navigation. Previous research has indicated that recent climate change (CC) has had significant impacts on local and regional hydrological regimes of this watershed. In this study, CC scenarios were integrated with a hydrological model to evaluate the influence of CC on water resources in the BRB. Historical and projected scenarios of dynamically downscaled temperature and precipitation from the REMO regional climate model (RCM) forced by the boundary conditions data of the Europe-wide Consortium Earth System Model (EC-ESM) and the Max Planck Institute-Earth System Model (MPI-ESM) general circulation models (GCMs) were used. The historical runs of the REMO simulations were first evaluated after which downscaled temperature and precipitation data were used as input for the HBV-Light hydrological model to simulate water balance components. The mean climate and hydrological variables for the historical (1981–2005) and the two future periods (2041–2065 and 2071–2095) were compared to assess the potential impact of CC on water resources in the middle and late twenty-first century under three greenhouse gases (GHGs) concentration scenarios, the Representative Concentration Pathways (RCPs) 2.6, 4.5 and 8.5. Our results show that (a) the HBV-Light hydrological model could effectively simulate the streamflow change in the BRB; (b) annual precipitation will decrease between 1 and 10% while both annual temperature and potential evapotranspiration (PET) will increase between 8–18 and 6–30%, respectively, under both scenarios, models and future periods; c) the combination of reduced precipitation and increase of PET results in a significant decrease in streamflow in the BRB (up to 51%) and this will move the basin to a much drier environmental state. Therefore, CC adaptation strategies and future development planning in this region must consider these important decreases of discharge.

Keywords Climate change · Water resources · REMO model · HBV-Light hydrological model · Dynamical downscaling · Benue River Basin

Introduction

Cameroon contributes significantly to the economy of Central Africa (CA), its water resources being a major source of this importance. However, within Cameroon, water is also recognized as the most important impediment for socioeconomic development because more than 70% of the population practices rainfed agriculture, which occupies about 95% of the land use (Molua and Lambi 2007). Other activities are also dependent on water resources: hydroelectricity production represents more than 95% of electricity in Cameroon. Additionally, Cameroon has the second-highest hydropower potential in CA after the Democratic Republic of Congo. However, in Cameroon, water resources are unequally distributed between the northern and southern parts. The

Electronic supplementary material The online version of this article (https://doi.org/10.1007/s12665-019-8614-4) contains supplementary material, which is available to authorized users.

✉ Rodric M. Nonki
norome31@yahoo.fr

[1] Laboratory for Environmental Modeling and Atmospheric Physics (LEMAP), Department of Physics, Faculty of Sciences, University of Yaounde I, Yaoundé, Cameroon

[2] Department of Physics, Faculty of Science, University of Douala, Douala, Cameroon

[3] Climate System Analysis Group, University of Cape Town, Cape Town, South Africa

[4] Laboratory of Mechanics, Department of Physics, Faculty of Sciences, University of Yaounde I, Yaoundé, Cameroon

Published online: 08 October 2019